D2.1 CFD CALCULATIONS

Creation Date:	2013-04-23
Revision Date:	2013-04-26
Project:	MoVe IT!
WP:	2
Deliverable:	2.1
Version:	1.1

Responsible: MARIN – Ir. K.H. van der Meij

TABLE OF CONTENT

DOCUMENT PROPERTIES

Document Name:	D2.1 Measurements
Document Author(s)	Ir. K.H. van der Meij, Dr. Ir. C. Veldhuis, Ir. J. Slot, Ir. L. Rueda, Ir. A. Lampe, Ir. F.H. Lafeber
Document Editor(s)	Ir. K.H. van der Meij, Dr. Ir. R.G. Hekkenberg
Date of delivery	2013-04-30
Nature of Deliverable	☒ Report ☐ Prototype ☐ Demonstrator ☐ Other
Document Status	☐ Draft ☐ Final ☐ Approved by SG Steering (or SP meeting type-D) ☐ Approved by reviewer ☐ Acknowledged by MOVEIT! Steering ☒ Issued to EC
Keywords	CFD calculations, Carpe Diem, Inflexible, Dunaføldvar, Herso-1, self propelled barge, pusher, barges, resistance, propulsive efficiency
Related MoVeIT! Reports	D1.2 Measurements

Partners involved

No.	Organisation Name	Name	Email
	MARIN	Ir. K.H. van der Meij	k.v.d.meij@marin.nl

Document history

Version	Date of delivery	Changes	Author(s) Editor(s)	Reviewed by
1.0	2013-04-25	Clarifications in text	K.v.d.Meij	R.G. Hekkenberg
1.1	2013-05-01		K.v.d.Meij	

INTRODUCTION

The goal of the EU project MoVe IT! is to develop a suite of options for the modernisation of inland ships that meet the challenges of over-aging of the fleet, climate change and stronger environmental objectives and provides decision support regarding the application of these options.

In WP1 the state of the art is defined by means of a literature study and by means of full scale measurements on board of five inland vessels. The goal of the measurements is to determine the performance of existing vessels in a controlled environment. Measurements have been done on board of five inland vessels and the performance of the selected vessels has been determined. For the vessels that perform below average CFD calculations have been performed within WP2 to determine the effect of retrofit measures. The results and analysis of the CFD calculations are presented in this report.

From the CFD calculation results a reduction in power due the retrofit measure will be retrieved. This is input for WP7 system integration and assessment.

The measurement results performed in WP1 showed that all vessels, except for the Veerhaven X pushboat were performing below average. For all vessels performing below average CFD calculation have been performed to investigate retrofit measures.

Each case had different aspects had to be investigated, therefore for each case a computation program was selected most suitable for investigating the retrofit measure. Since CFD calculations are a simulation of reality some simplification have to be taken into account. In the section of the CFD analysis of each vessel is written what simplification have been made to perform the calculations.

This report is divided into 4 Sections. In Sections 1 thru 4 the CFD calculation analysis of respectively Carpe Diem, Herso-I, Inflexible and Dunaføldvar are shown. Finally an overview of all the conclusions is presented.

SECTION 1:
CFD ANALYSIS CARPE DIEM

Written by : MARIN – Ir. L. Rueda

TABLE OF CONTENTS

1 INTRODUCTION

In WP1 full scale measurements have been performed on board the Carpe Diem. These full scale measurement showed the ship is performing below average when comparing with the benchmark. Therefore in WP2 possible retrofit measures for the Carpe Diem are investigated, to determine reduction in fuel consumption.

For the Carpe Diem two retrofit options are investigated. First there the bow of the vessel is investigated by means of MARIN's potential flow code RAPID. The objective is to determine if modifying the bow can significantly reduce the wave making resistance. Secondly the flow around the gondolas is investigated with MARIN's viscous flow code PARNASSOS. The objective is to determine the resistance reduction when the gondolas are partly cut off.

The CFD code RAPID is selected for the investigation to the modification of the bow, because this is the most suitable CFD code available at MARIN to investigate the wave making resistance. For the investigation of the flow around the gondolas PARNASSOS is selected, because PARNASSOS is an efficient tool to calculate viscous flow phenomena and has been validated against model tests and full-scale results.

2 PARTICULARS OF SHIP AND PROPELLERS

The main particulars of the ship *Carpe Diem* are listed below:

Table 1. Main characteristics of the ship.

Description	Symbol	Original Hull	Unit
Length between perpendiculars	L_{pp}	109.36	m
Breadth at still waterline (moulded)	B	11.40	m
Moulded draught moulded on FP	T_F	2.80	m
Moulded draught moulded on AP	T_A	2.80	m
Displacement volume moulded	Δ	3096.05	m^3
Wetted surface	S_{TOT}	1710.95	m^2
LCB position forward ½ Lpp	LCB	55.81	%
Block coefficient	Cb	0.887	-

The geometry of the ship is shown in *Figure 1* and *Figure 2*.

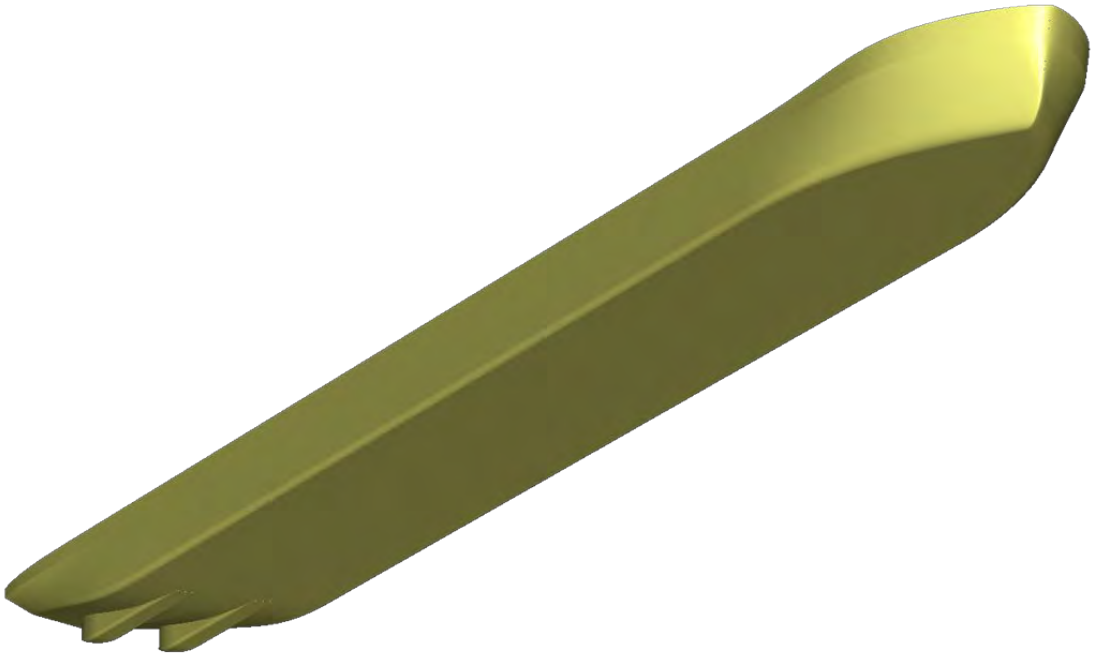

Figure 1. 3D View of the bow of the ship (Carpe Diem)

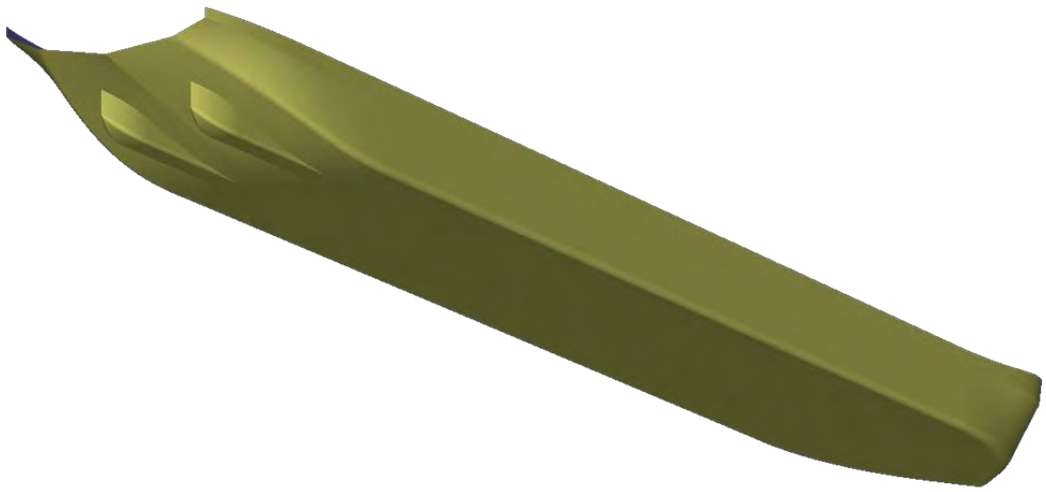

Figure 2. 3D view of the Stern of the ship (Carpe Diem)

The ship is equipped with two gondolas for course-keeping ability and with two propellers (behind the gondolas). Their main characteristics are gathered in Table 2.

Table 2. Propellers characteristics

Propeller diameter	1500	mm
X prop [distance ahead of the aft perpendicular]	4000	mm
Y prop [distance outside the centreline]	± 2250	mm
Z prop [distance above of the basis]	1000	mm

The ship is also equipped with fish-tail rudders and tunnels (Figure 3) to prevent propeller ventilation. These tunnels are necessary to start the ship moving from zero speed.

Figure 3. Aft view of the ship. Above: Tunnels and propeller nozzle. Down: Starboard gondola of the ship.

3 REVIEW OF THE CALCULATION

A PARNASSOS computation for Carpe Diem has been performed to analyse the fluid around the hull. The conclusions taken from this calculation will be used to propose a improvement of the ship, if necessary.

Two calculations have been carried out:

1. *PARNASSOS* calculation for Carpe Diem without actuator disc.
2. *PARNASSOS* calculation for Carpe Diem with actuator disc.

The calculation has been performed in shallow water condition. The Water-depth/draught ratio of this sailing condition is 1.61, so it is expected a big impact of the bottom on hull pressure distribution with respect to deep water.

All the calculations have been carried out in full scale. The trim and sinkage applied to the ship has been calculated by RAPID, potential solver which studies the steady inviscid flow around the ship hull and estimates the wave pattern.

The general characteristics for all the calculations are gathered in Table 3.

Table 3. Main characteristics of the ship and computation

Length between perpendiculars [m]	221.5
Draught [m]	2.8
Water depth [m]	4.5
Ratio depth/draught	1.61
Ship speed [km/h]	15.0
Factor scale	1
Thrust per propeller [kN]	35
Froude number	0.127
Reynolds number	4.0E+08
Trim [deg] (bow down)	0.09
Sinkage [m] (ship moves downward)	0.1545

The ship has been modelled without the tunnels, this means the absolute value of the calculated resistance is lower than in reality. However, relatively hulls can be compared. The results will provide information on the alignment of the tunnel with the local flow. The geometry of the tunnels added to the ship model is shown in *Figure 4*.

Figure 4. Aft view of the model ship with tunnels. Tunnels haven't been included in calculations.

The ship domain (Figure 5) has the following characteristics:

Inflow (distance in front of bow)	88	m
Left exterior	190	m
Bottom	4.5	m
Outflow (distance behind transom)	164	m
Type of grid	Structured multi block	
Number of Grid Cells	Around 7.9 millions	
Number of hull surface elements	Around 17 000	

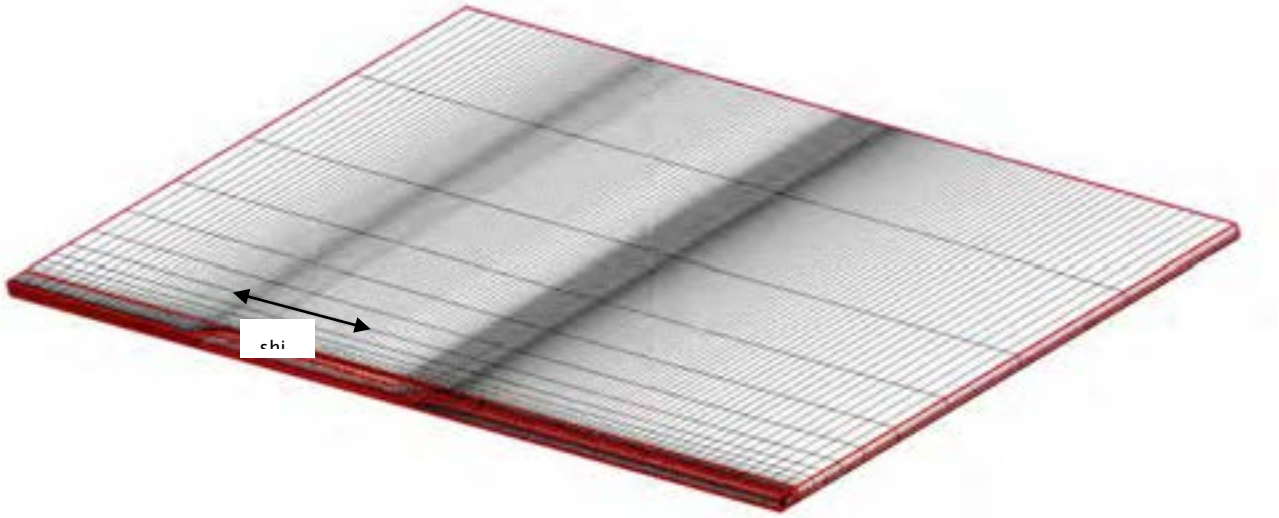

Figure 5. The used computational domain. Number of visualized grid cells is reduced by a factor of four in all directions.

The level of convergence for the calculations is well below 1 X 10^{-5} with a maximum y+ value of 2.0 for the nominal computation and 1 X 10^{-4} with a maximum y+ value[1] of 1.8 for ship with the actuator disc. The maximum y+ values are rather high, however this very locally due to flow separation areas. In general the y+ value over the hull is around 1.

[1] The y+ value is a non-dimensional parameter for the location inside a turbulent flow boundary layer. An y+ value of around 1 means the first cell height of the grid is well within the sublayer of the (fully turbulent) boundary layer.

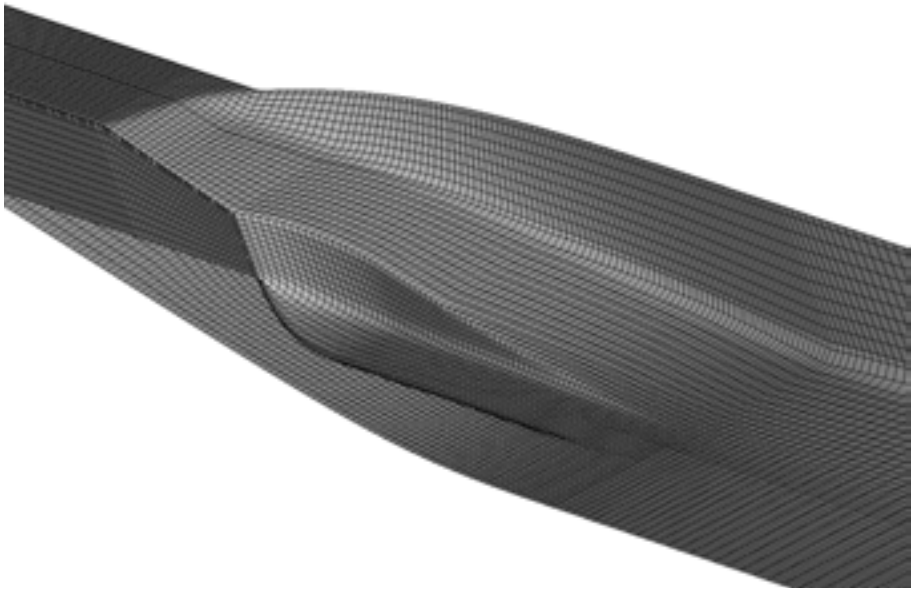

Figure 6. Detail of panel distribution on the hull (Gondola).

4 PRESENTATION AND DISCUSSION OF THE RESULTS

In this chapter the results of the calculation will be presented and discussed.

4.1 Analysis wave pattern

The wave pattern produced by the ship Carpe Diem is show in Figure 7.

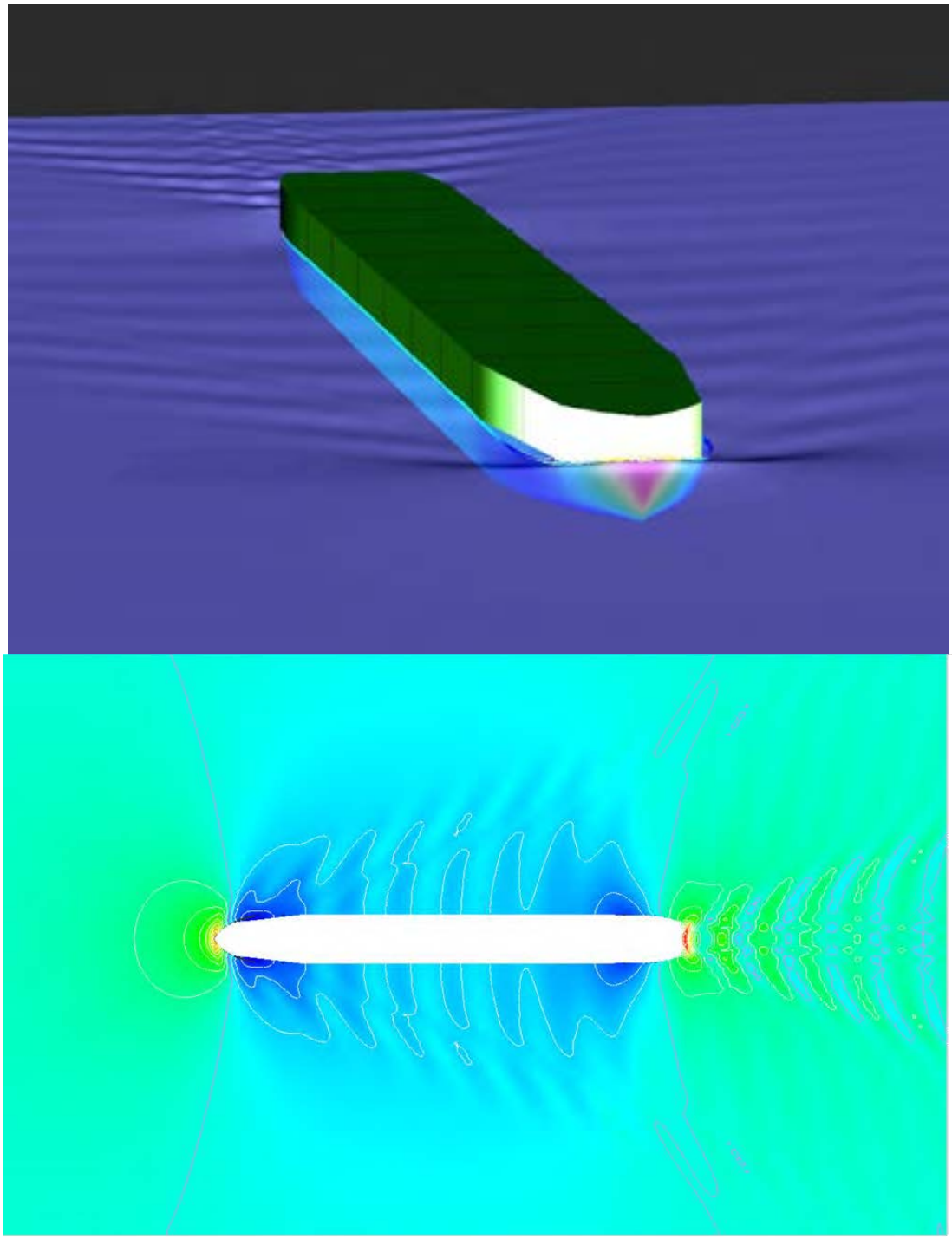

Figure 7. Wave pattern approached by RAPID.

The wave pattern produced by the ship shows a moderate wave height. A small transverse wave system is present. For this water depth and speed this could be improved slightly, however the calculation results at a water depth of 4.5 m show a reduction in the transverse wave system. Therefore due to the changing water depths, there is no reason to modify the bow. The transom also generates some waves, however compared to other calculation of wave patterns of inland vessels the Carpe Diem perform rather well.

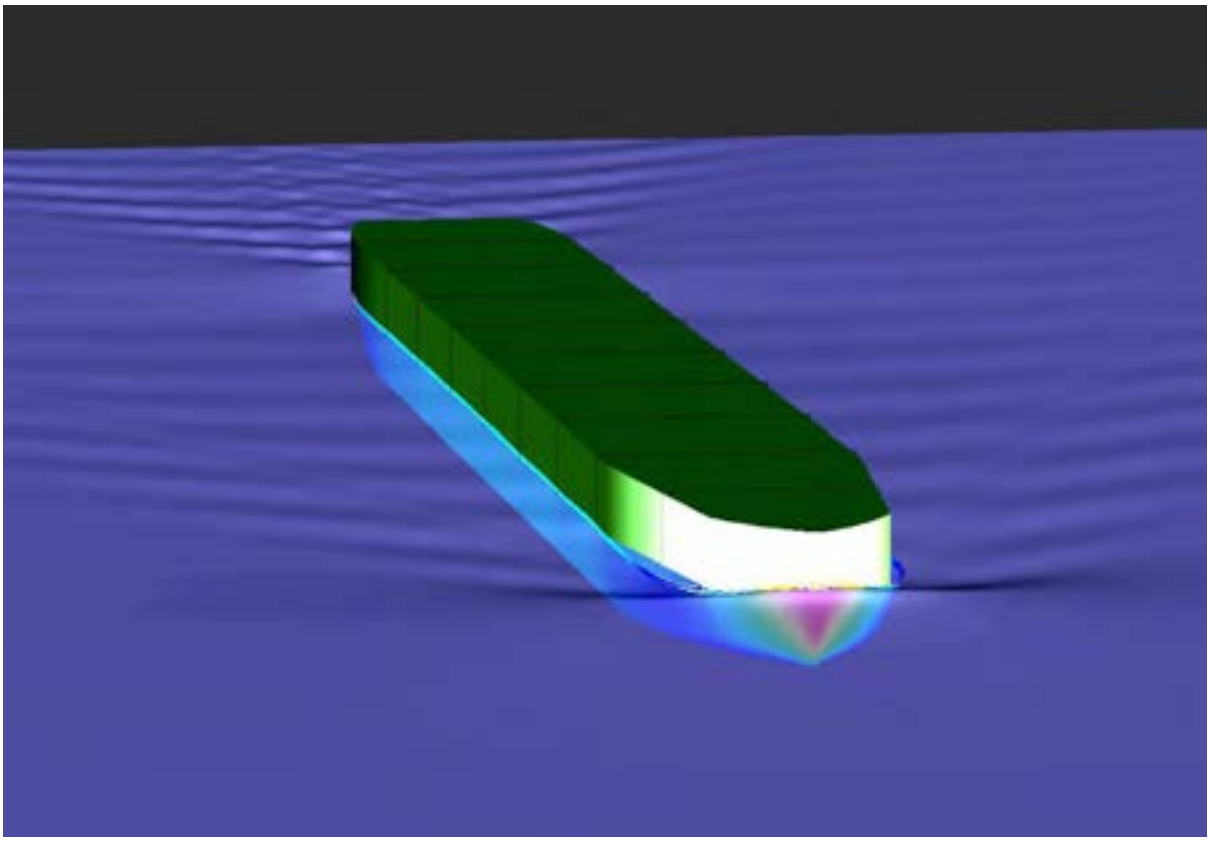

The pressure distribution on the fore hull calculated is shown in Figure 8. The low pressure area (most blue area in Figure 8) is considered to be very low and it should be avoid if possible. This peak is due to the sharp corner of the ship on that area. Moreover, when a ship is sailing in shallow water condition, the fluid under the ship is speeded up, and the low pressure peak increases.

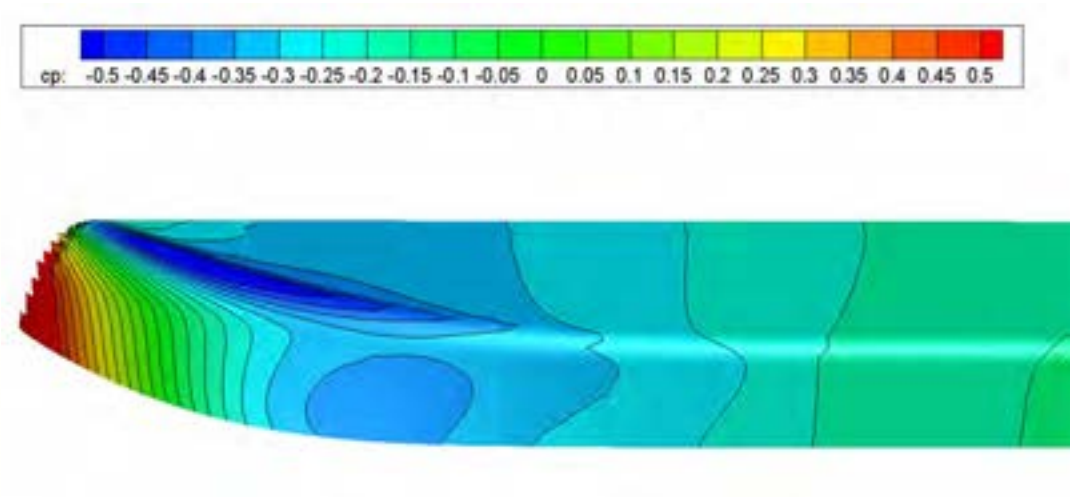

Figure 8. Pressure distribution on Fore part of the hull

4.2 Analysis ship without actuator disc

Figure 9 shows the pressure distribution on the aft hull. Most of the attention should be paid on the stern since is in this part where the viscous effect becomes important. The pressure on the aft part of the ship increases smoothly along the hull, and the hull forms seems good except for the gondolas.

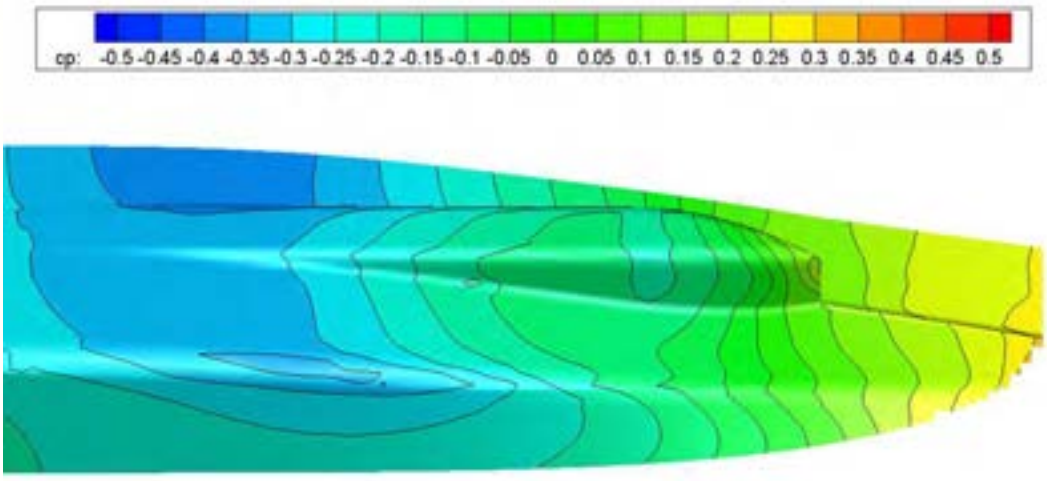

Figure 9. Pressure distribution on Aft part of the hull

Because the pressure distribution has a transverse gradient, the flow has a transverse component as well. In Figure 10 can be observed that the direction of the limiting streamlines on the gondola are slightly oriented inward.

The consequence is that the streamlines on the gondola are forced to detach it on the sharp corner (around 90 degrees). In Figure 11 the place where the streamlines detach the hull has been circled in red.

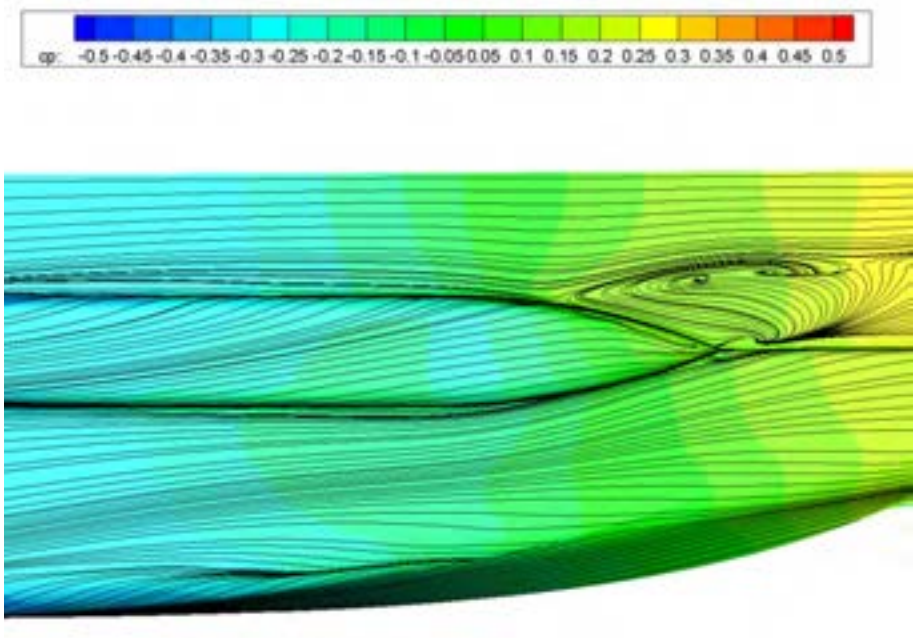

Figure 10. Limiting streamlines on the aft part of the hull.

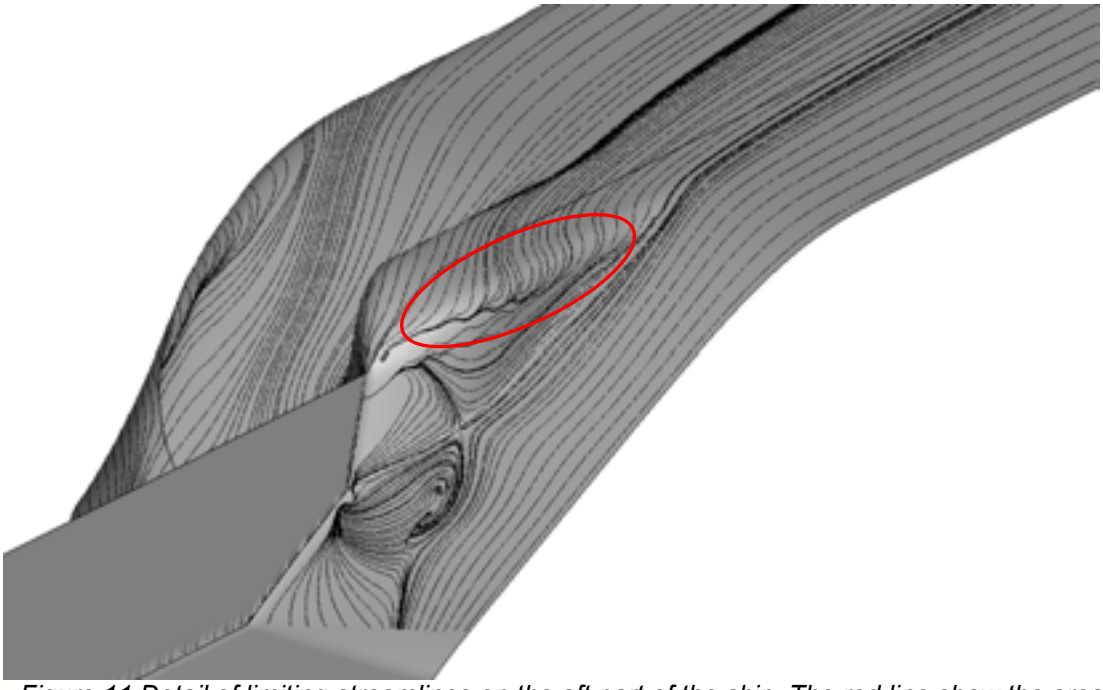

Figure 11.Detail of limiting streamlines on the aft part of the ship. The red line show the area where the streamlines are detached from the gondola and the flow separation appears.

As a consequence of this sharp corner, a big flow separation volume appears in the inner part of the gondola. It has been represented as a black surface in Figure 12.

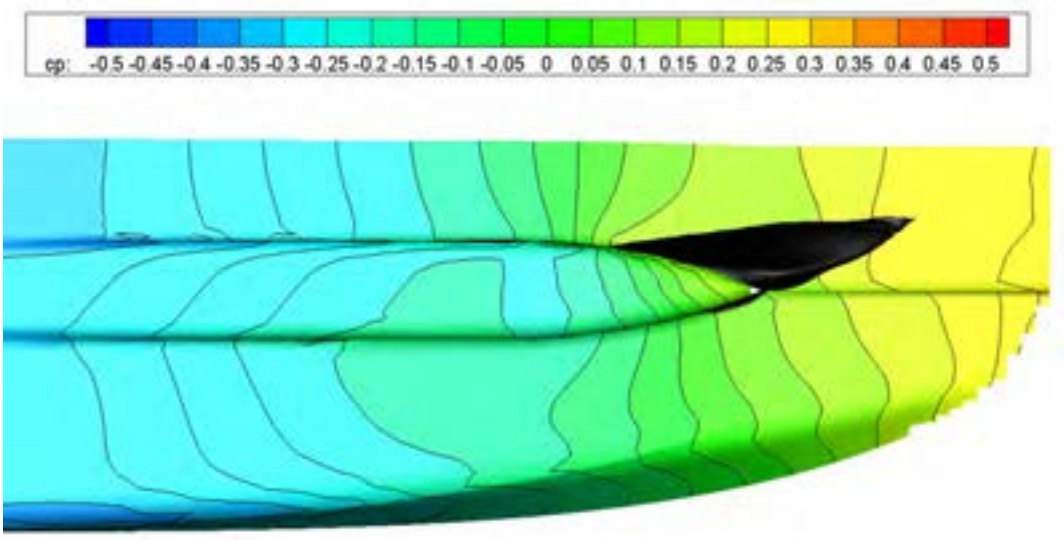

Figure 12. Pressure distribution on the aft part of the hull with flow separation area represented in back.

This flow separation area communicates with the outer part of the gondola and a small flow separation volume appear around there (Figure 13).

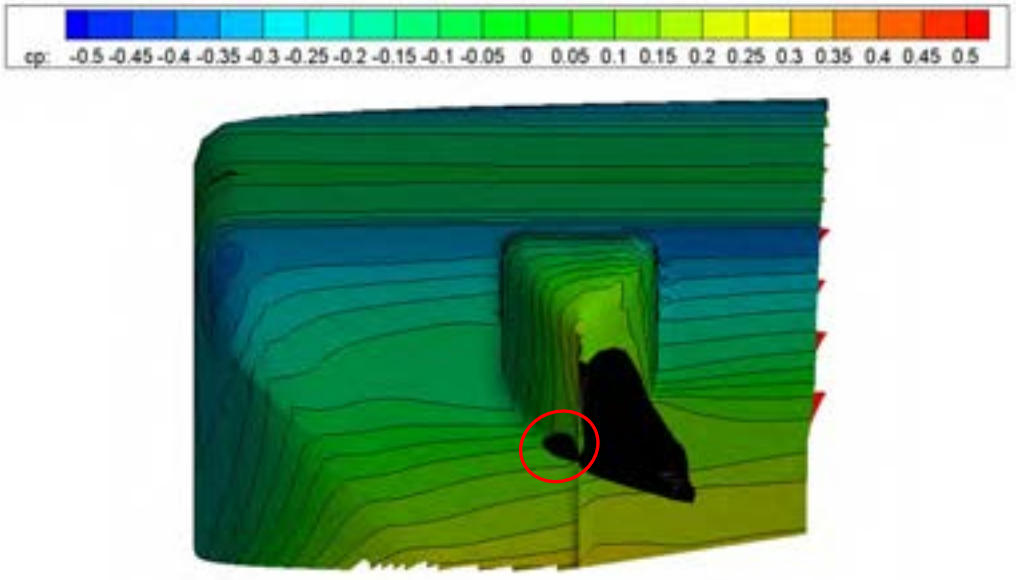

Figure 13. Flow separation behind the gondola. The big volume of flow separation inward is creating a small flow separation area outward.

The alignment of the tunnels with the limiting streamlines is shown in Figure 14.

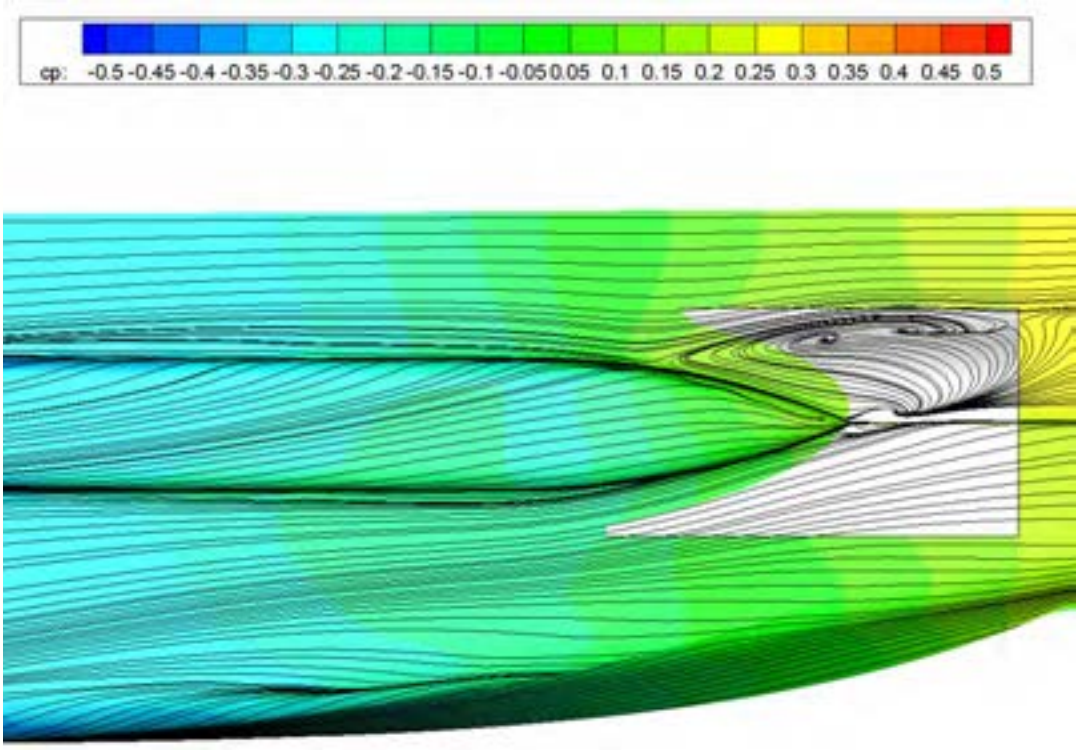

Figure 14. Alignment of the tunnels with limiting streamlines.

The flow at the location of the propellers and tunnels is totally influenced by the presence of the gondolas. The nominal flow distribution is shown in Figure 15, where the black area represent the flow separation area. The small distance between the end of the gondola and the propeller position reduce the amount of water flowing through the propellers.

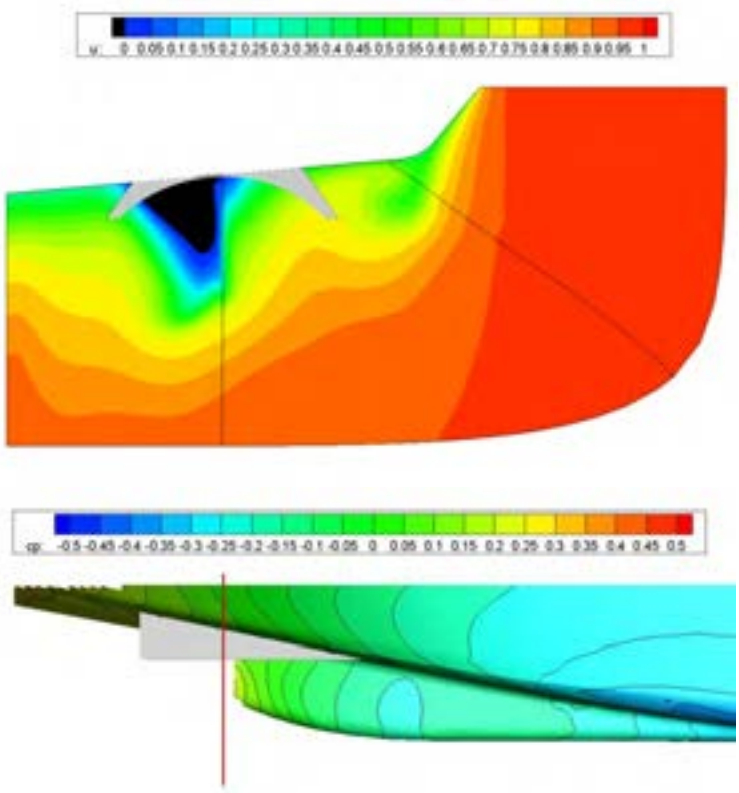

Figure 15. Ux distribution of the flow at a plane just behind the ship. Tunnel has been included (grey area). Down picture represents the location of the plane.

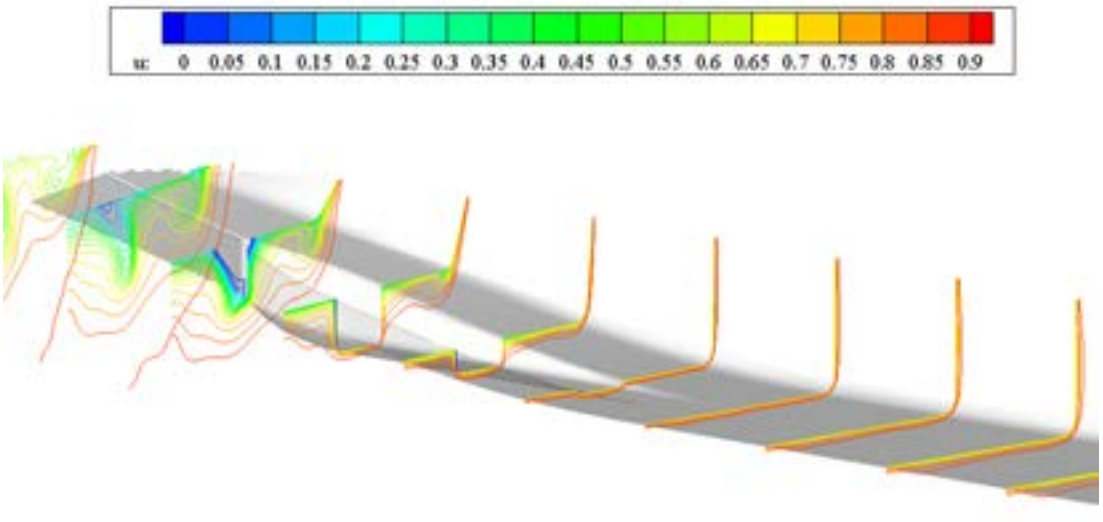

Figure 16. Axial velocity field at several streamwise planes at the aftbody.

4.3 Analysis of the influence of the actuator disc on the ship

Up till now the calculations have been performed without the effect of an propeller. Therefore an actuator disc is applied in the calculation. With an actuator disc the axial force of the propeller is modeled in the calculation. The fore part of the ship is not influenced by the presence of the actuator disc. Therefore, the main differences with the nominal solution are found at the stern of the ship.

The thrust coefficient of the actuator disc has a value of 2.0. This is a rather high value and big differences with respect the nominal solution are expected.

Figure 17 shows the differences in the pressure distribution between the ship with and without actuator disc. The presence of this actuator speeds up the fluid towards the propeller plane, and as a consequence of it the pressure isolines (both forwards and aft ward of the propeller) are stretched towards it. The transverse gradient of the pressure distribution remains also in this case.

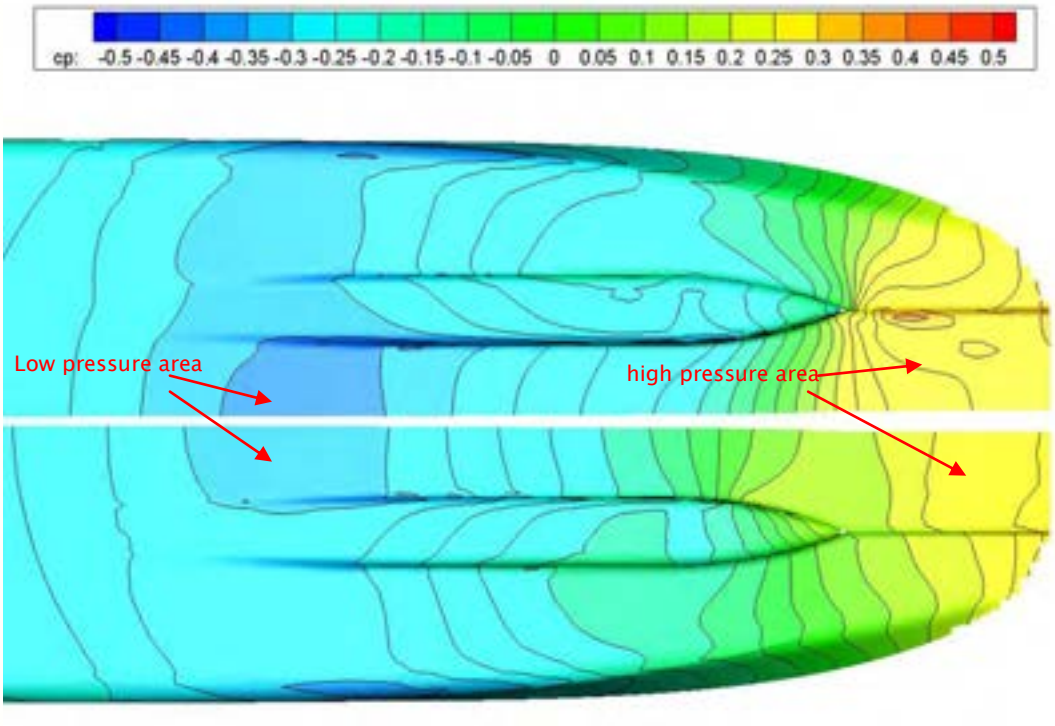

Figure 17. Pressure distribution on the hull. Above: Ship with actuator disc. Down: Ship without actuator disc.

The low pressure peak on the hull remains on the same area but has decreased a 10% with respect to the nominal solution due to the suction of the propeller. The high pressure area after the propeller has been moved backward towards the propeller. The average coefficient of the high pressure values behind the propeller has increased around 50% with respect to the nominal solution due to the propeller suction. These differences will have an impact on the resistance values.

The limiting streamlines of both ships are shown in Figure 18. In both cases this lines are slightly oriented inward as a consequence of the transverse pressure gradient. The flow separation area has significantly decreased (Figure 20) due to the suction effect of the actuator disc which stretches the streamlines toward it. However, the calculations have been performed modeling neither the tunnels nor the nozzles. Part of these structures are allocated where the flow separation is and a reduction of the flow separation is expected.

The change of direction of streamlines due to the actuator disc worsen the alignment of the flow with the tunnels.

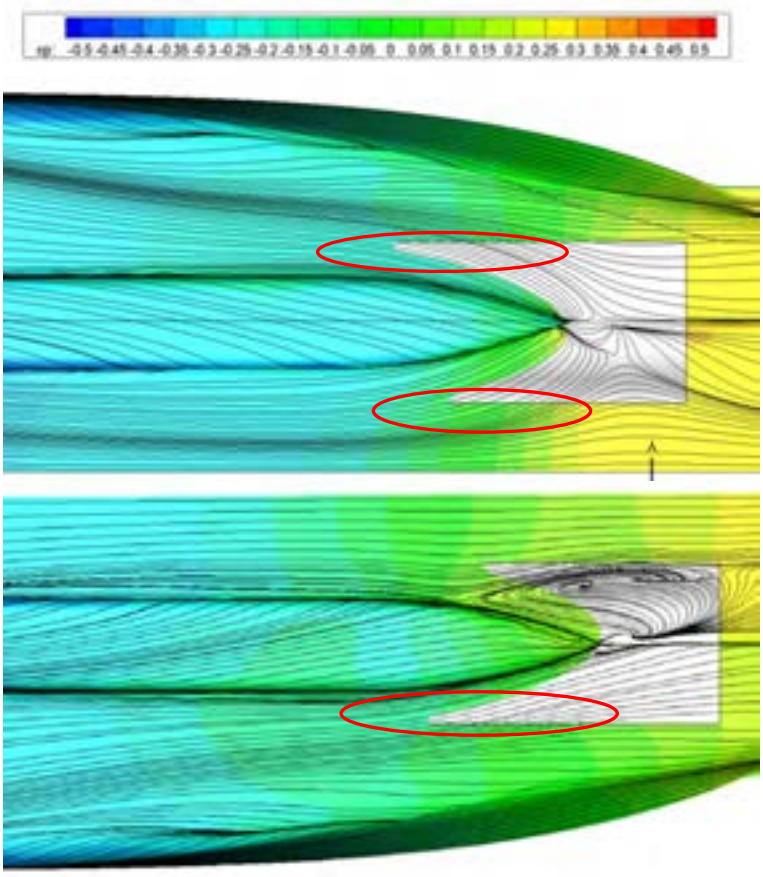

Figure 18. Limiting streamlines on the hull with the presence of the tunnel for both ships. Above: Ship with actuator disc. Down: Ship without actuator disc. Black areas represent flow separation.

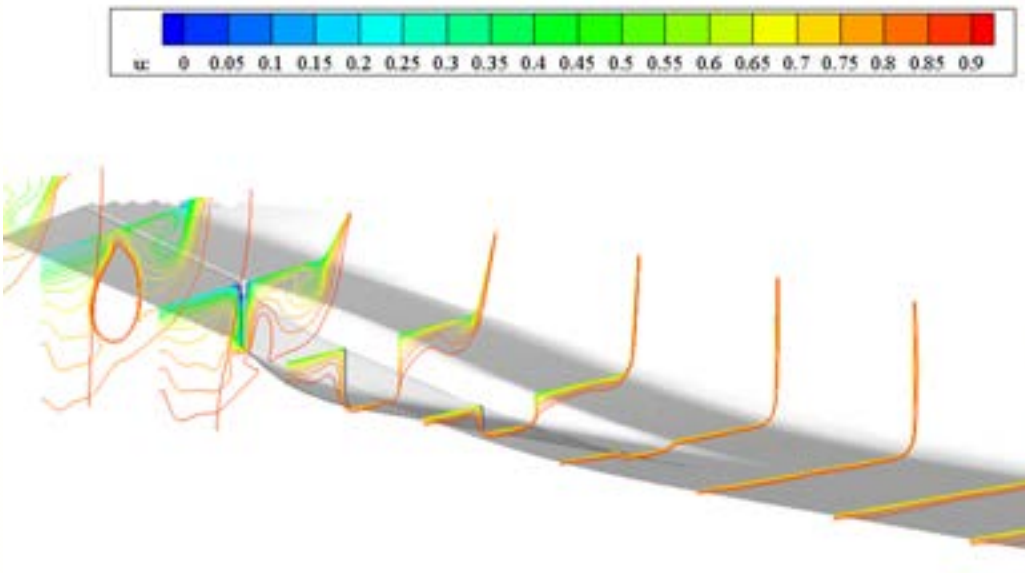

Figure 19. Axial velocity field at several streamwise planes at the aftbody.

Figure 21 shows the top view of the differences of the flow separation volume in the ship for both cases. It can be seen in Figure 21 that the flow separation of the ship with actuator disc is totally located above it. The tunnel and duct are allocated around this area and the flow separation volume is expected to reduce.

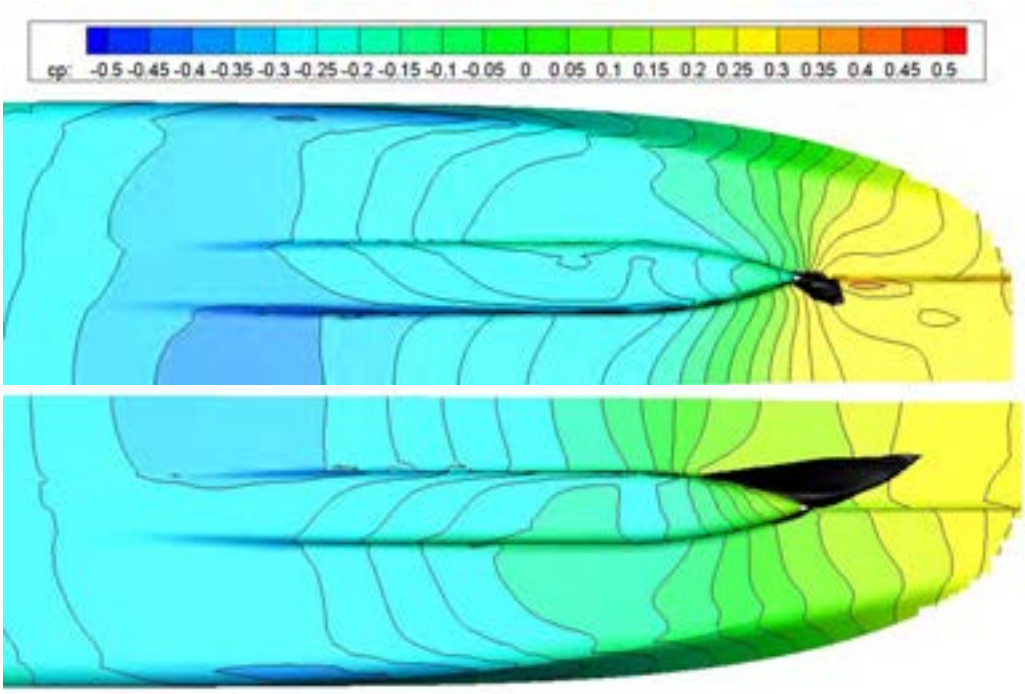

Figure 20. Pressure distribution on the aft part of the hull. Above: Ship with actuator disc. Down: Ship without actuator disc. Black areas represent flow separation.

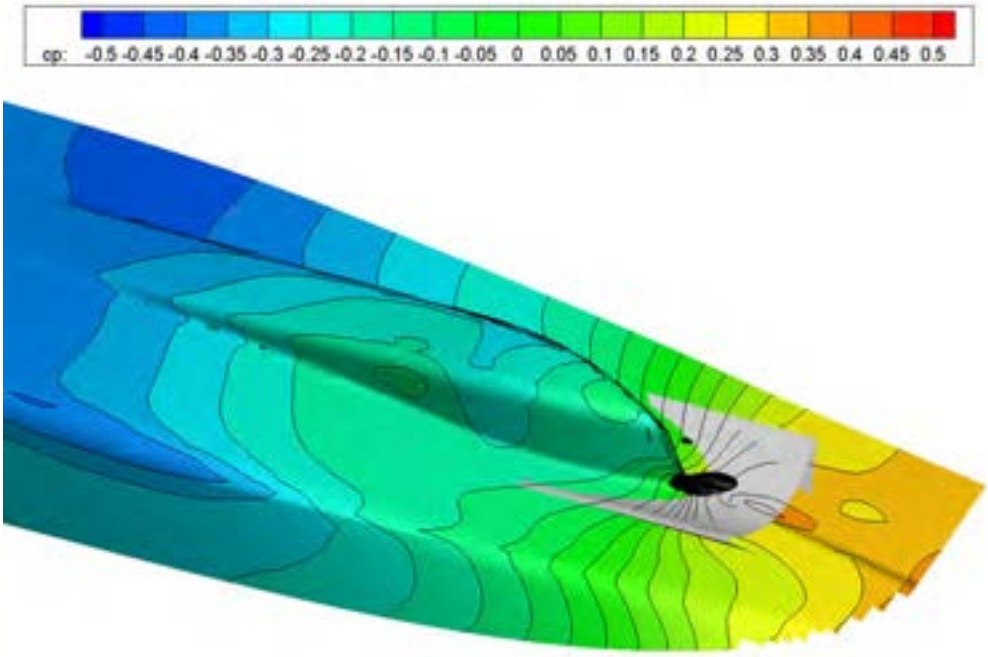

Figure 21. Representation of the flow separation area of the ship with actuator disc. The tunnel has been added in the figure, but is not taken into account in the calculation.

4.4 Resistance computation

An estimation of the resistance value has been performed. The presence of the flow separation complicates the resistance computation. However, these values are useful to compare the fluid behavior between both conditions.

The estimated thrust deduction factor is 0.28. The resistance results are gathered in Table 4.

Table 4. Resistance prediction by Parnassos.

Total resistance coef.	2.4177E-03
Form factor 1+k ITTC 1957	1.4052

Resistance [kN]	**36.91**

5 CONCLUSION

After the analysis of the ship Carpe Diem, the followings recommendation are stated:

- The wave generated by the ship is good compared to that of similar vessels, therefore no significant gain is expected after modifying the bow.
- The gondolas should be oriented slightly inward in order to be aligned with the fluid and avoid the flow separation.
- The size of the gondolas are considered big. A reduction of it length is recommended.
- An increase of the distance from the end of the gondola to the propeller plane is recommended in order to improve the wake field.
- Smooth the end of gondola.

Based on this study, MARIN has proposed a hull modification of the ship Carpe Diem. Since the ship is already built, the modification proposed tries to has a small impact on the design. The main differences between the proposed and current ship is shown in the Figure 22.

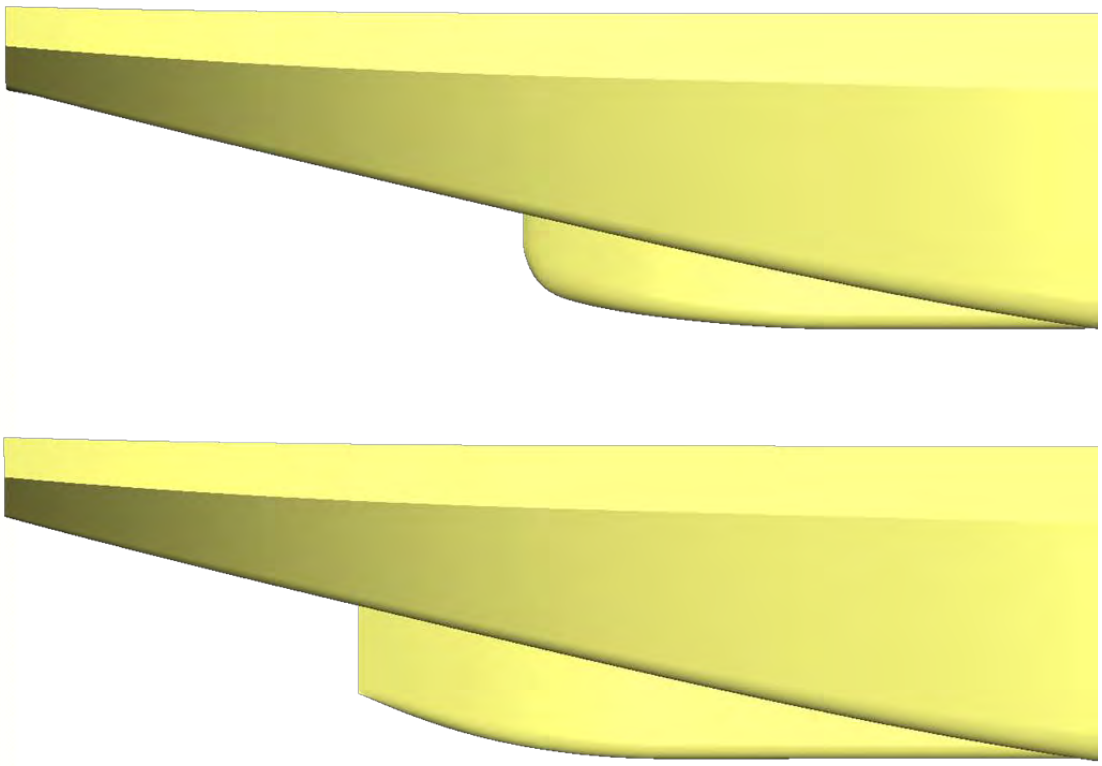

Figure 22. Side view of ship. Above: New hull lines proposed by MARIN. Below: Original hull lines.

A CFD calculation for the new ship hasn't been performed at the moment of writing this report, and it is a material out of this report.

SECTION 2:
CFD ANALYSIS HERSO-I

Written by : MARIN – Dr. Ir. C. Veldhuis

TABLE OF CONTENTS

1 INTRODUCTION

In WP1 full scale measurements have been performed on board the Herso-I. These full scale measurement showed the ship is performing below average when comparing with the benchmark. Therefore in WP2 possible retrofit measures for the Herso-I are investigated, to determine reduction in fuel consumption.

During the full scale trials Herso-I was sailing without a barge in front. However in normal operation the vessel is sailing with the barge Leonie-SL. In a discussion with the shipowner it was decided to investigate the effect of smoothened transition between pusher and barge (trapeze).

Therefore the flow around the pusher-barge combination Herso-I-Leonie SL has been investigated with MARIN's viscous flow code PARNASSOS. PARNASSOS was selected because it is an efficient tool to calculate viscous flow phenomena and has been validated against model tests and full-scale results. The main objective was to determine the viscous flow and resistance for the combination without and with the trapeze.

2 PARTICULARS OF THE SHIP

At the start of the CFD calculations no hull lines were available. Hull lines of a sistership were found and used as input for the CFD calculations. The hull lines (Figure 1) used for the CFD are based on the following drawing:

Hull lines sistership HERSO.jpg	"DE MERWEDE" Bouw No. 562-563

The aftbody of the hull lines in the CFD calculations deviate from the actual ship shown in Figure 2. Further the hull lines used for the CFD calculations and the vessel are very similar. For the investigation of the effect of a Trapeze this has no significant influence.

The main particulars of the ship Herso-I are:

Description	Symbol	Original Hull	Unit
Length between perpendiculars	L_{pp}	84.95	m
Breadth at still waterline (moulded)	B	9.50	m
Moulded draught moulded on FP	T_F	2.1	m
Moulded draught moulded on AP	T_A	2.1	m
Displacement volume moulded	Δ	1426.2	m^3
Wetted surface	S_{TOT}	1024.3	m^2
LCB position forward ½ Lpp	LCB	40.93	%
Block coefficient	Cb	0.842	-

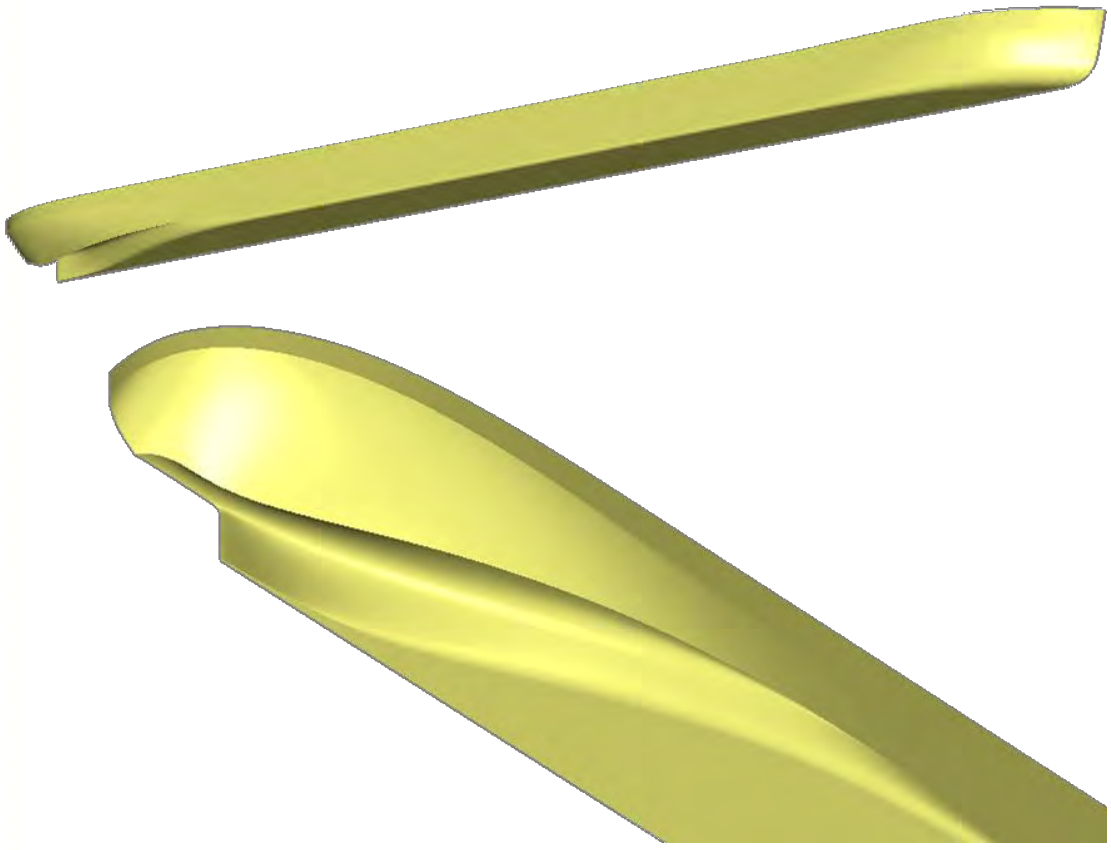

Figure 1: Ship (Herso-I): Total ship and zoom on tunnel in the aft ship

Figure 2: Ship (Herso-I): Entire ship and aft ship arrangement

For the barge Leonie-SL no hull lines were available, therefore based on pictures and the main dimension, the hull lines of the barge were developed at MARIN.

The main particulars of the barge are:

Description	Symbol	Original Hull	Unit
Length between perpendiculars	L_{pp}	70.75	m
Breadth at still waterline (moulded)	B	10.44	m
Moulded draught moulded on FP	T_F	1.9	m
Moulded draught moulded on AP	T_A	1.9	m
Displacement volume moulded	Δ	1251.6	m^3
Wetted surface	S_{TOT}	914.9	m^2
LCB position forward ½ Lpp	LCB	39.155	%
Block coefficient	Cb	0.892	-

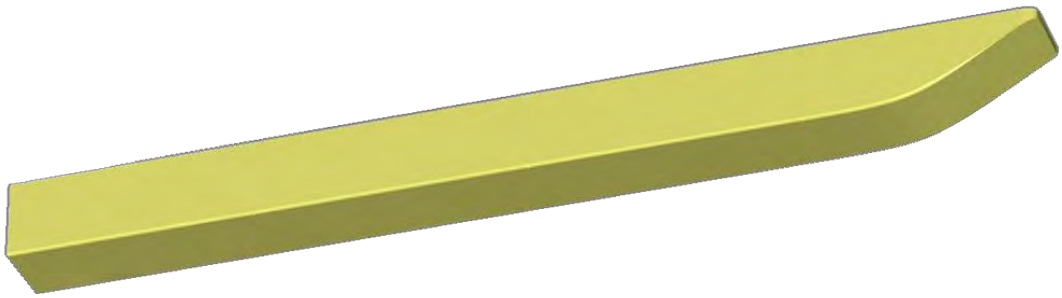

Figure 3: Barge (Leonie SL)

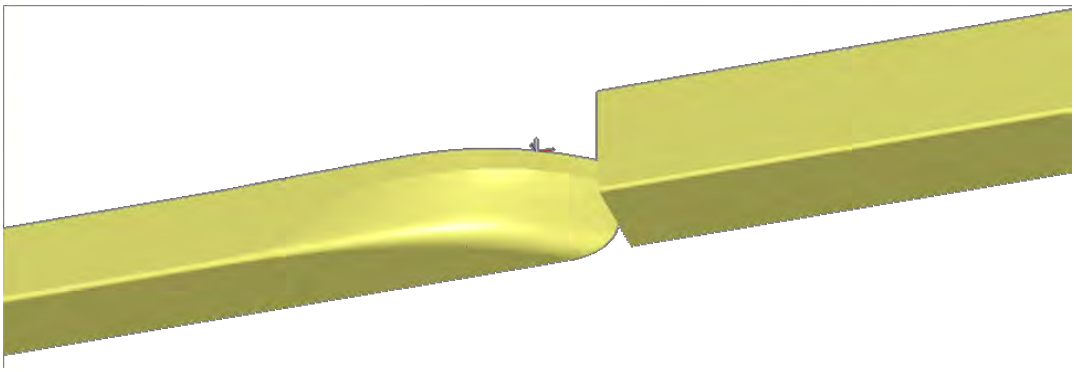

Figure 4: Pusher (Herso-I) and barge (Leonie SL)

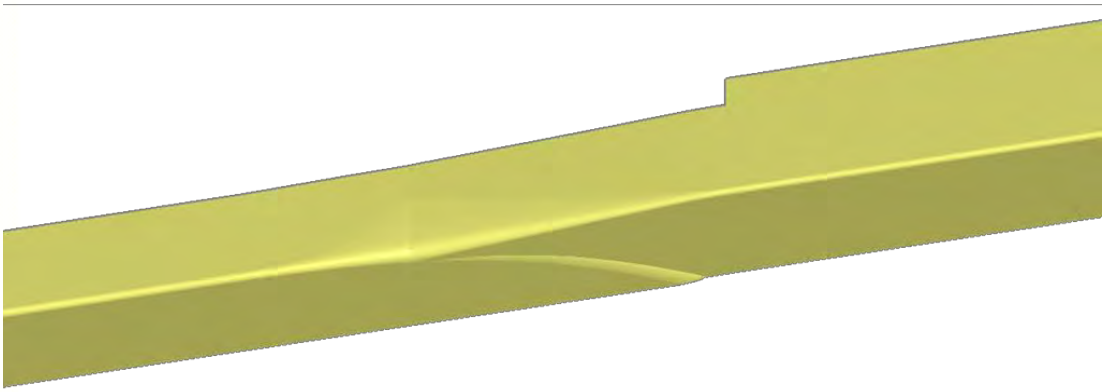

Figure 5: Pusher (Herso-I) and barge (Leonie SL) with smoothened transition

3 REVIEW OF THE CALCULATIONS

Three calculations have been performed:

1. The pusher (Herso-I) without barge (Leonie SL)
2. The pusher (Herso-I) with barge (Leonie SL)
3. The pusher (Herso-I) with barge (Leonie SL), with smoothened transition

A sailing condition was selected based on the measurements performed in WP1. The speed trials conditions at Komarom, Hungary were selected for the CFD calculations. The width at that location is large enough to eliminate canal effects.

The following sailing conditions were used for these calculations:

Ship speed	15	km/h
Water depth	4.6*)	m
Scale	full	m
Trim	0.0	deg
Sinkage	0.0	

*) During the calculations the bottom was not modeled because previous calculations showed that the bottom effects are negligible for a Wd/T-ratio of 2.14.

A calculation domain with a flat free surface (Double Body approach) with the following characteristics was made:

Inflow (distance in front of bow of barge)	85m
Left Exterior	85m
Bottom	Deep, 85m
Outflow (distance behind transom of pusher)	160m
Type of Grid	Structured multi blocks
Number of Grid Cells	Around 5.4 millions
Number of hull surface elements	Around 21 000

The level of convergence for the calculations is well below $1x10^{-4}$ for all residuals, except in regions with flow separation where the convergence level reached $1x10^{-3}$. A maximum y+-value[1] of 0.5 was reached.

[1] The y+ value is a non-dimensional parameter for the location inside a turbulent flow boundary layer. An y+ value of around 1 means the first cell height of the grid is well within the sublayer of the (fully turbulent) boundary layer.

4 PRESENTATION AND DISCUSSION OF THE RESULTS

The results for the three calculations are presented by comparing several aspect of the 3D flow. The results will be presented in three steps: flow at the bow of the barge, the transition area, and the stern of the pusher.

4.1 Flow at the bow of the barge

The pressure distribution on the bow of the barge is shown in Figure 6. The transition from bow to bottom is smooth and shows rather modest under pressures. The transition from the bow to the side is rather sharp due to the pram shape. This low pressure region causes cross-flow in the boundary layer which results in a longitudinal vortex running along the barge (see Figure 7).

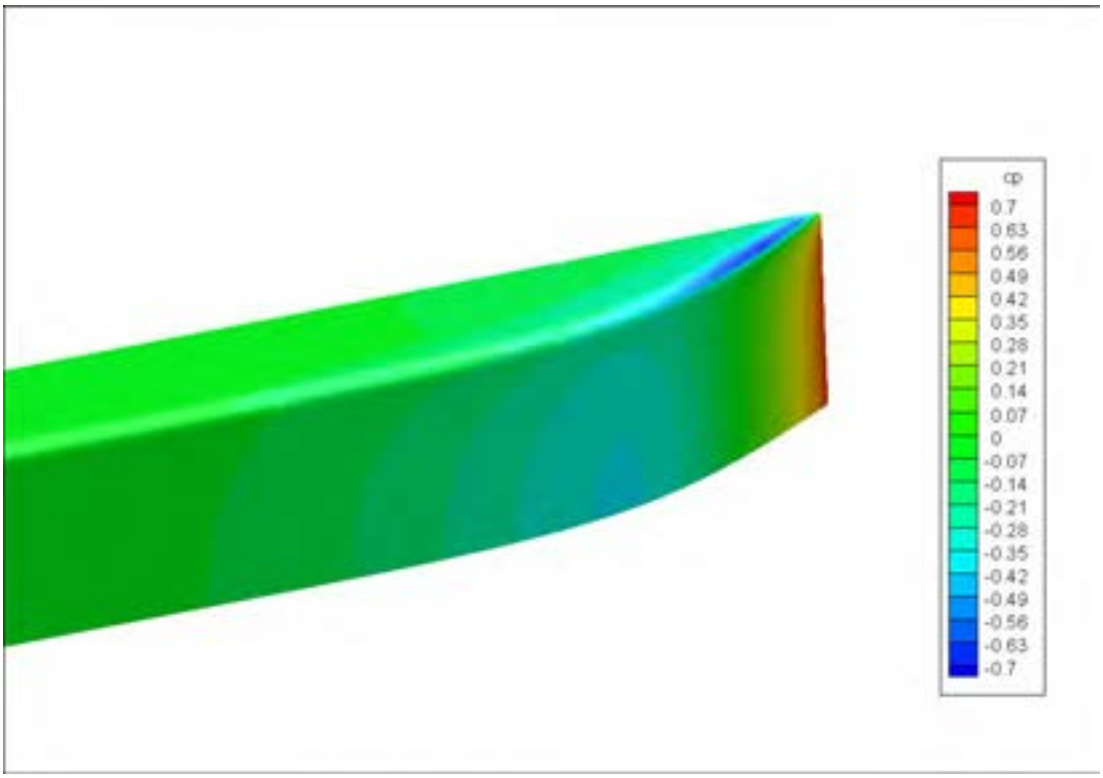

Figure 6: Pressure distribution on hull of the barge

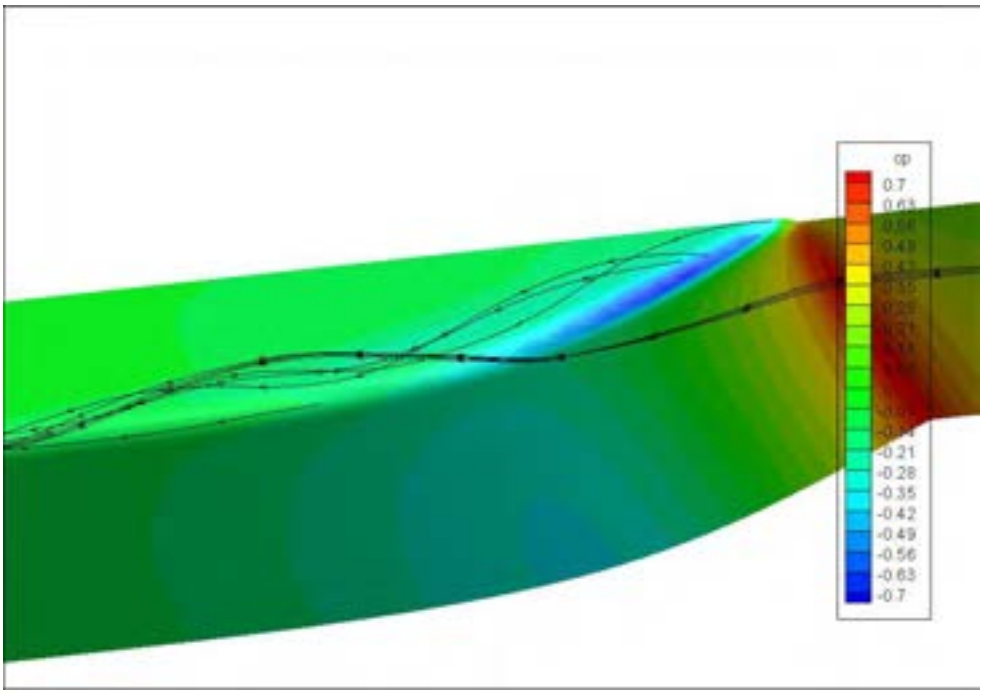

Figure 7:Pressure distribution on hull of barge and streamtraces

The vortex originating at the bow of the barge runs all the way up to the transom (see Figure 8). If changes to the hull of the barge are allowed a more gentle transition from bow to side is preferred. Of course this depends on the internal arrangement of the barge and constructional restrictions.

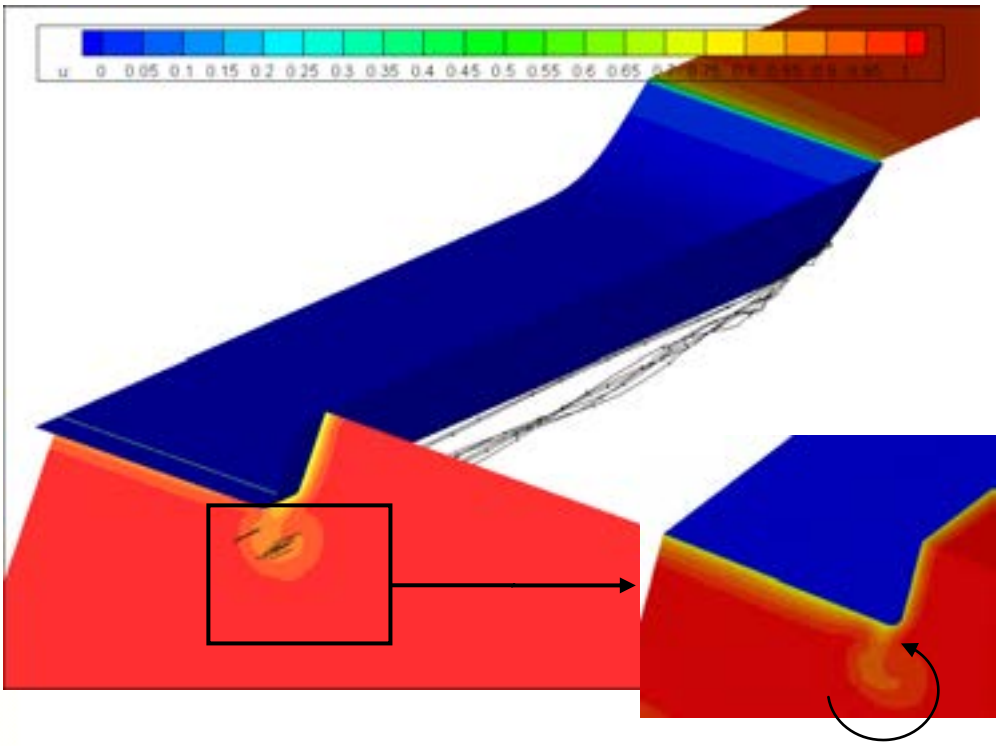

Figure 8: Axial velocity just before transom of barge and streamtraces and detail and arrow indication longitudinal vortex

4.2 Flow at the transition area

Figure 9 shows the pressure distribution on the hull at the transom of the barge and the bow of the pusher. The flow along the barge runs in axial direction and no pressure gradients on the hull are observed. On the bow of the pusher the pressure gradients are also minor. Comparing these results to the case without barge (Figure 10) shows the impact of the barge in front of the pusher. The pusher without barge encounters the free-stream flow and a stagnation area (high pressure) will appear at the bow. With the barge in front this stagnation area vanishes.

The smoothened transition between barge and pusher shows a similar smooth pressure distribution (see Figure 11).

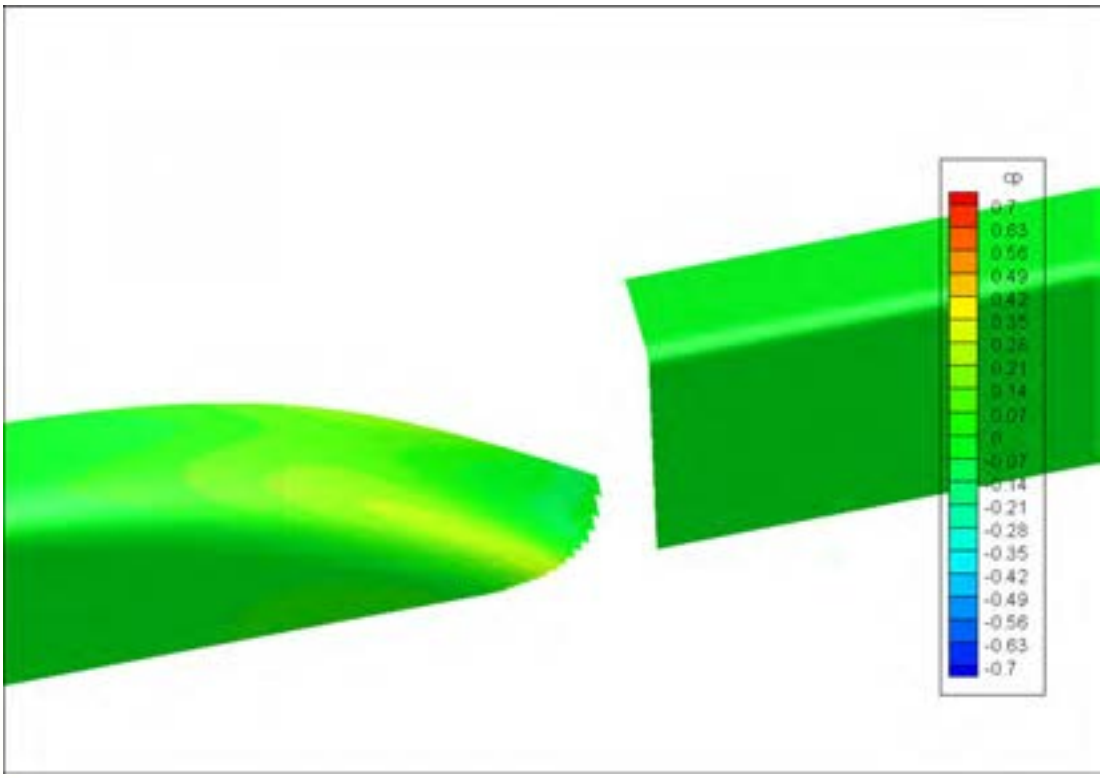

Figure 9: Pressure distribution on the hull:pusher+barge

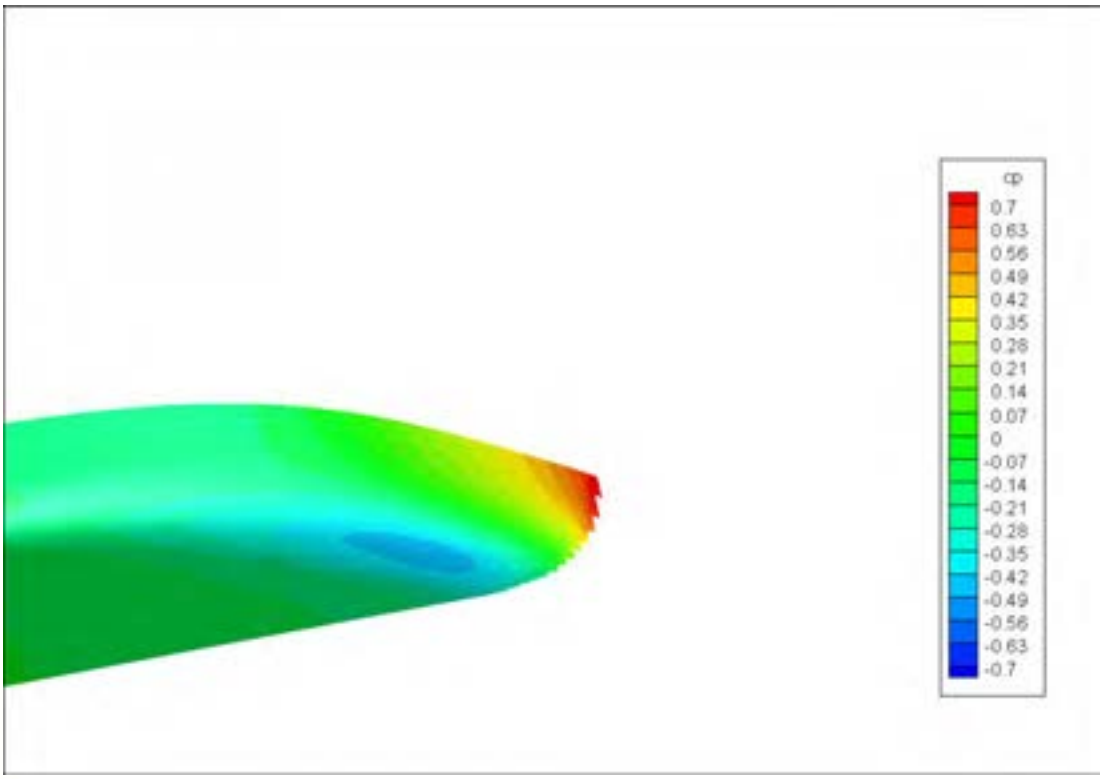

Figure 10: Pressure distribution on the hull: barge without pusher

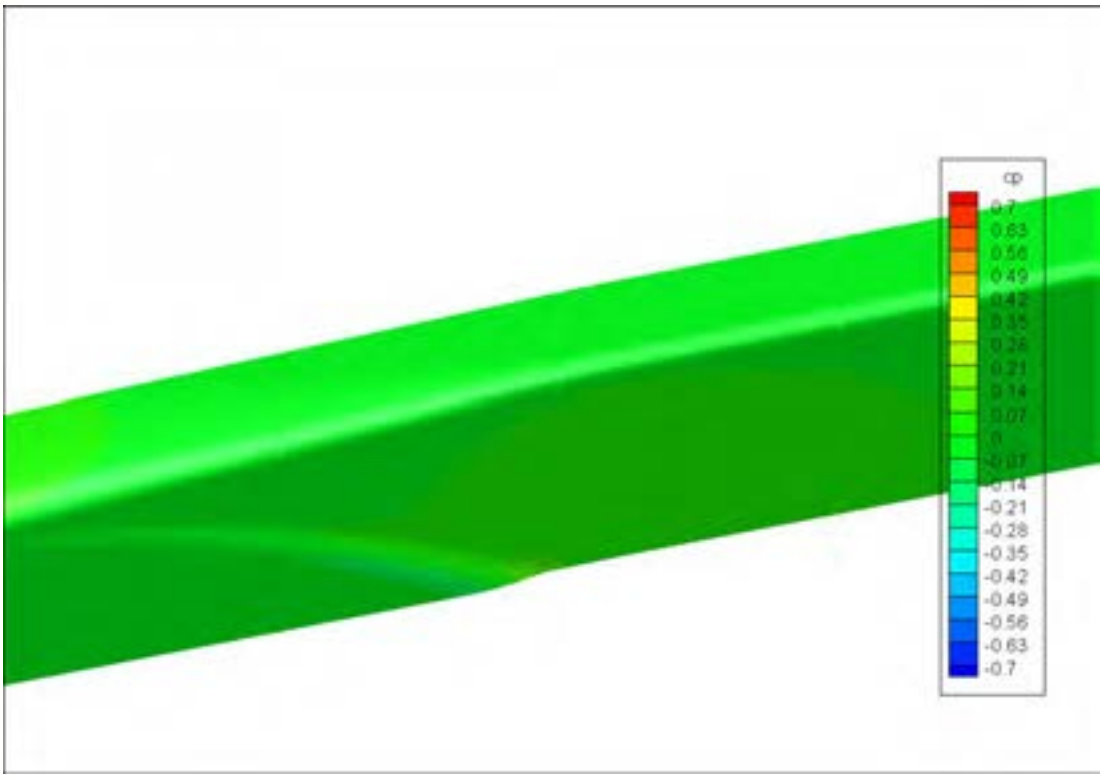

Figure 11: Pressure distribution on the hull: pusher and barge with smoothened transition

The flow aft of the transom of the barge can be visualized by means of streamline tracing. In order to do so, streamlines are released at the bow of the pusher close to the hull and outside the boundary layer in the free stream. The stream traces clearly show the dead water region behind the transom of the barge (Figure 12): the main flow will pass along this flow reversal area. Figure 13 shows the stream traces (released at the same location) for the case without barge in front. This is followed by Figure 14 for the case with the smoothened transition.

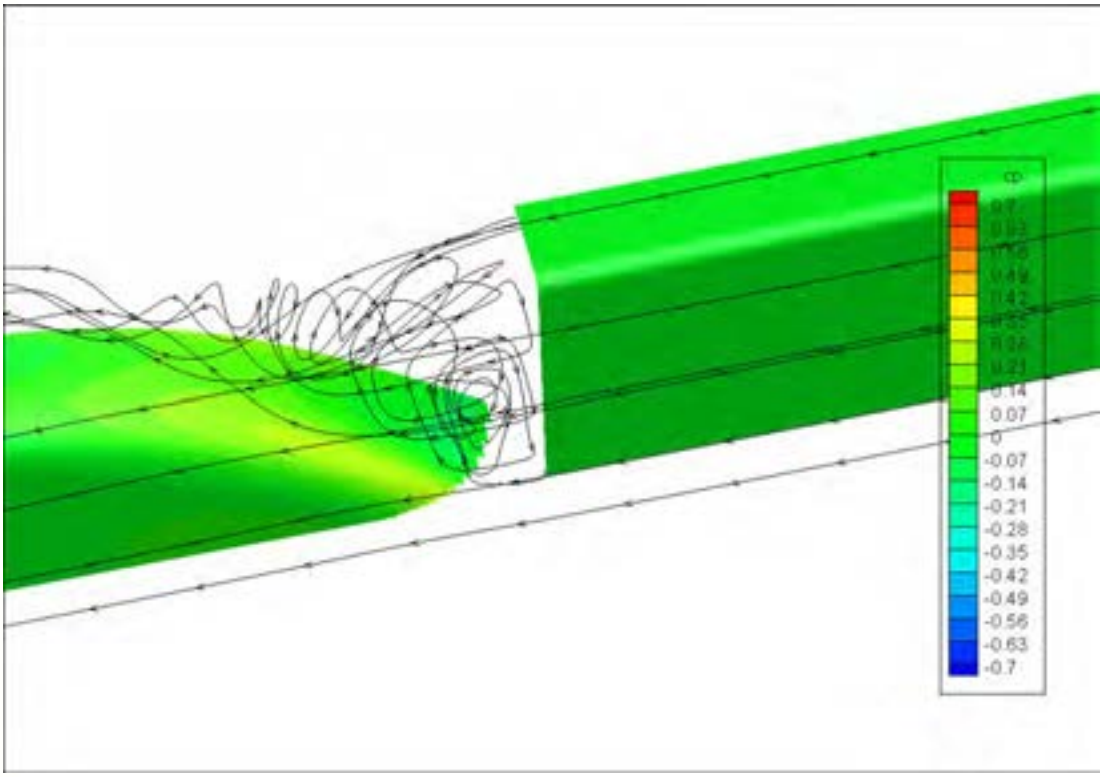

Figure 12: Pressure distribution on the hull and streamtraces: pusher and barge

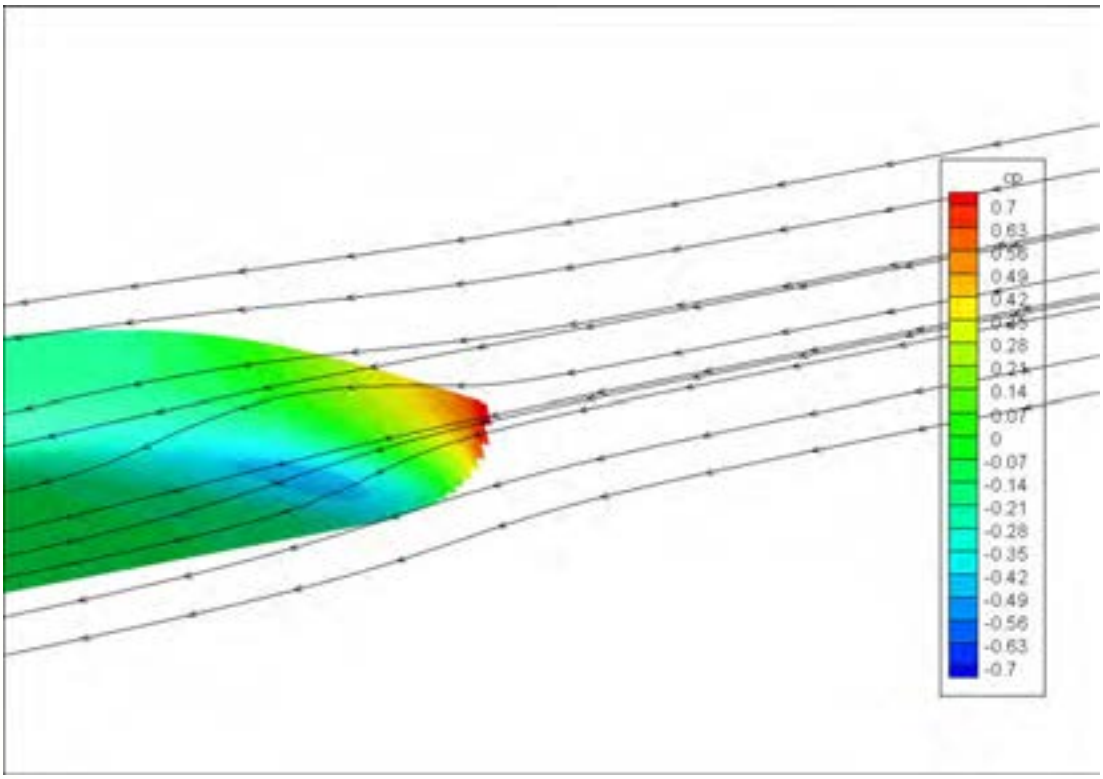

Figure 13: Pressure distribution on the hull and streamtraces: pusher without barge

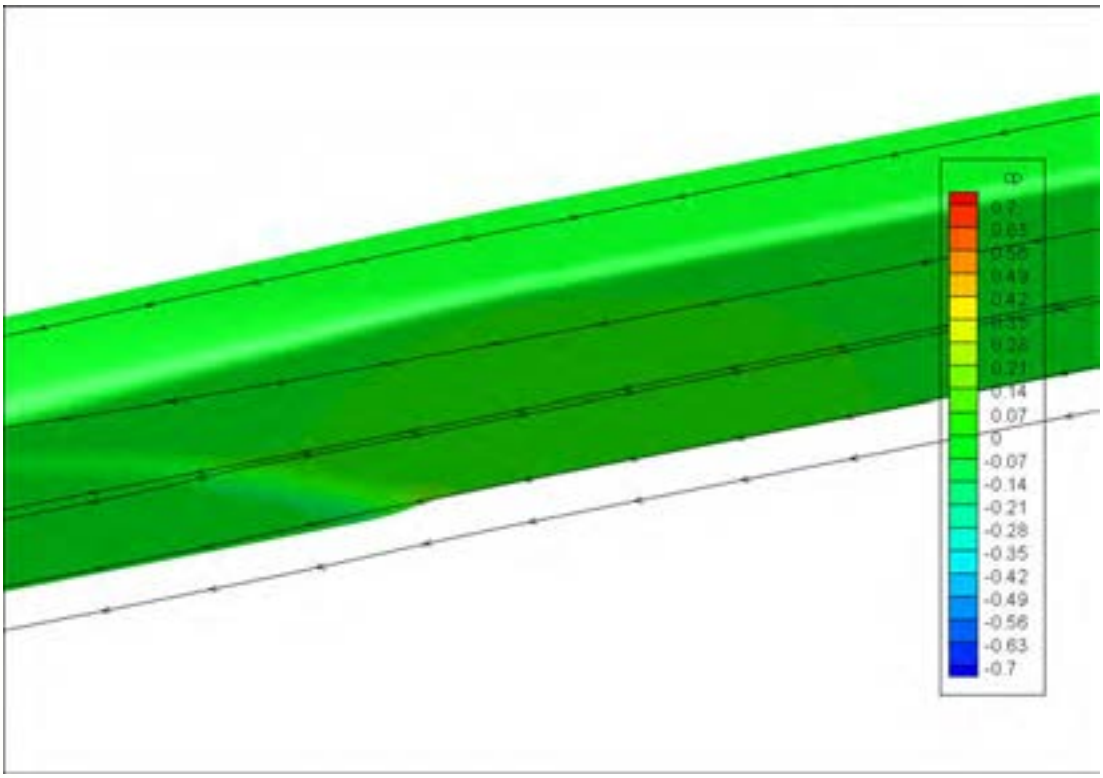

Figure 14: Pressure distribution on the hull and streamtraces: pusher and barge with smoothened transition

In the dead water region aft of the transom the velocities are very low and even negative. Figure 15 shows the area with negative axial velocity and some vortical flow originating from this area.
Figure 16 shows the axial velocity distribution on the flat free surface for the case with pusher and barge; the low velocity region is clearly visible. This low velocity area explains the smooth pressure distribution on the bow of the pusher with the barge in front: due to the barge the flow speed at the bow of the pusher is much lower. Therefore the pressure gradients on the bow of the pusher are much smoother compared to the case without barge in front.

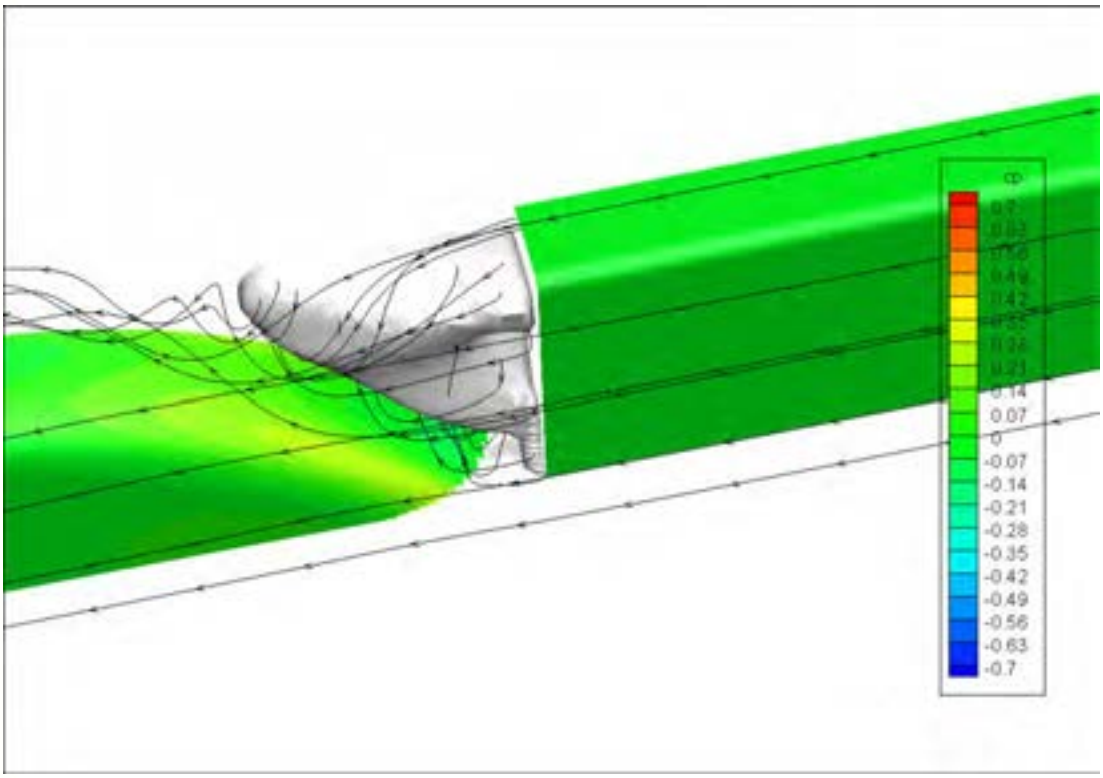

Figure 15: Pressure distribution on the hull, streamtraces, and flow reversal area in white/grey :pusher and barge

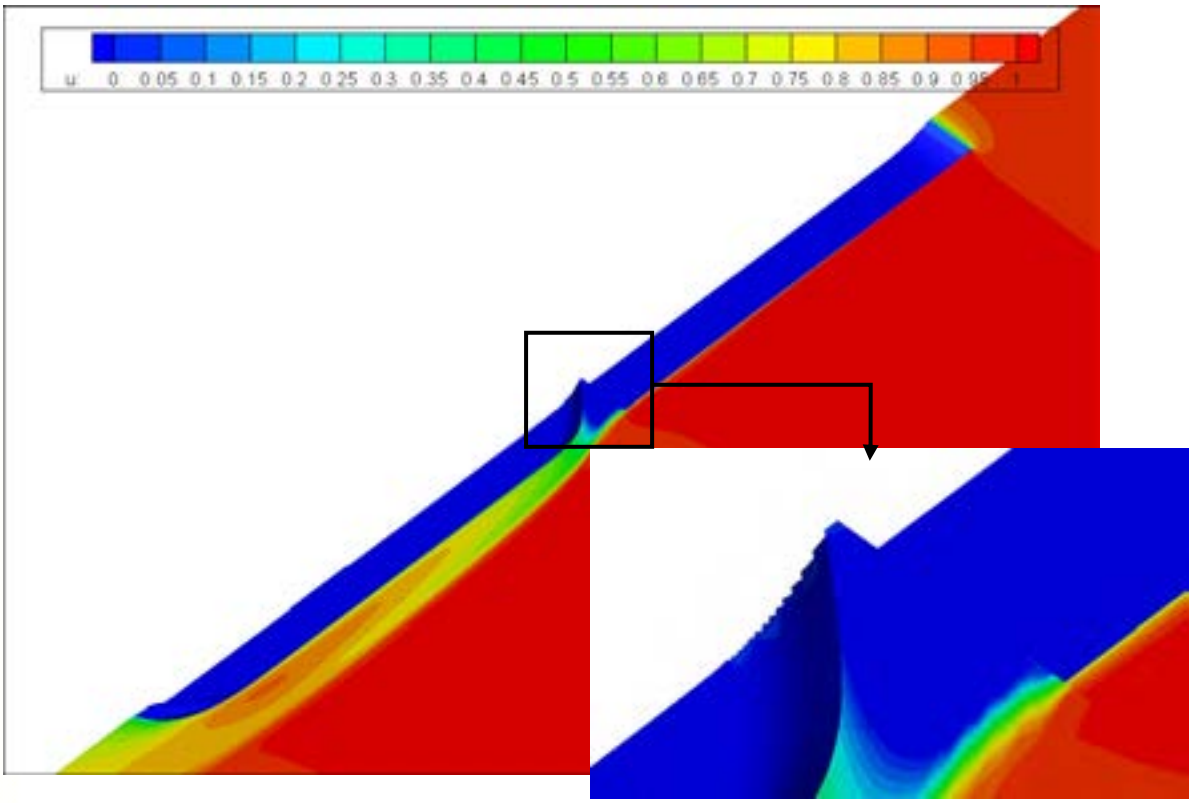

Figure 16:Axial velocity at water surface: pusher+barge with detail on flow at transom of the barge

Comparison of Figure 16 with Figure 18 and Figure 19 shows that the boundary layer along the pusher is rather thick due to the flow reversal behind the barge. The single pusher and the case with the smoothened transition show a much smoother velocity distribution and thinner boundary layer.

Figure 20 and figure Figure 21 show the comparison of the boundary layer of the original pusher-barge combination and the case with the smoothened transition. The thinner boundary layer is beneficial from resistance point of view; an indication for the resistance with and without smooth transition shows a resistance decrease of 20%.
The transition as calculated here might be impractical to built. A less drastic approach could be followed leading to less resistance decrease than indicated before. However, most of the resistance decrease is related to the removal of the flow reversal area. Hence, for a smooth transition to be effective at least this flow reversal should be dealt with. A possible solution could be a “notch”-type pusher-barge combination where the transom of the barge is changed (see Figure 17).

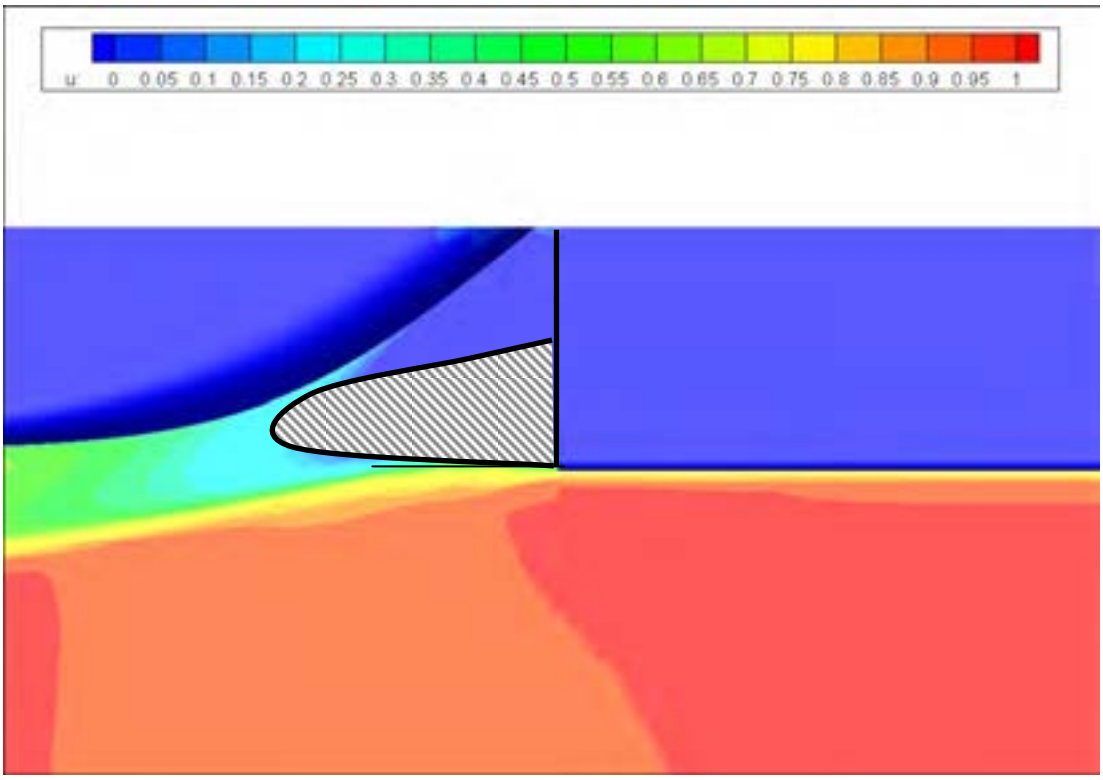

Figure 17:Topview on the axial velocity at water surface: pusher+barge with indication for a "notch"-type barge transom.

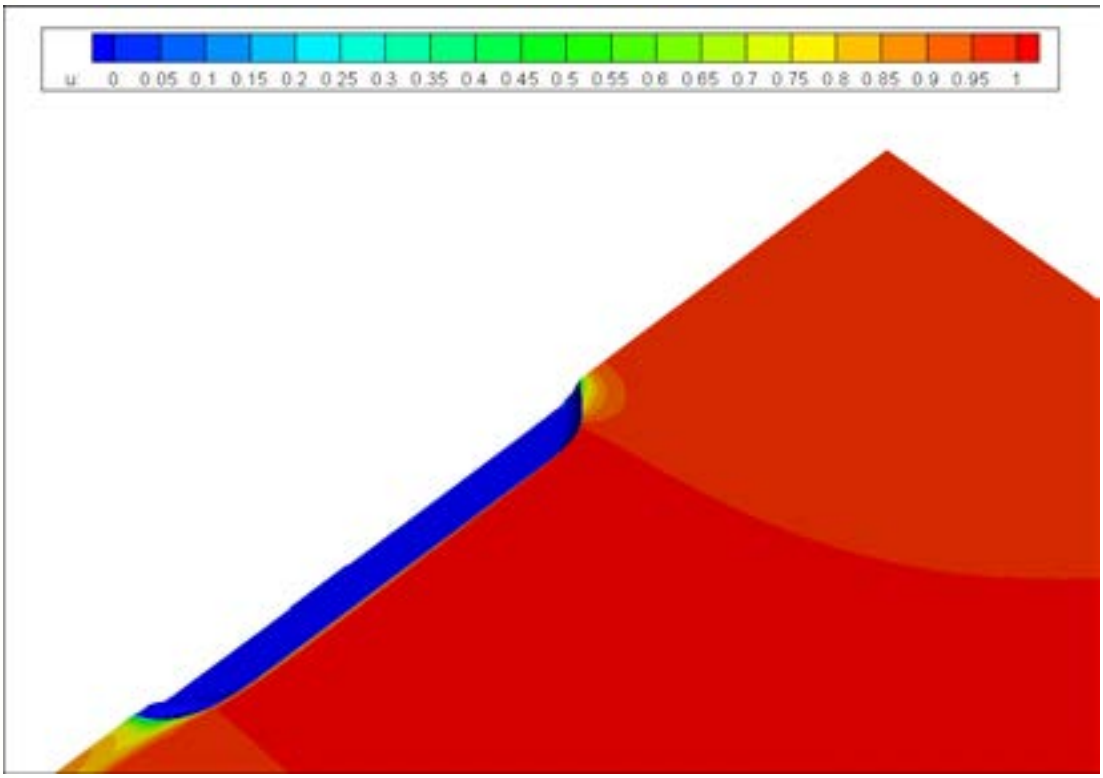

Figure 18:Axial velocity at water surface: pusher without barge

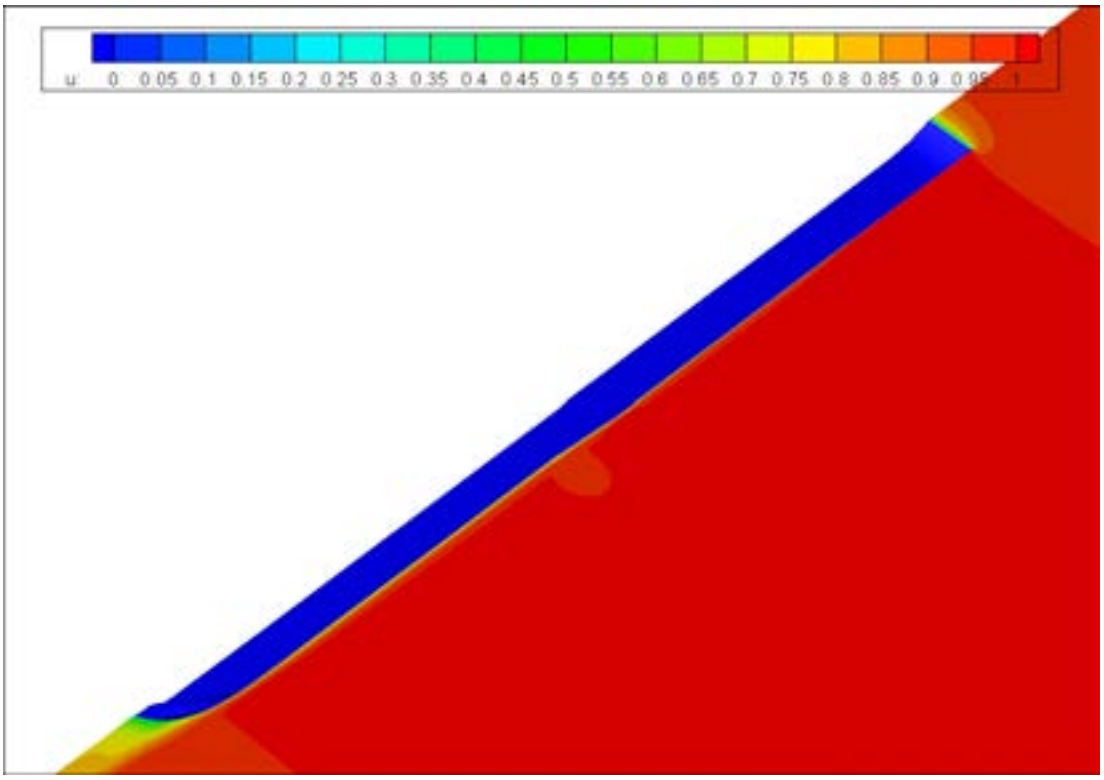

Figure 19:Axial velocity at water surface: pusher+barge with smoothened transition

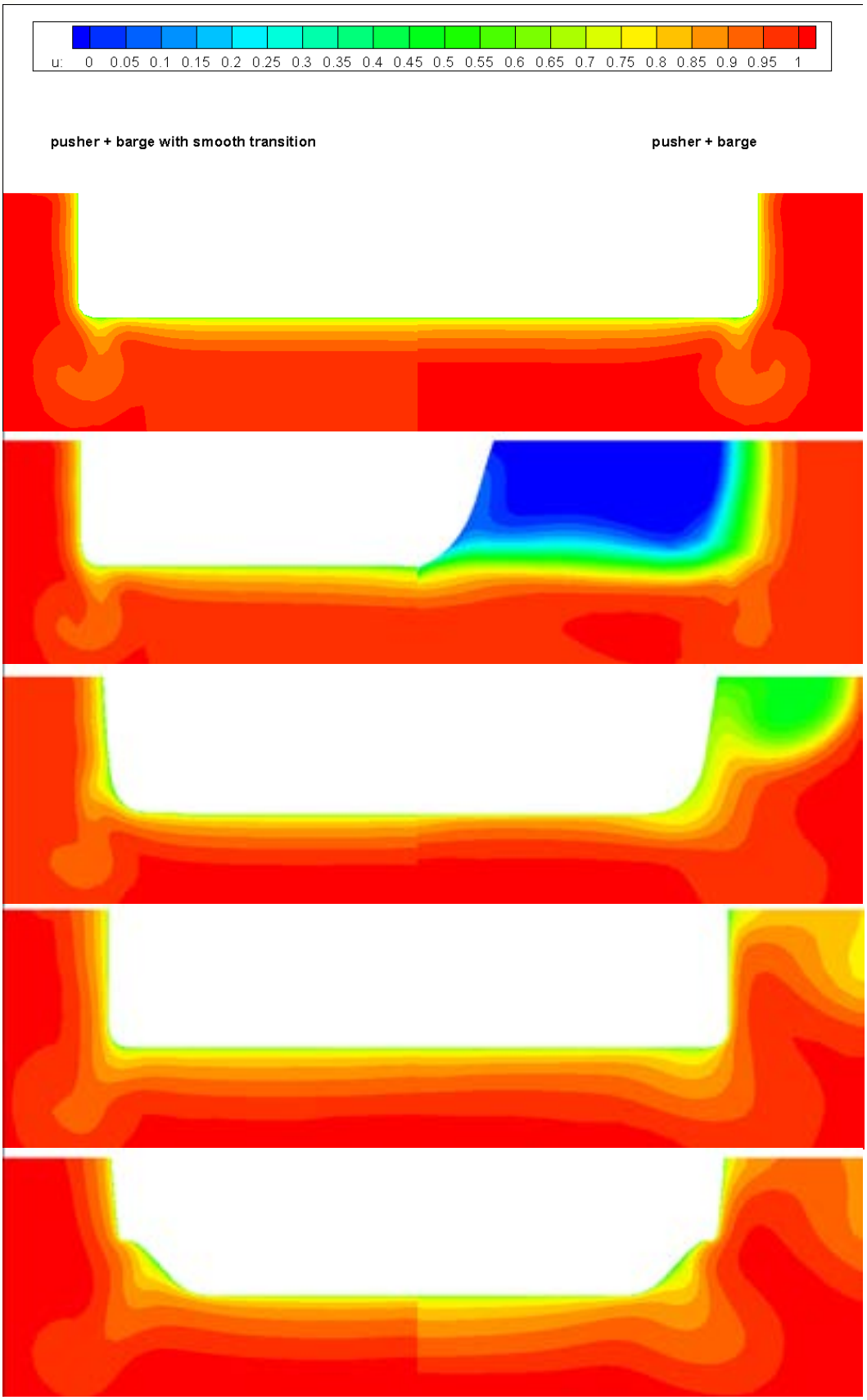

Figure 20:Axial velocity in slices from transom of barge to transom of pusher: Left: smooth transition, right: original.

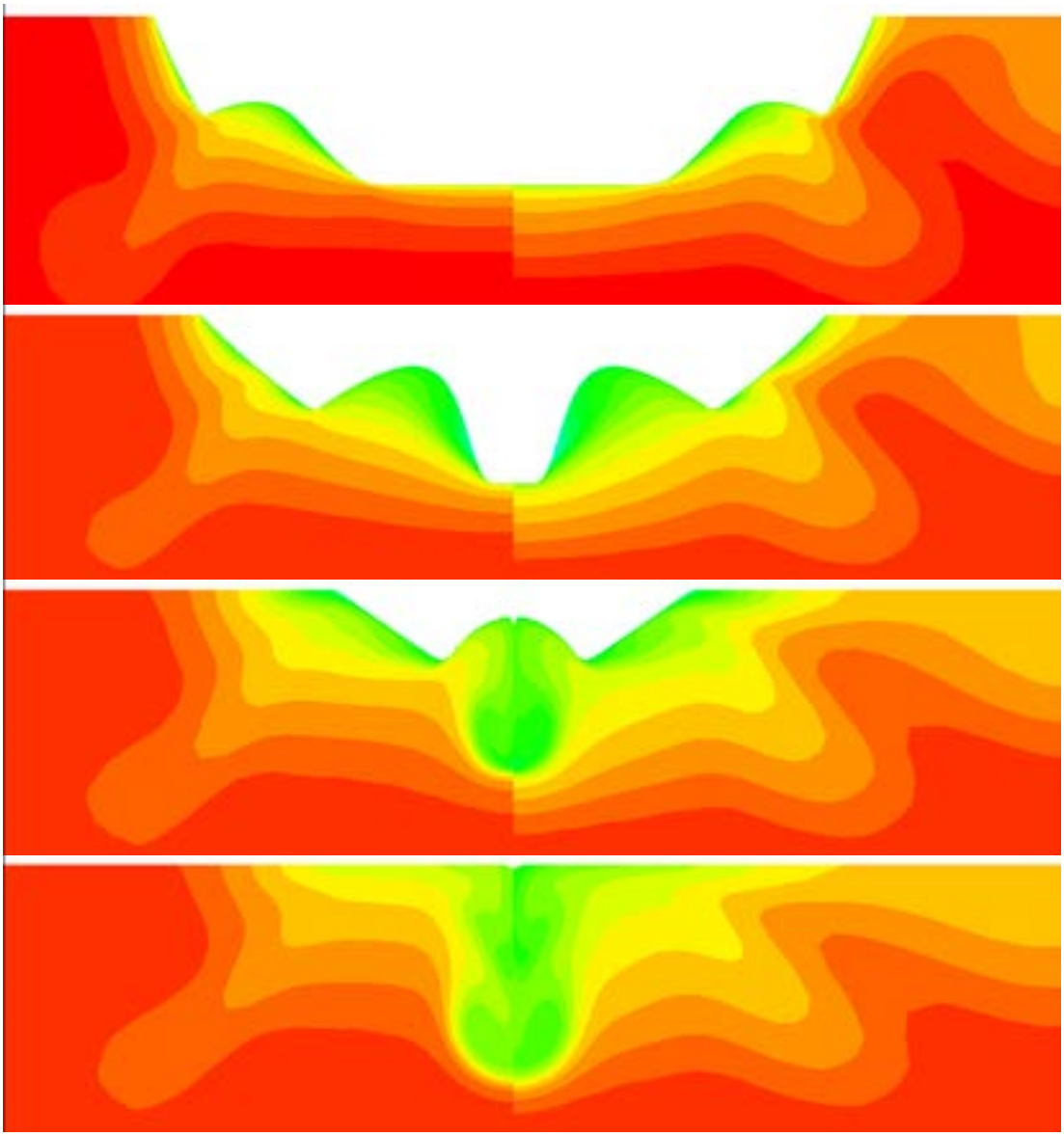

Figure 21:Axial velocity in slices from transom of barge to transom of pusher: Left: smooth transition, right: original (continuation).

4.3 Flow at the stern of the pusher

Figure 22 shows the pressure distribution on the hull at the stern of the pusher. Although the boundary layer changes significantly from one case to the other, the pressure distribution on the hull does not change enough to be visible on this legend scale. Therefore only one stern visualization is given.

Figure 23 shows the axial velocity distribution just before the transom of the pusher. Two longitudinal vortices are observed (figure Figure 24 and figure Figure 25) originating from the bilge area and the knuckle at the top of tunnel. The under pressure around the bilge is reasonable. A smoother transition from bottom to buttock flow could smoothen the pressure distribution and reduce the longitudinal vortex. The knuckle line in the tunnel is sharp but more or less aligned with the flow, resulting in a smooth pressure distribution and a modest vortex. Note that the suction effect of a propeller (not modeled) will locally change the flow direction more towards the propeller plane. This effect is limited to 1-2 propeller diameters upstream of the propeller.

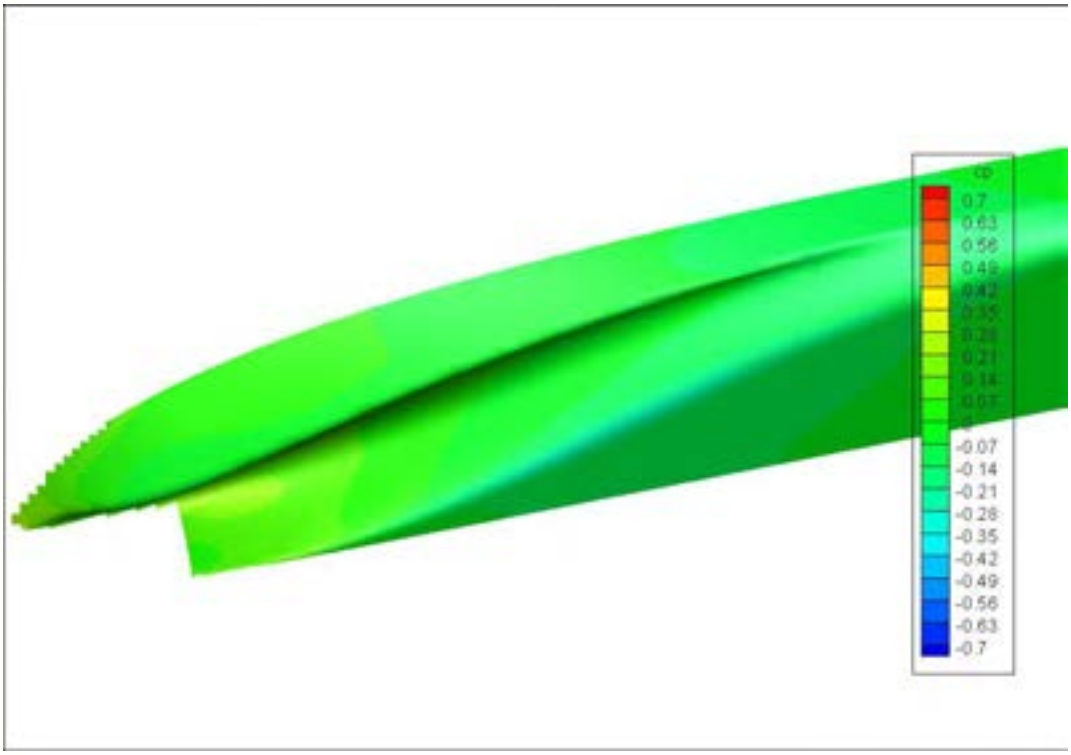

Figure 22: Pressure distribution on the hull: stern of the pusher

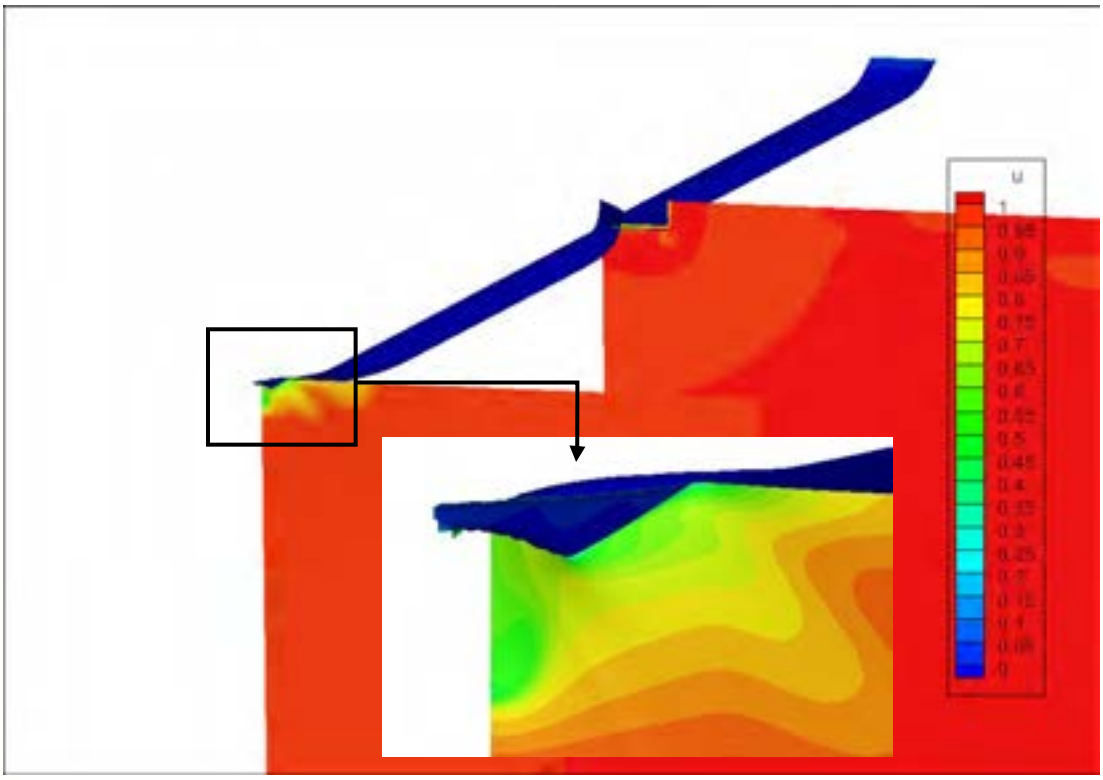

Figure 23: Axial velocity at transom of the barge and just before the transom of the pusher and detail of boundary layer at transom of the pusher

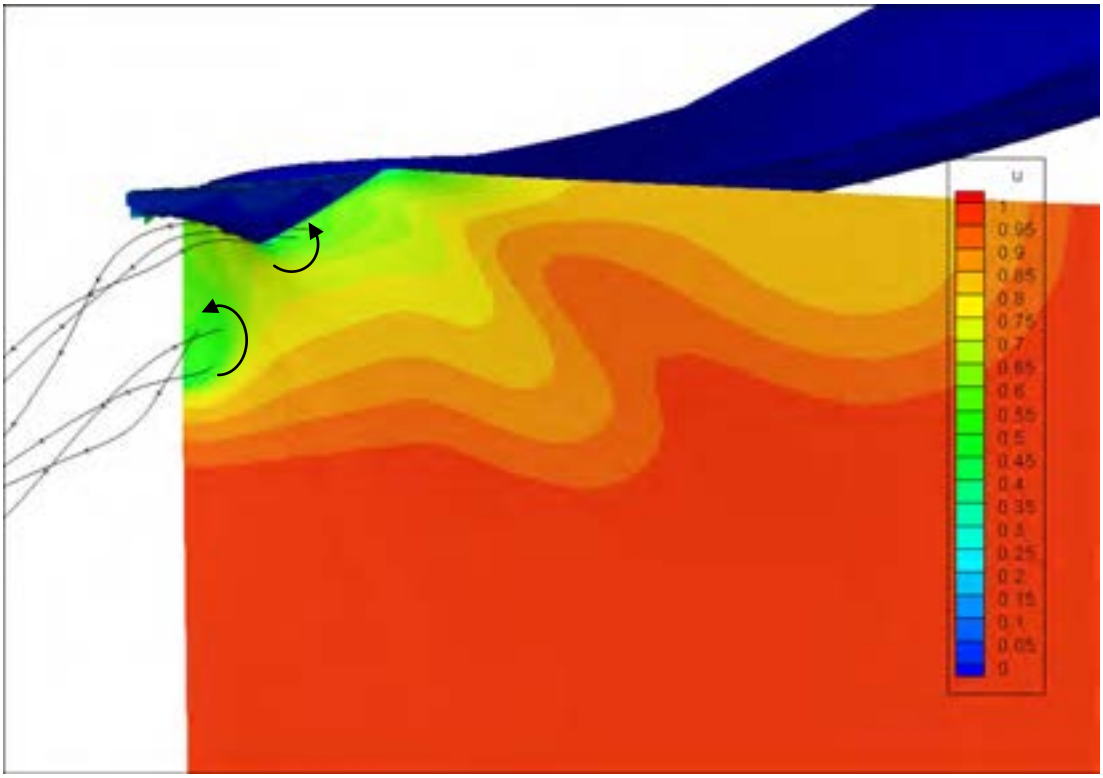

Figure 24: Axial velocity just before the transom of the pusher and streamtraces and arrows to indicate vortical motion

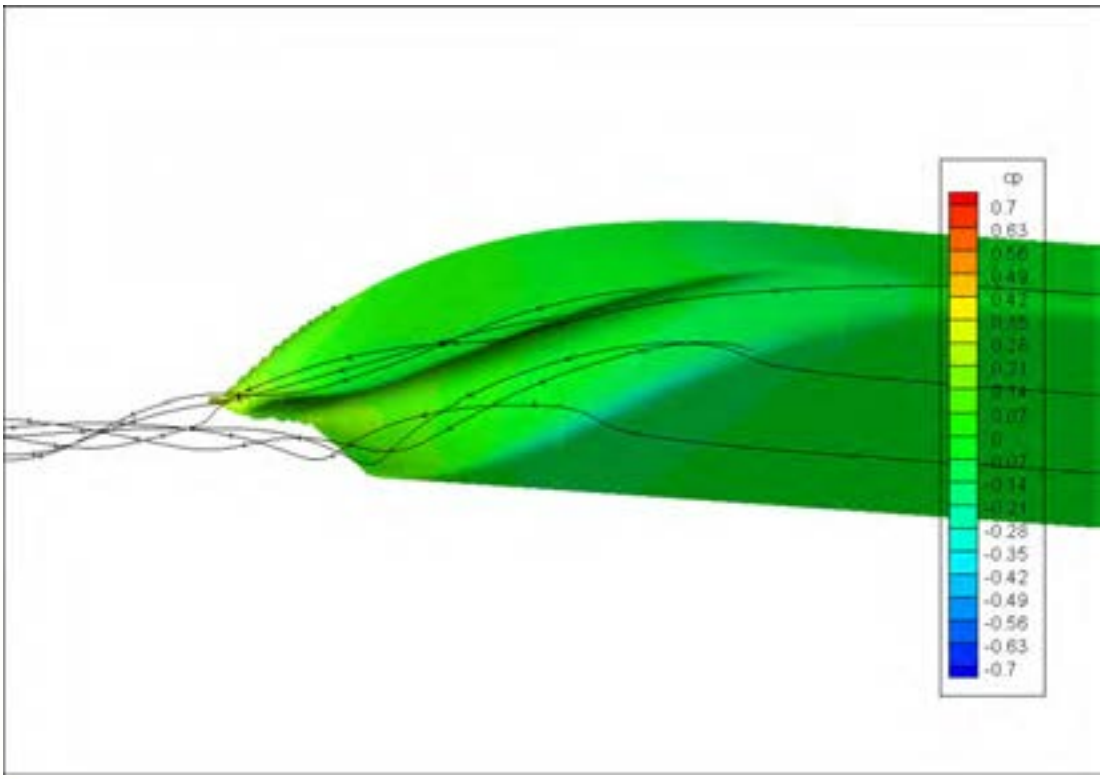

Figure 25: Pressure distribution on the hull of the pusher and streamtraces to indicate vortical motion

5 CONCLUSIONS

From the CFD calculation results discussed in this chapter, the following conclusions can be drawn:

- The flow around the bow of the Leonie SL shows a smooth transition from bow to bottom. The transition from the bow to the side is rather sharp due to the pram shape, which causes a large vortex.

- When not applying a smoothened transition the boundary layer along the pusher is rather thick due to the flow reversal behind the barge. When applying a smoothened transition the boundary layer becomes thinner. The thinner boundary layer is beneficial from resistance point of view; an indication for the resistance with and without smooth transition shows a resistance decrease of 20%.

- The transition as calculated might be impractical to build. A less drastic approach could be followed leading to less resistance decrease than indicated before. However, most of the resistance decrease is related to the removal of the flow reversal area.

- The axial velocity distribution just before the transom of the pusher shows two longitudinal vortices originating from the bilge area and the knuckle at the top of tunnel. These vortices increase the resistance of the vessel.

SECTION 3:
CFD ANALYSIS INFLEXIBLE

Written by : MARIN – Ir. J. Slot

TABLE OF CONTENTS

1 INTRODUCTION

In WP1 full scale measurements have been performed on board the Inflexible. These full scale measurement showed the ship is performing below average when comparing with the benchmark. Therefore in WP2 possible retrofit measures for the Inflexible are investigated, to determine reduction in fuel consumption.

For the push boat Inflexible, shown in Figure 1, the flow around the aftship has been investigated using PARNASSOS. The CFD code PARNASSOS was selected, because PARNASSOS is an efficient tool to calculate viscous flow phenomena and has been validated against model tests and full-scale results.

The CAD geometry used in PARNASSOS in shown in Figure 2. Moreover, the alignment of the strut has been examined. The locations of the struts is visualized in Figure 3. This report on the CFD discusses the main features of the flow and can serve as starting point for further analyses and discussion.

2 PARTICULARS OF SHIP AND PROPELLERS

The hull lines used for the CFD are based on the following drawing:

PR99-154 RevB Lines Plan Inflexible CFT.pdf	Received by email dated April 4, 2012

The initial main particulars of the ship and sailing conditions are:

Description	Symbol	Original Hull	Unit
Length between perpendiculars	Lpp	22.1	m
Breadth at still waterline (moulded)	B	9.45	m
Moulded draught moulded on FP	TF	2.5	m
Moulded draught moulded on AP	TA	2.5	m
Displacement volume moulded	Δ	353	m3
Wetted surface	STOT	289	m²
LCB position forward ½ Lpp	LCB	11.73	%
Block coefficient	Cb	0.68	-

The table below indicates some relevant propulsion details of the ship:

Diameter	D	1850	mm
Hub Diameter	DHUB	413	mm
Distance Ahead of transom	XPROP	2511	mm
Distance Outside the centreline	YPROP	2700	mm
Distance Above the base	ZPROP	665	mm
Thrust		75.71	kN

The table below indicates the location of the leading edge of the struts:

Inner strut				
		at shaft:	at duct:	
Distance ahead of transom	XI	-3363	-3254	mm
Distance outside the centreline	YI	2570	1950	mm
Distance above the base	ZI	837	1660	mm
Lower strut				
		at shaft:	at duct:	
Distance ahead of transom	XL	-3363	-3263	mm
Distance outside the centreline	YL	2700	2700	mm
Distance above the base	ZL	450	-500	mm
Outer strut				
		at shaft:	at duct:	
Distance ahead of transom	XO	-3363	-3254	mm
Distance outside the centreline	YO	2830	3450	mm
Distance above the base	ZO	837	1660	mm

Figure 1: CFT Inflexible

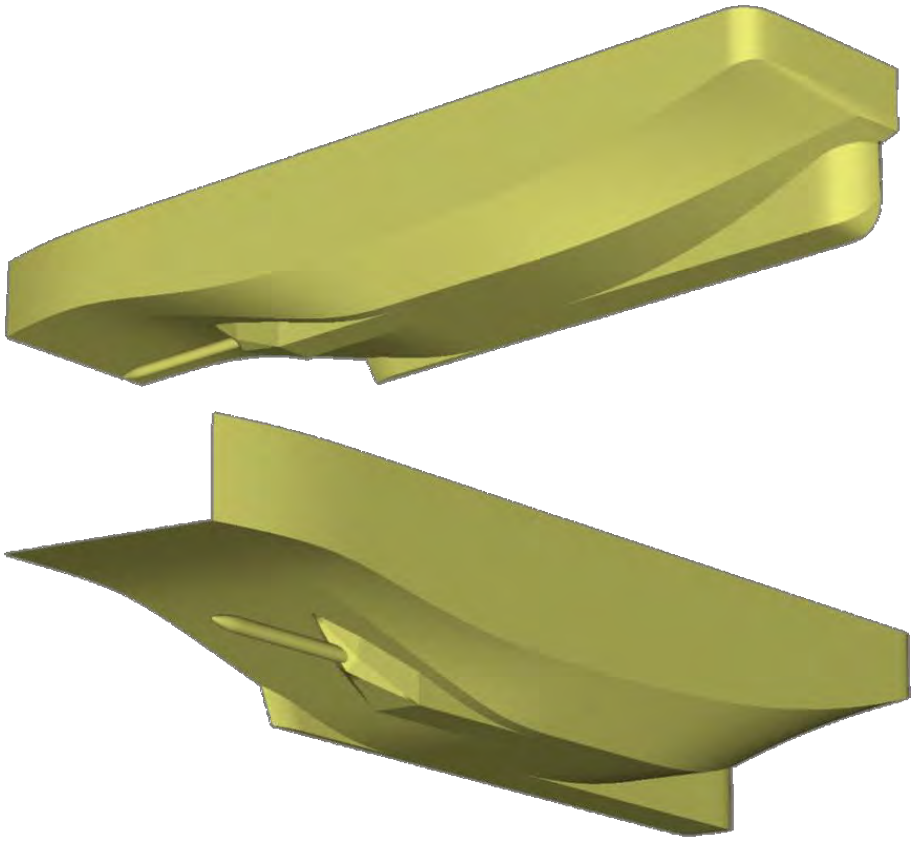

Figure 2: Ship geometry used in PARNASSOS

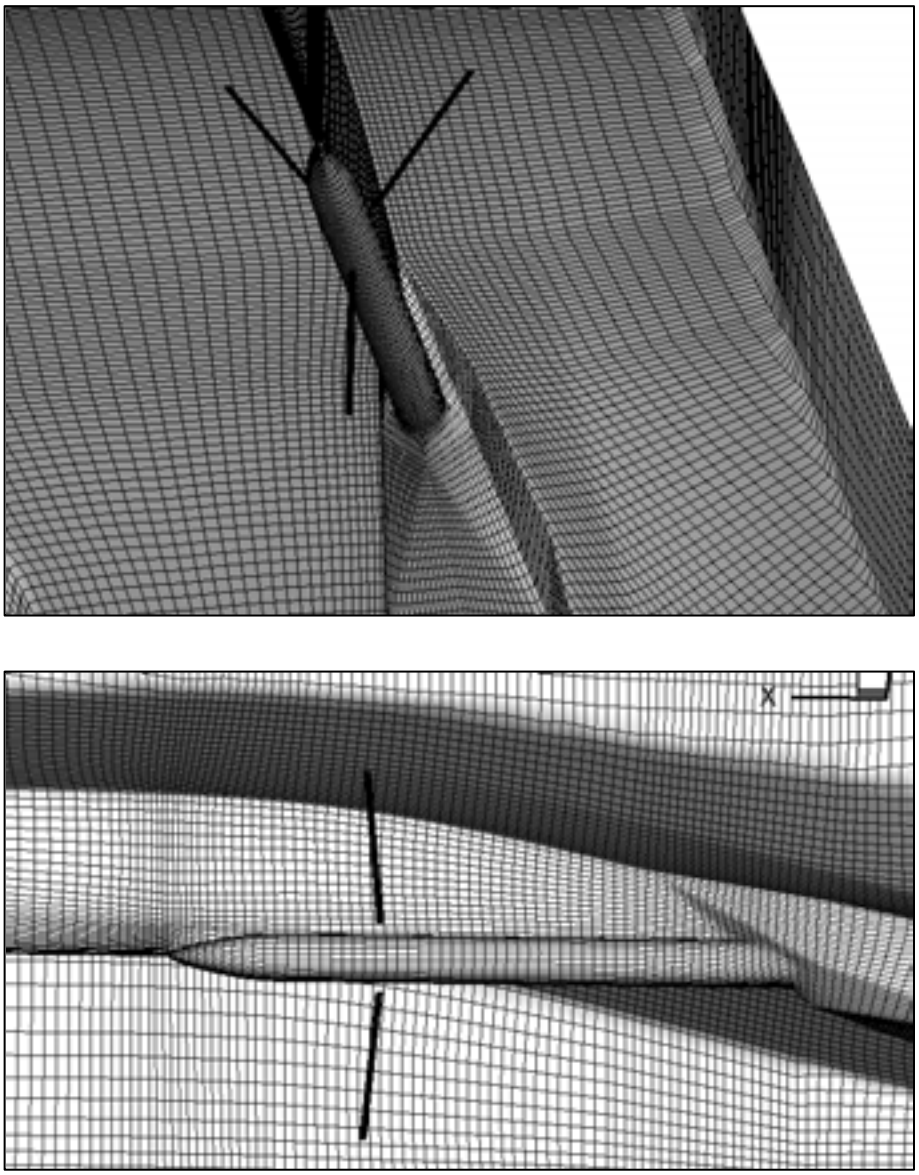

Figure 3: Locations of the struts; bottom view from aft (top) and side view (below).

3 REVIEW OF THE CALCULATION

PARNASSOS is an efficient CFD program to calculate the steady incompressible viscous flow around a ship hull using a higher order discretization on a structured mesh. It provides detailed information on the velocity and pressure field around the hull, the wake field in the propeller plane, the possible occurrence of flow separation and the viscous resistance.
All calculations were performed without barges in front of the pushboat.

Three calculations have been carried out:

1. CFT Inflexible without the shaft.
2. CFT Inflexible with the shaft.
3. CFT Inflexible with the shaft and an actuator disk.

A sailing condition was selected based on the measurements performed in WP1. The speed trials conditions at Canal de Tancarville, France were selected for the CFD calculations. The width at that location was limited so canal effects were present during the on board measurements, this is not taken into account in the CFD calculations. This resulted in the following sailing conditions:

Ship speed	15	km/h
Water depth	6.5	m
Scale	full	m
Trim	0.0	deg
Sinkage	0.0	m

A calculation domain with a flat free surface (Double Body approach) with the following characteristics was made:

Inflow (distance in front of bow)	22.1 m
Left Exterior	49 m
Bottom	6.5 m
Outflow (distance behind transom)	44.2 m
Type of Grid	Structured multi blocks
Number of Grid Cells	Around 10.4 millions
Number of hull surface elements	Around 26 000

3.1 Geometry change

Knuckle lines in the geometry led to problems in the mesh generation. Therefore, some nodes are moved inward to reduce the large angles of elements at the knuckle line. In effect, this make the edges slightly more rounded. The maximum translation of a node is about 25 mm, the majority of geometry alterations are smaller.
Due to the use of structured meshes, the original knuckle lines are not well captured. The inaccuracies introduced by the geometry changes are of similar magnitude and should therefore not lead to a substantial additional error. Figure 4 shows the new mesh in black on the side of the push boat, with the original mesh in blue.

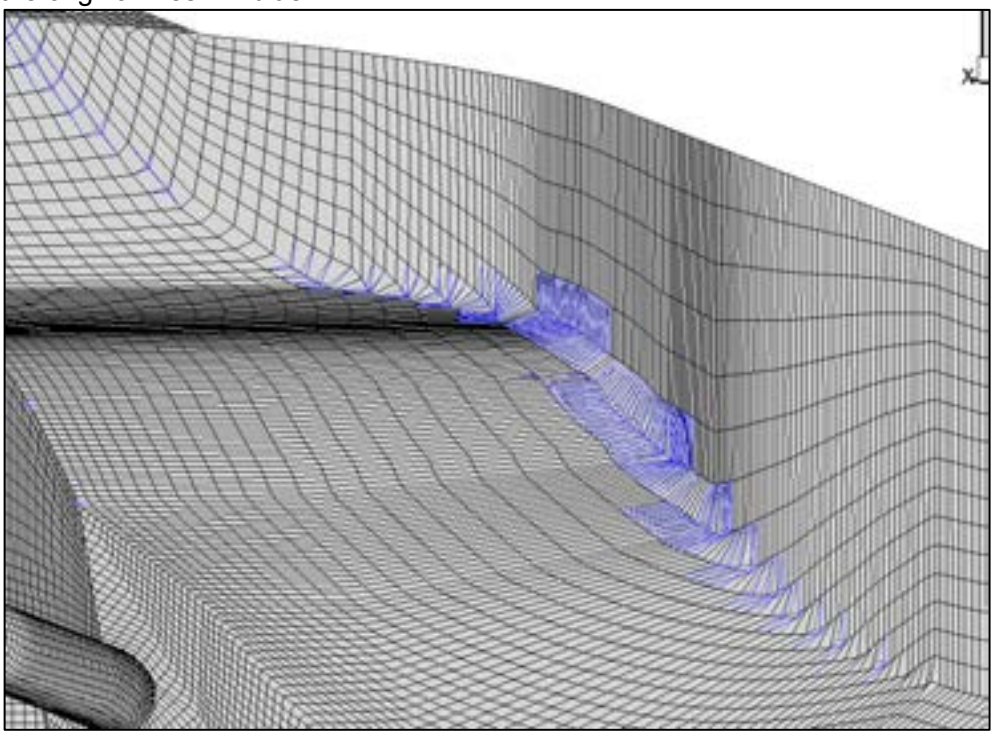

Figure 4: Changes in geometry: black new geometry, blue original shape.

3.2 Bottom boundary layer

The bottom boundary layer is not resolved. While the normal velocity at the bottom is set to zero, a no-slip condition is not applied. At a depth of three times the draught, the boundary layer is expected to be weak and its impact on the flow near the ship is expected to be negligible. Not resolving the bottom boundary layer will save additional pre-processing work and computational costs.

3.3 Convergence level

Some convergence issue were encountered at the bow and behind the gondola. Comparison with the fully-converged solution without shaft, which uses at different mesh, showed very similar results near the bow. Thus the flow around the bow in the case with shaft is deemed reliable, even if the residual are relatively high. Behind the gondola, the maximum residuals are located well after the transom.
No wall-function are used in the calculations. The maximum y+[1] in the calculations is 0.7.

[1] The y+ value is a non-dimensional parameter for the location inside a turbulent flow boundary layer. An y+ value of around 1 means the first cell height of the grid is well within the sublayer of the (fully turbulent) boundary layer.

4 PRESENTATION AND DISCUSSION OF THE RESULTS

The three-dimensional flow around bow and stern, the flow into the propeller plane and alignment of the struts are discussed.

4.1 Bow region

Figure 5 shows limiting streamlines and the pressure distribution on the hull near bow. A very low pressure area is observed near the bottom of the bow thruster housing. Low pressure indicated that the local speed is very high and flow separation may occur.

Figure 6 shows re-circulation region just upstream of the bow thruster housing near the centreline. The flow cannot follow the convex shape of the bow near the centreline. Subsequently, the flow is deflected outwards due to the presence of the bow thruster housing. A horse-shoe vortex emanates from re-circulation flow region. Vortices contain kinetic energy, which is not recoverable and as a result lead to increased resistance. Therefore, vortices should be avoided or their strength should at least be minimized. Note that the flow will change if a barge is present.

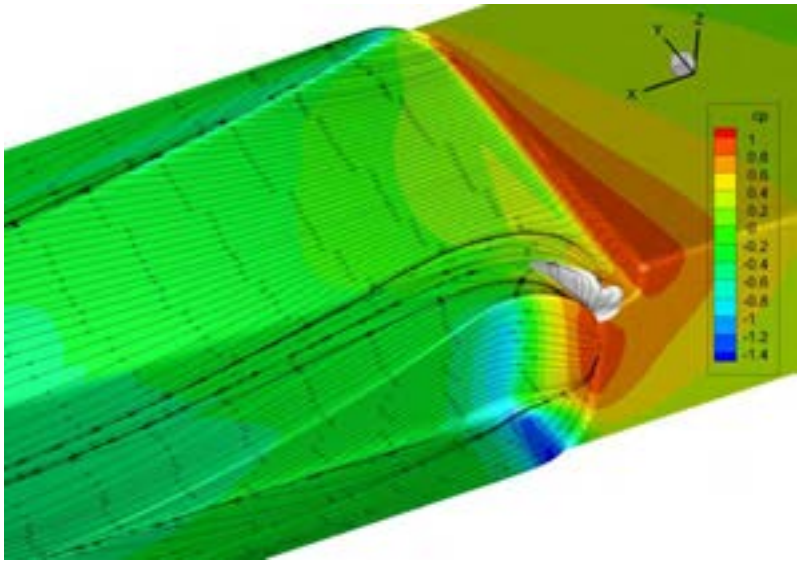

Figure 5: Limiting streamlines and pressure distribution on the hull near the bow.

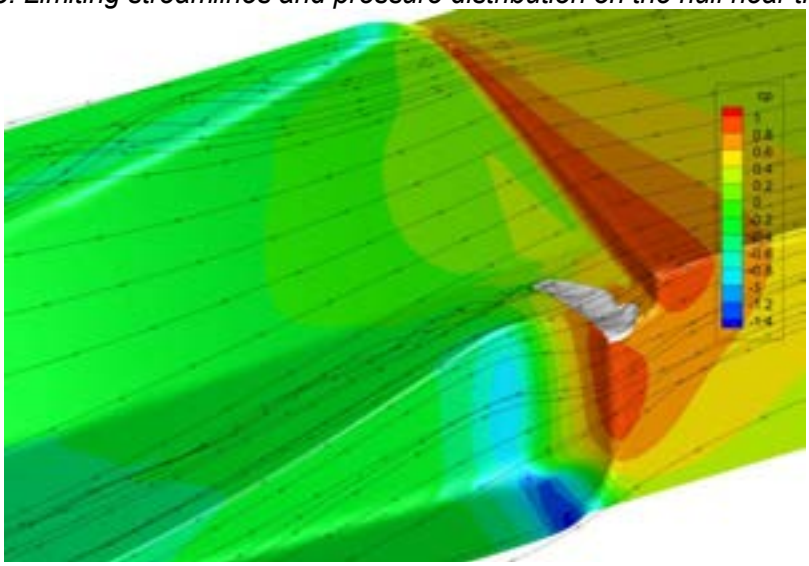

Figure 6: Region of negative axial velocity (grey region) and streamlines near the bow. On the hull the Cp distribution is given. Vortices emanating from bilge and from re-circulation region.

4.2 Stern region

In Figure 7 a bottom view is given of limiting streamlines and the pressure distribution near the stern. A low pressure area of is seen between the skeg and the bossing, locally the pressure coefficient reaches a minimum of -0.7, which indicates high local velocities.
Along the bossing of the shaft, a cross-flow towards the centreline is seen. This is consistent with the low pressure region on the inner side of the bossing. This region can be clearly seen in Figure 8. The limiting streamlines converge towards the location of the propeller. Near the sharp edge of the bossing small, low pressure spikes are seen. These are caused by the mesh. Similar spikes can be seen at the bilge in Figure 7.
Figure 8 also shows a small region of flow separation as white region. The region of flow separation is observed at the sharp edge at the inner side of the bossing. Due to bad grid quality at these locations, the occurrence of flow separation at this position may be numerical in nature.

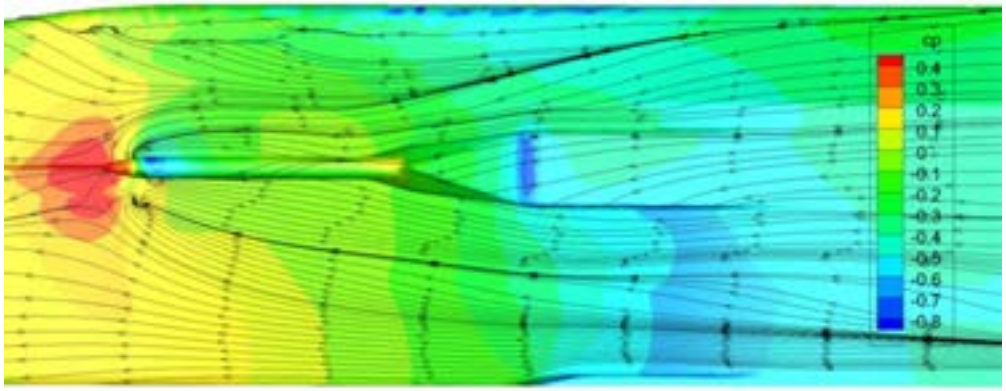

Figure 7: Limiting streamlines and pressure distribution on the hull near stern, view from bottom.

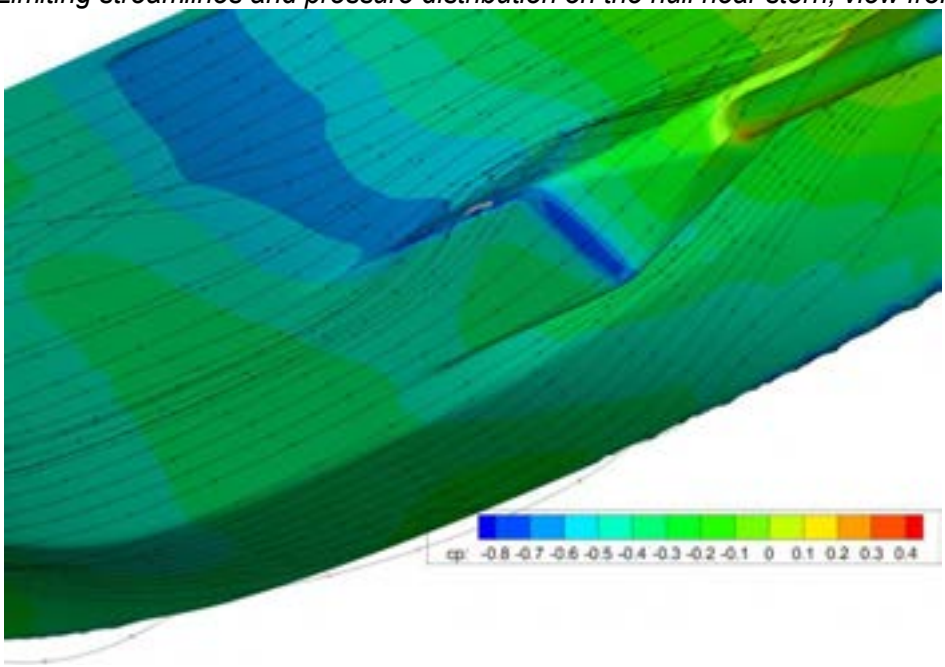

Figure 8: Small flow separation (grey regions) and streamlines near bossing. On the hull the Cp distribution is given.

4.3 Axial velocity distribution

The axial velocity in the bulk flow below the ship for the case without and with actuator disk is given in figure Figure *9*. The contour lines are drawn at every frame.
Vortices generated at the bilge, re-circulation separation region at the bow, bow thrusters housing and the shaft bossing can clearly be seen. The vortex originating from the flow separation region at the bow is transported to the inner side of the bossing. Here it merges with the vortex coming of the bossing. In between the vortices from bow thrusters housing and the re-circulation region, vortex layer separation is seen. This is also indicated by the converging limiting streamlines at this location shown in Figure 7. The presence of the actuator disk does not alter the formation of the vortices.

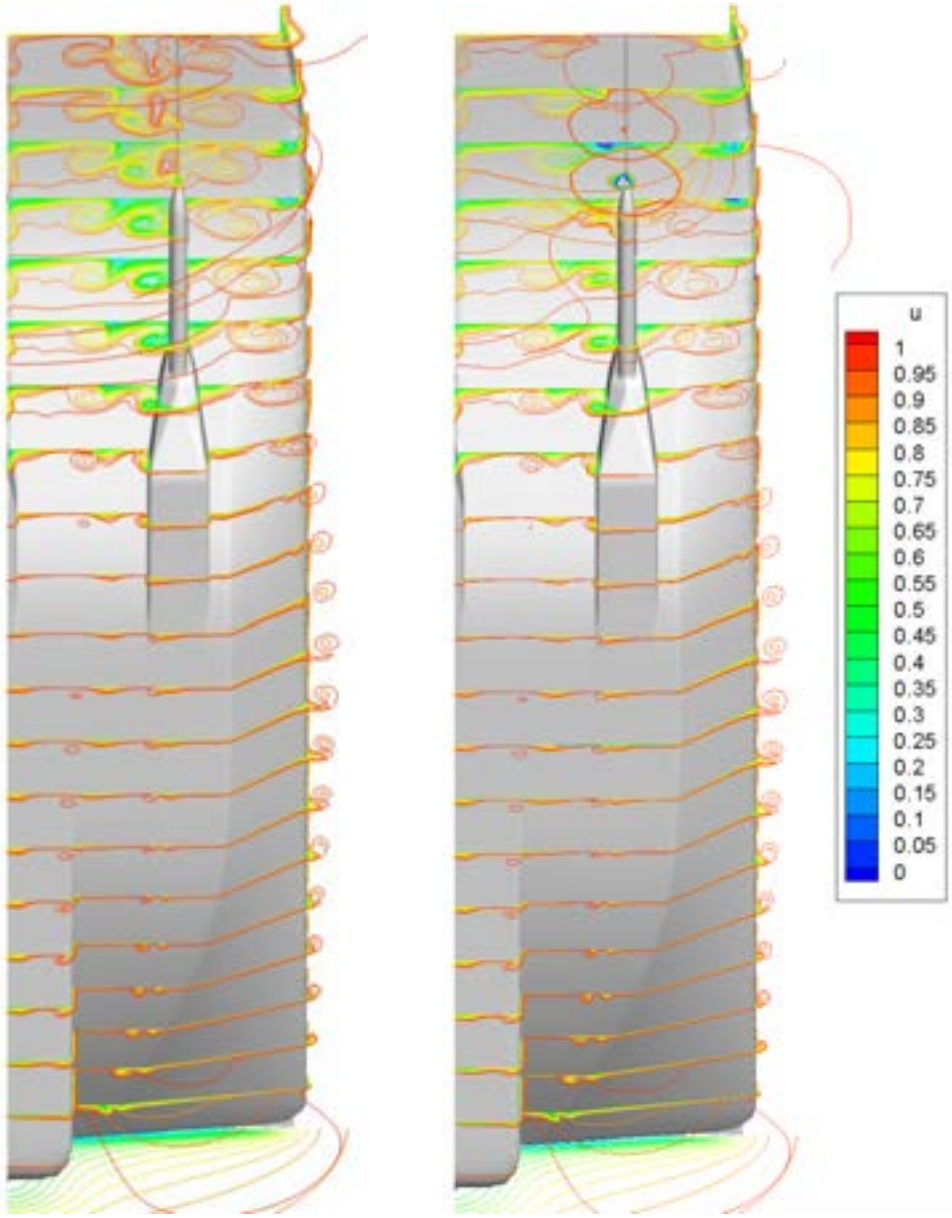

Figure 9: Contour plots of axial velocity, normalised by ship speed for cases without (left) and with (right) 75.71 kN actuator disk. Contour-lines plotted at every frame.

4.4 Propeller

Overview
A complicated nominal wake is seen. Further insight can be gained by using streamlines for the case without actuator disk to trace the origin of the various wake peaks. Figure 10 and Figure show the rear and side view, respectively, of the ship with the axial velocity indicated at the propeller plane.

Three regions of low axial velocity are seen:

1. The region near the top of the propeller plane, crossed by the red streamlines, is caused by the presence of the bossing. It is shifted inwards due to the overall fluid motion near the hull towards the centreline.
2. The large vortex on the left, crossed by yellow streamlines, is generated at the inner side of the bossing.
3. In the upper-right corner, the third region is present caused by the knuckle line along the bilge. Two distinct low velocity regions, indicated by the green and blue streamlines are seen. These streamlines represent vortices generated at location with substantial cross-flow over the rather sharp bilge.

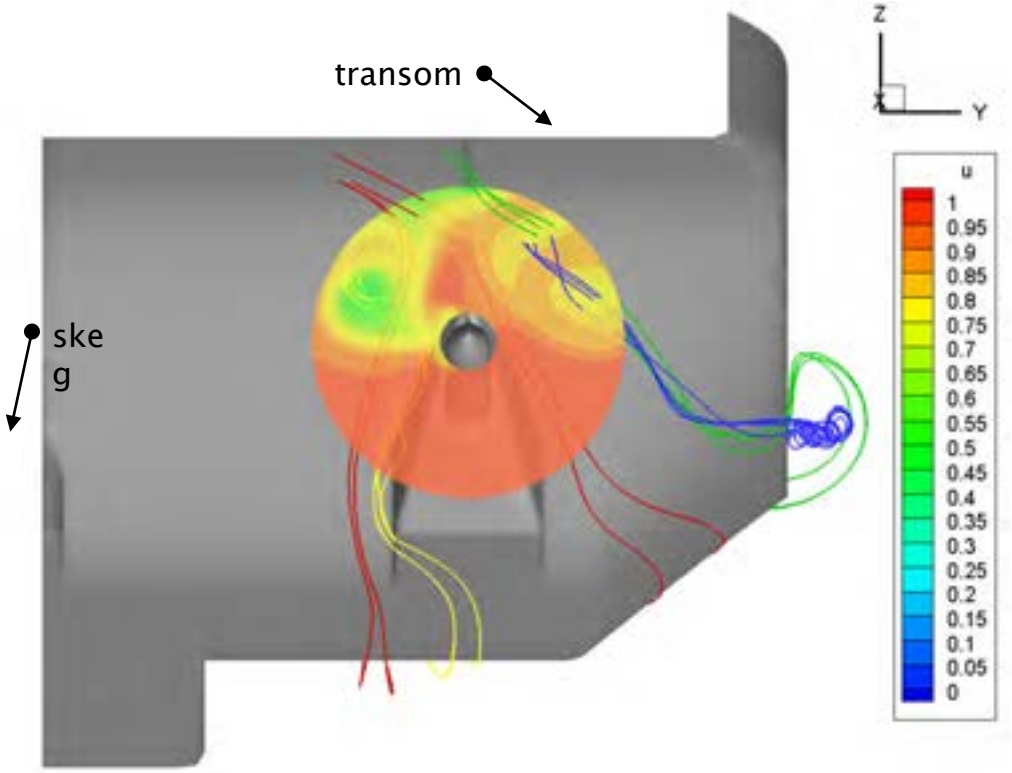

Figure 10: Rear view of hull with nominal wake field indicated at the propeller plane. Streamlines drawn through wake peaks indicating causes of low axial velocity.

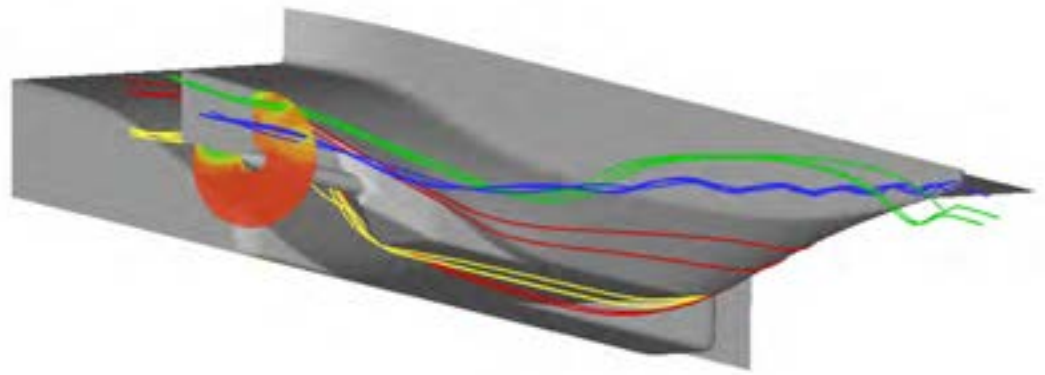

Figure 11: Side view of Figure 10 showing vortices, captured by green and blue streamline sets, being generated at the knuckle line of the bilge.

Influence of shaft

Figure 12 shows the axial velocity in propeller plane with (left) and without (right) shaft, both cases without actuator disk. The vectors are two-dimensional and show the velocity tangential to propeller plane. In both propeller planes similar regions are present, indicated by the numbers 1 to 3.

The shaft however blocks the inward and upward flow seen without the shaft. The reduced flow area results in a higher speed above the shaft. The blockage of the shaft leads to a low velocity region on the inner side on the shaft. A counter-clockwise rotation is observed in the flow around the inner side of the shaft, which interacts with the vortex coming from the bossing.

It should be mentioned that the computation with shaft uses a finer mesh. Therefore, vortical structures are better resolved in that calculation.

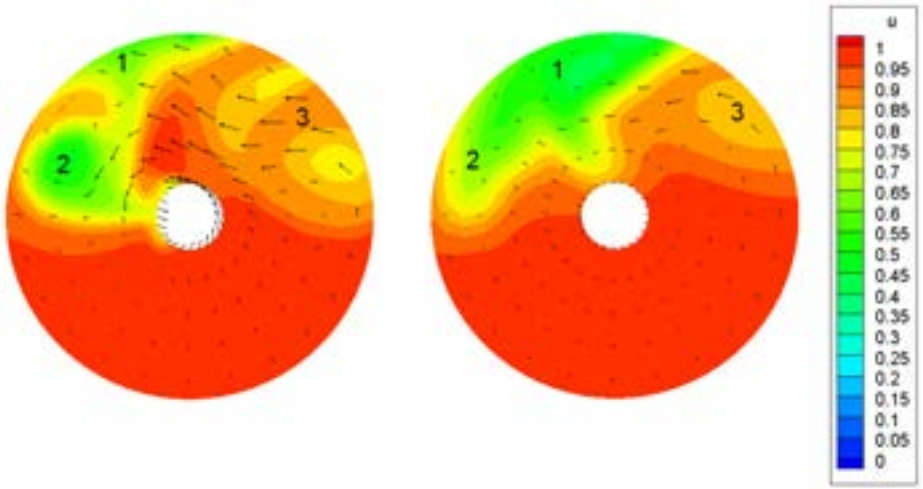

Figure 12: Nominal axial velocity in the starboard propeller plane with (left) and without (right) shaft. 2D Vectors indicate velocity tangential to propeller plane.

Wake field velocity distribution

The axial and tangential velocity in the nominal wake field are given in figures Figure *13* and Figure *14*. Angle θ is zero at the '6 o'clock' position and increases in counter-clockwise direction. Data for more values for r/R with and without shaft is available in excel-sheet format.

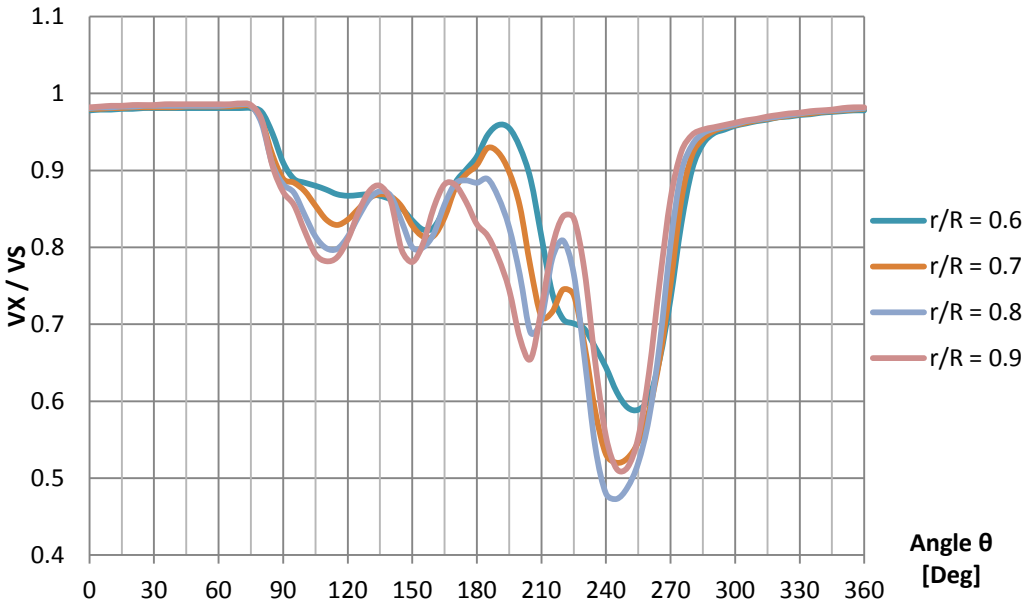

Figure 13: Non-dimensional axial wake velocities for case with shaft.

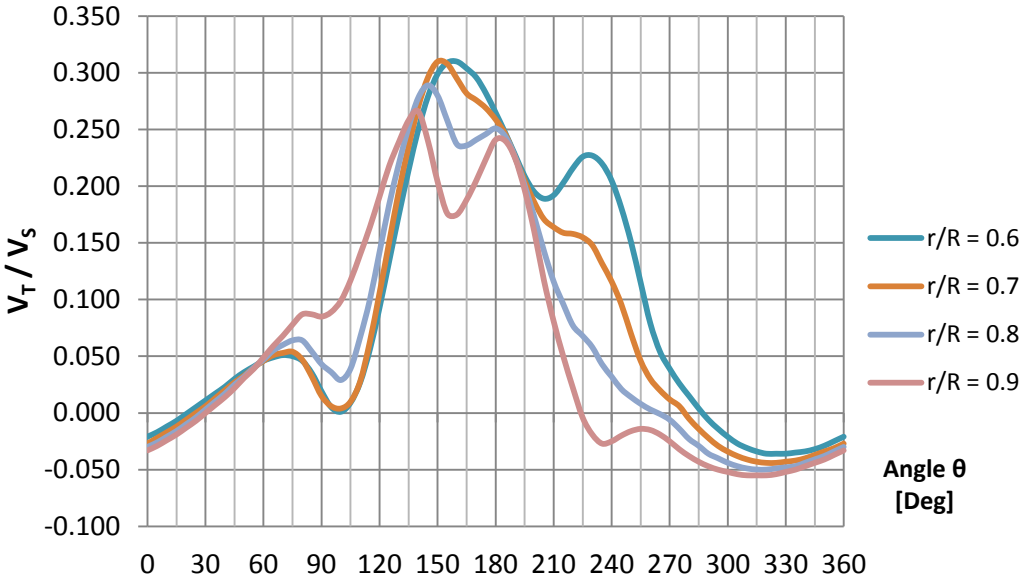

Figure 14: Non-dimensional tangential wake velocities for case with shaft.

4.5 Alignment of struts

Three struts are attached to the shaft. These are not modelled in PARNASSOS. The locations of these strut are given in chapter 2 and they are visualized in Figure 3. Their alignment with the flow is given in figures Figure 15, Figure 16 and Figure 17 for the lower, inner and outer strut, respectively. An actuator disk was used in the calculation of these results. The graph shows how far the strut should be rotated, in its own coordinate system, to be aligned with the flow. A positive angle entails a rotation of the trailing edge towards the centreline. The current struts are believed to have a zero angle with respect to the axial direction, based on photos.
With flow angles up to 20° the upper struts are poorly aligned, creating additional wake peaks in the wake field. Note that the duct is not modelled and can have an effect on the local flow direction.
When struts are not well aligned, flow separation can occur on the struts which increases the resistance of the vessel. In addition the not aligned struts can cause a retarded flow into the propeller, which can cause vibration problems.

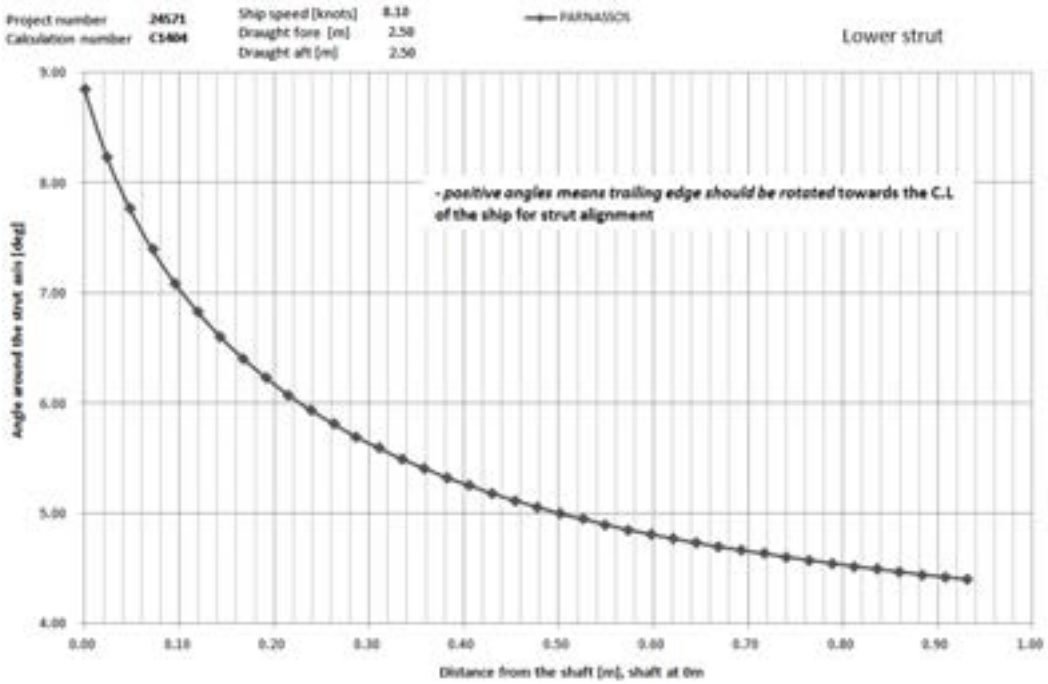

Figure 15: alignment with the flow of the lower strut.

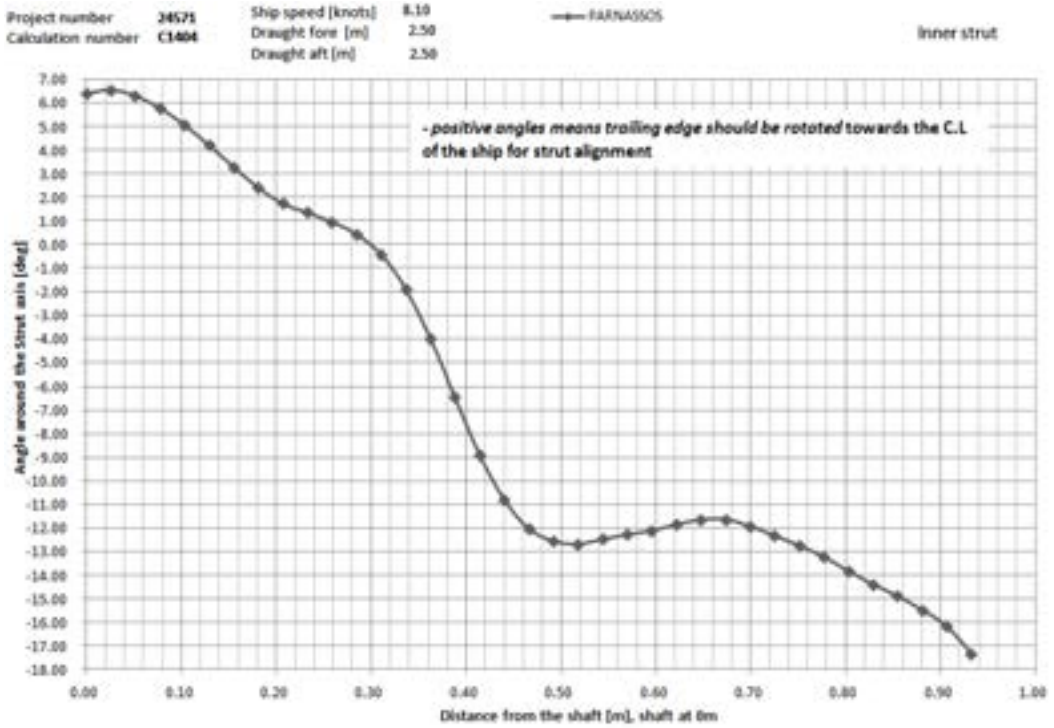

Figure 16: alignment with the flow of the inner strut.

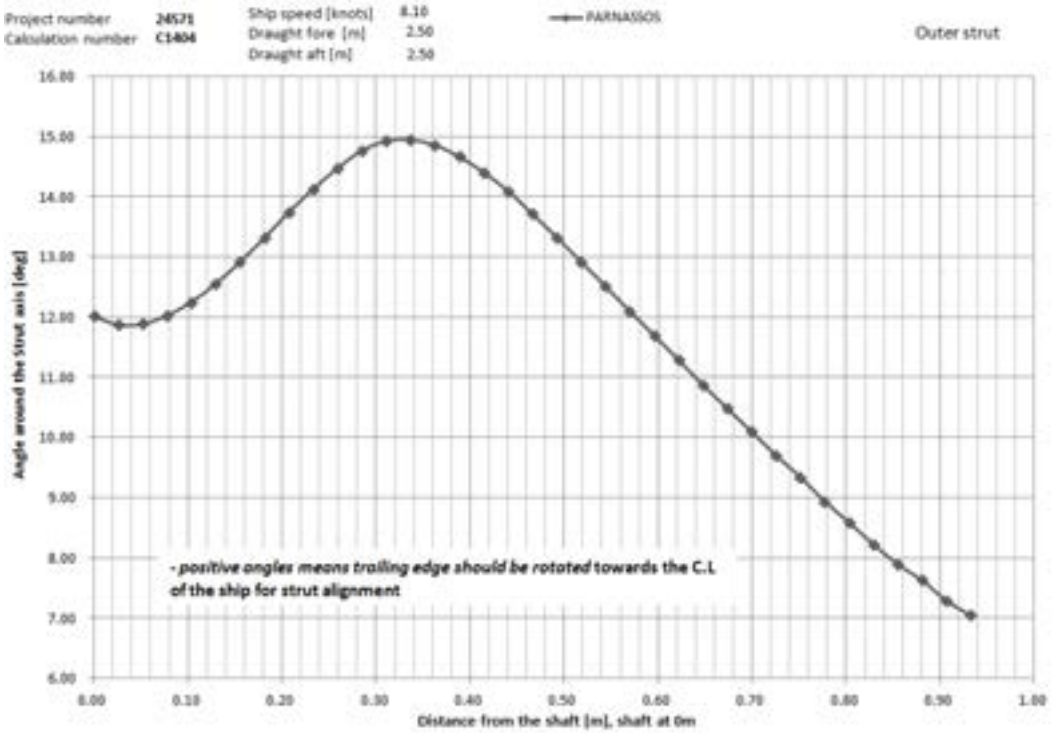

Figure 17: alignment with the flow of the outer strut.

4.6 Results for re-designed hull shape

Based on the previous results a modification of the hull shape has been designed. The new hull shape features a more rounded bow thrusters housing and shaft bossing. It is also advised to eliminate the hard knuckle lines in the hull shape, however this seems a very expensive retrofit measure.
The pressure distribution near the bow for the two hull shapes is compared in Figure 19. Some streamlines are released close to the hull to visualized the flow pattern. The more slender and rounded entrance of the bow thrusters greatly reduces the strength of the horse-shoe vortex. In addition, the region of negative axial velocity is no longer present. The under pressure on the bottom of the bow thrusters housing is also substantially reduced.
The pressure distribution on the stern region for the improved and original hull shapes is shown in Figure 20. The flow over the bossing is visualized by streamlines. These indicate that no vortex is generated along the inner side of the bossing for the improved hull shape. However, some vorticity is introduced in the flow at the location where the shaft leaves the bossing.
Figure 21 shows the nominal wake field in the starboard propeller plane for both hull shapes. Due to the rounding of the bossing the large vortex on the inner side of the shaft is absent for the improved hull shape. This vortex contributes to the rotation of the flow seen around the shaft for the original hull. The rotation is in counter-clockwise direction in Figure 21. Therefore the increased flow towards the centre line above the shaft is not observed for the improved hull. The wake coming from the bossing is thus not pushed out of the propeller plane as is seen for the original hull.
The axial and tangential wake velocities in the propeller plane for the improved hull are shown in Figure 22 and Figure 23. Comparison with figures Figure *13* and Figure *14* shows that the wake peak is deeper for the improved hull.
For the current ship the accurate prediction of the resistance is difficult to determine. So bear in mind there is an uncertainty in the prediction. However, the improved hull shape has an estimated 8 % reduction in resistance compare to the original shape. For the whole convoy this corresponds with a resistance reduction of 1 to 1.5 %

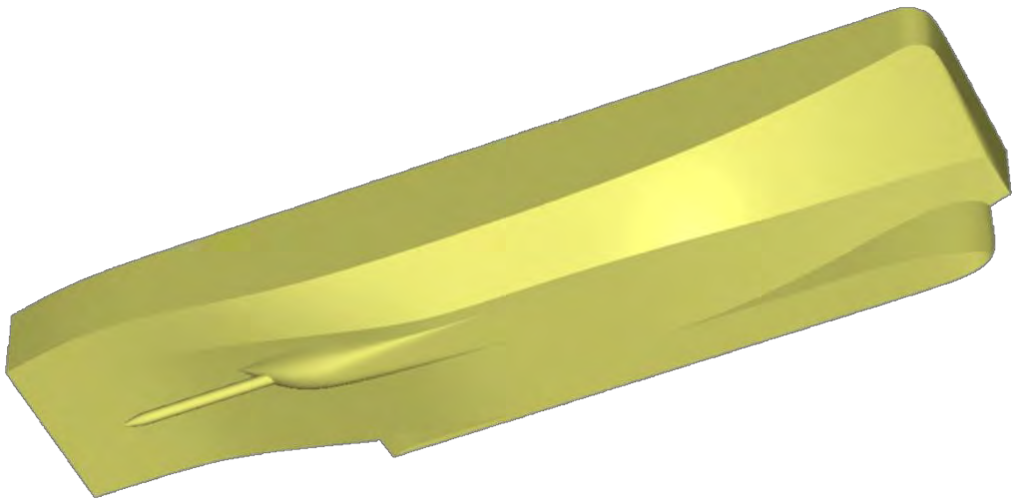

Figure 18: Improved hull shape with a slender entrance of the bow thrusters housing and a rounded bossing.

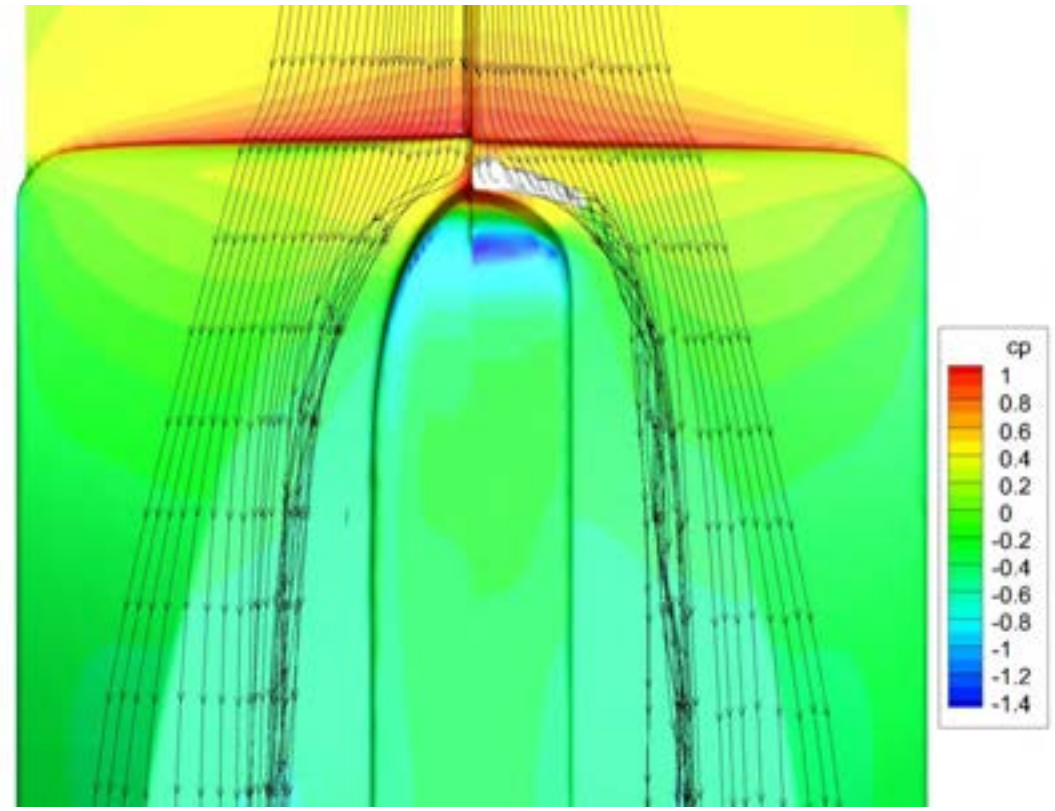

Figure 19: Bottom view of pressure distribution on the bow region for the improved (right) and the original (left) hull shape. Bulk streamlines are released close to the hull. The improved hull shape shows no region of negative axial velocity (gray region), a much weaker horse-shoe vortex and less extreme under pressure on the bow thruster housing.

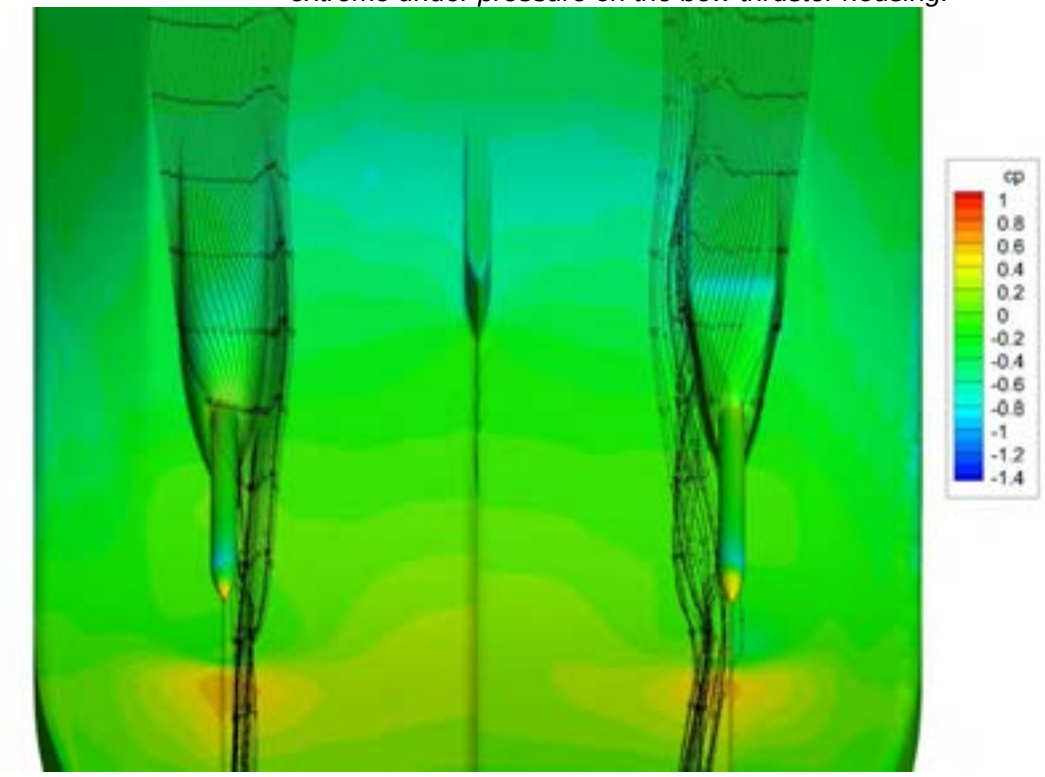

Figure 20: Bottom view of pressure distribution on the stern region for the improved (right) and the original (left) hull shape. Bulk streamlines visualize the flow near the surface of the bossing. No vortex is generated along the inner side of the bossing for the improved hull shape. Some vorticity is introduced in the flow at the location where the shaft protrudes from the bossing.

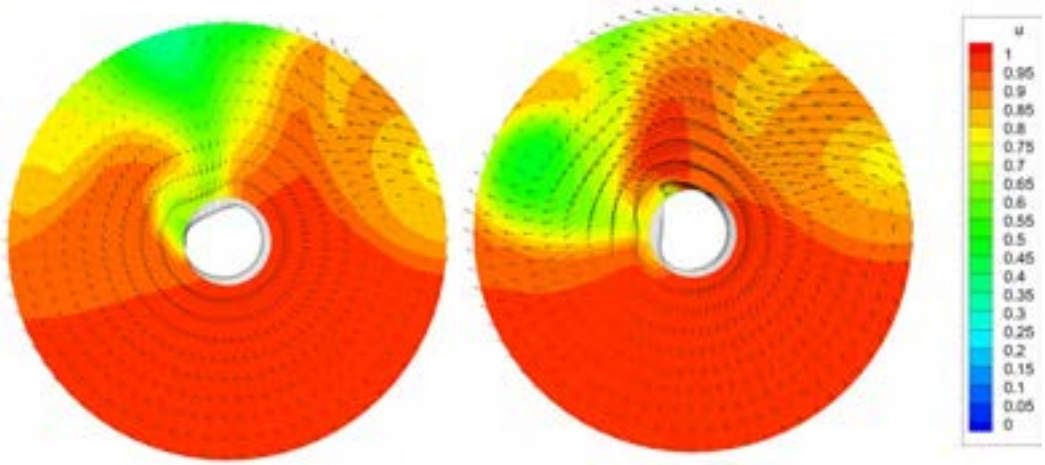

Figure 21: Nominal wake field in the starboard propeller plane for the improved (left) and the original (right) hull shape. For the improved hull the large vortex on the inner side of the shaft is absent and less rotation of the flow around the shaft is seen.

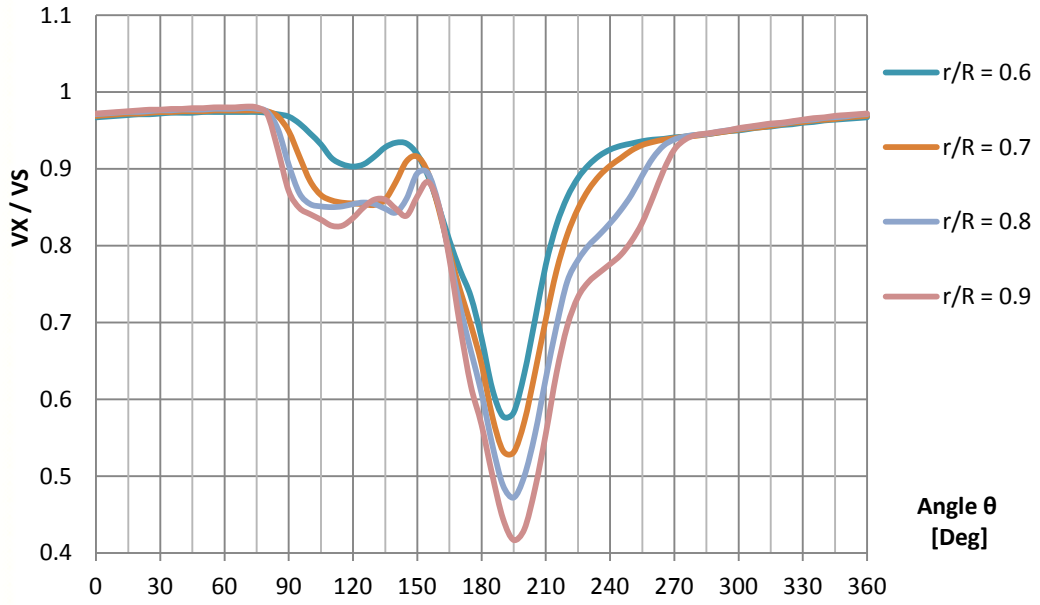

Figure 22: non-dimensional axial wake velocities for case with improved hull shape.

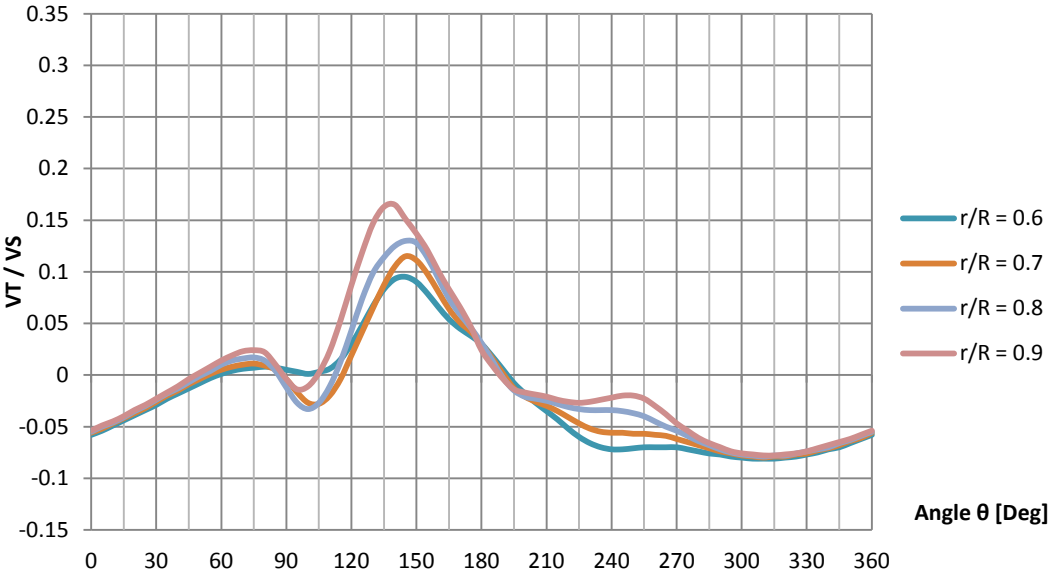

Figure 23: non-dimensional tangential wake velocities for case with improved hull shape.

5 CONCLUSIONS

5.1 Summary of results

- Vortex sheet separation due to streamline convergence is seen on sharp edges at bow thrusters housing, bilges and bossing.
- Flow separation occurs at the bottom of the bow due to the strong curvature of the hull and the further deceleration on the flow caused by the downstream bow thrusters housing. When sailing with barges in front of the pusher, the local flow will be different.
- The shaft bossing is poorly aligned with the flow. This leads to the formation of a strong vortex, which crosses the propeller plane and causes vibrations
- Some flow separation is seen at the inner side of the bossing.
- The nominal wake field is characterised by various wake peaks stemming from different sources.
- The upper two struts are misaligned, locally at an angle up to 17° with the flow direction. The outer strut experiences just flow towards the centreline. However, the inner strut has incoming flow at both positive and negative angles. Please note that the calculation is performed for only one condition, variations in draught, trim and water depth can change the neutral angle.
- Rounding of knuckle lines substantially reduces the generation of strong vortices.
- The improved hull shape has an estimated 8 % reduction in resistance compare to the original shape. For the whole convoy this corresponds with a resistance reduction of 1 to 1.5 %

5.2 Recommendations

- **Nozzle**: The duct of the nozzle seems quite thick. Perhaps improvements can be made by using a more slender nozzle.
- **Knuckle lines**: Sharp edges in the hull can be made more rounded. Perhaps the depth of the bossing can be increased to accommodate this geometry change. Note that currently the duct is lower than the base.
- **Propeller**: Improvements can be made by using an optimized propeller. This is in the order of magnitude of 2 % power reduction
- **Rudder**: The rudders seem quite large and bulky. The more efficient design may increase manoeuvrability and decrease resistance.
- **Transom:** The transom immersion is relatively deep, creating a rather large recirculation zone behind the ship. A lower immersion reduces drag, but will necessitate geometry changes

SECTION 4:
CFD ANALYSIS DUNAFØLDVAR

Written by : MARIN – Ir. A. Lampe

TABLE OF CONTENTS

Page

1 INTRODUCTION

In WP1 full scale measurements have been performed on board the Dunaføldvar. These full scale measurement showed the ship is performing below average when comparing with the benchmark. Therefore in WP2 possible retrofit measures for the Dunaføldvar are investigated, to determine reduction in fuel consumption. The objective is to investigate the effect of removing the flanking rudders on the performance of the ship.

The computations comprise of resistance computations on two grids and propulsion computations on one grid using propulsion values from the full scale measurements.

This report gives the results of these viscous flow computations. Chapter 2 gives the computational setup, chapter 3 and 4 discusses the results of the computations on the hull and propeller respectively and finally in chapter 5 conclusions are drawn.

2 COMPUTATIONAL SETUP

2.1 CFD code

For all viscous flow computations the in-house RANS code ReFRESCO for incompressible fluids is used. ReFRESCO uses a finite-volume discretization, unstructured mesh, variables defined in cell-centered (collocated) and has a segregated solver using SIMPLE for Pressure-velocity coupling. The numerical approach is comparable to e.g., STAR-CCM+, OpenFOAM and Fluent. For all computations the k-ω SST turbulence model and QUICK discretization of the convective part of the momentum equations was used. All computations were steady state (i.e. no time dependence). All computations were made for full scale without using wall functions (y+ ~ 1).

Some computations on the propeller have been made, this is done using the in-house Boundary Element Method (BEM) code PROCAL which is based on potential flow (i.e. no viscosity). With this code unsteady computations can be performed including cavitation. For these computations a wake field is necessary which is taken from the viscous flow computations.

2.2 Geometry

In the computations use is made of the symmetry thus only half the ship is modeled. The ship and propeller are drawn according to the drawings received by email from Helogistics. The result for the 3D solid model is shown on page F1. The form plan of the propeller is on page F2. Some slight adaptations from the drawings are made for gridding purposes, among which are the creation of several fillets, the slight extension of the endplates of the rudder near the leading and trailing edges and the adaptation of the struts near the lower connection with the nozzle. None of these geometrical adaptations cause significant changes in the results to the author's opinion.

Furthermore a stream cap is attached to the transom of the ship shown in blue on page F1. This prevents excessive flow separation regions in the solution since these can cause difficulties in the computations. This has no impact on the flow around the flanking rudders. The main particulars are shown in the next table.

Parameter		Unit
Length over all (LOA)	37.2	m
Beam	12.54	m
Draught fwd / aft	2.1 / 2.1	m
Water depth	5.4	m
Number of propellers	3	-
Propulsion configuration	5 bladed FPP in nozzle	-
Propeller diameter	1.700	m
Total engine power (MCR)	3 x 515	kW
Maximum engine RPM	600	RPM
Main engine type	Skoda 6 27.5 A2L	-

Table 1: Main particulars of Dunaføldvar

2.3 Domain and flow parameters

The computation uses a double body approach which means that for the water surface a symmetry plane is taken. This means no waves are computed. For the computational domain the parameters of the boundaries are summarized in the next table.

Boundary	location	Boundary condition
Inlet	150m (~4 times LOA) upstream of AP[1]	Velocity specified
Outlet	150m downstream of AP	Zero gradients (outflow)
Side	150m sideways from centerplane	Constant pressure
Water surface	2.1m above keel	Symmetry plane
Symmetry plane	at the centerplane	Symmetry plane
Bottom	3.3m below keel	Free-slip wall

Table 2: Boundary conditions of computational domain

The velocities, water depth and propeller loading are chosen from the trial condition on shallow water (5.4m water depth) and ship speed of 8.5km/h. For the propeller the trials give the propeller RPM and torque. However, no thrust is measured. For this PROCAL is used. The condition is summarized in the next table.

Parameter	Value	Unit
Ship speed	2.36	m/s
Propeller speed	245	RPM
Delivered power per propeller	289	kW
Thrust per propeller	41.2	kN
Water density	998	kg/m^3
Water kinematic viscosity	$1.139 \cdot 10^{-6}$	m^2/s

Table 3: Ship and propeller conditions and water properties.

In the viscous flow computation the propeller is modeled as an actuator disk. This resembles a propeller with an infinite number of blades. The loading in radial direction is taken as the loading of a Ka4-70 propeller since the actual radial loading is hard to compute. The loading is scaled to the required thrust, see page F4. In circumferential direction the propeller loading is constant.

In total four computations are made:

Computation	Details
Resistance normal grid	no propeller action
Resistance high resolution grid	no propeller action
Propulsion normal grid	actuator disk as propeller
Propulsion normal grid, no flanking rudder	actuator disk as propeller

Table 4: List of performed computations

[1] Aft Perpendicular

2.4 Grid generation

For grid generation the commercial package Hexpress is used. This creates an unstructured grid using only hexahedral cells. For all grids and y+ value[2] of around one is aimed at, which creates large amount of cells in the viscous layer for full scale computations like these. However, in this case no wall-functions[3] need to be used. An impression of the coarsest grid is shown on page F3. In total three grids are made, listed below.

Grid	Size	description
normal res	19.7 mln. cells	Half domain
high res	26.9 mln. cells	Half domain
norm res noFlank	13.8 mln. cells	Half domain, no flanking rudders

Table 5: Computational grids

Hexpress uses for grid generation a basic hexahedral cell size which is divided by eight for every refinement step (sides of the cubic are halved). This means that changing the basic cell size changes the whole grid density. This is what is done for the high resolution grid. The sides of the basic cell size are two thirds of that of the normal grid which means that there are locally about 1.5^3 = 3.4 times more internal grid cells. However, the total grid size is not 3.4 times larger due to lack of geometric similarity of the grids but mostly because of the viscous layer which scales differently. This layer that captures the detailed gradients in the flow near a surface comprises the larger part of the grid cells (e.g. for the normal resolution grid only about 20% of the cells are *not* in the viscous layer). In other words, the increment from 19.7mln cells to 26.9 mln. cells is deceptive and a significant increase in resolution is obtained.

[2] The y+ value is a non-dimensional parameter for the location inside a turbulent flow boundary layer. An y+ value of around 1 means the first cell height of the grid is well within the sublayer of the (fully turbulent) boundary layer.

[3] Wall functions are functions that describe the boundary layer according to some flow parameters. These are less accurate since the shape of the boundary layer is assumed, not calculated.

3 RESULTS VISCOUS FLOW COMPUTATIONS

An analysis of the results is made in this chapter. First the accuracy of the computation is discussed using the two resistance computations. Then the flow around the ship including propeller action is analysed. Improvements are suggested and the influence of the flanking rudders is discussed.

3.1 Resistance computations

The resistance computations are done with two different grid densities. Qualitatively no significant differences are encountered except maybe for the extent of the flow separation areas, see page F5. This shows the sensitivity of the flow to separation regions. The table below summarizes the forces in forward direction.

Force on	normal resolution [kN]	high resolution [kN]	difference [%]
Hull	6.12	6.14	+0.6%
Center nozzle	0.542	0.382	-29.5%
Port side nozzle	0.187	0.125	-33.2%
Inner flanking rudder port	0.001	0.018	-
Outer flanking rudder port	0.462	0.430	-6.8%
Total	8.04	7.72	-4.1%

Table 6: Forces from the resistance computation compared

First note that the total forces do not equal the sum of the other forces, this is because the forces on the shafts and struts are not included in this overview.

The total forces on the hull with a normal resolution and a high resolution differ approximately 4%, which is not very large. However large differences exist between the appendages. On closer inspection it is noted that the difference is mainly due to the pressure forces, not the frictional forces. Page F6 shows a detail near the separation area on the port side nozzle. The blue area at the leading edge, near the separation region, is a suction peak on the nozzle which locally creates a forward force. However, in this case a clear difference is seen between the normal and high resolution computations. The suction peak is apparently influenced by the separation region. On its turn the separation area is apparently quite sensitive to grid resolution, this confirms earlier experience and is probably due to the instable nature of these separation regions. Fortunately, when the propeller action is modeled, less flow separation occurs at important locations like pressure peaks, see next section.

3.2 Propulsion computations

The results in terms of forces are summarized in the table below.

Force on	incl flank ruds [kN]	excl flank ruds [kN]
Hull	25.86	26.12
Center nozzle	-24.24	-23.96
Port side nozzle	-24.24	-23.79
Inner flanking rudder port	1.43	-
Outer flanking rudder port	0.83	-
Axes and struts	13.16	13.4
Total	-29.2	-32.12
Thrust per propeller	-41.2	-41.2

Table 7: Forces from propulsion computation; Negative means forward force.

The total force in the case including propulsion is directed forward, note that the propeller thrust is not yet added. This is solely due to the nozzle which are expected to give a substantial forward force when highly loaded. A large forward force is expected because the condition which is taken from the full scale trials is including barges. These barges are not taken into account here.

The next major difference is the hull resistance. This is a factor four higher than in the resistance case. When comparing the pressures on page F7 it is evident that it is due to the jet exiting the nozzles. Due to the curvature of the hull the jet hits the aft part of this hull which causes a high pressure resistance of the hull.

The flanking rudders have a combined resistance of 4.52kN for the ship. This is 3.0% of the total forward force of the pusher. Note on the figures on pages F10 and F11 that these rudders are perfectly aligned with the flow in this case. The streamlines are not bend due to the rudder and there is no suction peak on it as well. This means this 3.0% is a minimum.

Flow separation is shown on page F8. Note that the blue ring around the inlet of the nozzle is actually not flow separation. This is shown on page F9, due to the high loading of the nozzles the flow is more or less bend around the inlet of the nozzle creating a small region of flow in forward direction.

The region between the nozzles has flow separation due to the high loading of the nozzles and propellers. This is best shown on page F12. Streamlines that enter half way between the two nozzles roll up in a vortex and go into the nozzle at the last moment.

The figure on page F13 show the limiting streamlines on the surface. There is a strong flow over the side edge of the aft part of the hull. This is often seen for ships in shallow water and is due to the propellers that need to ingest high quantities of water. However, due to the high curvature at this edge a vortex is generated due to so called 3D flow separation which is shown in the lower figure on the same page.

Other vortices that are generated are shown in the same figure. Below the axes vortices emerge due to the axes not being aligned with the flow. This is inevitable. However, the endplates of the rudder are also not aligned with the flow which also creates strong vortices. These vortices are ingested by the propeller, also shown on page F14, causing disturbances on the wake field of the propeller. This may cause extra cavitation and extra vibrations.

4 RESULTS OF PROPELLER COMPUTATIONS

In this chapter an indicative analysis will be performed on the propeller using PROCAL. Some changes in the propeller design was attempted using the next starting points:

- The thickness of the propeller is not altered, this stems mainly from strength considerations. The blades are thicker than necessary from a pure hydrodynamic perspective but some extra strength is probably required due to large objects that may be encountered in the shallow inland waters.
- The propeller has the same working point as the original propeller, i.e. the same power absorption at the same rotation rate. No analysis is made weather a different working point would be beneficial due to lack of reliable thrust data. However, a good analysis in this respect can be greatly beneficial.

4.1 Wake field

Since PROCAL is not yet able to do unsteady computations including a nozzle, the effect of the nozzle needs to be included in the wake field. The wake field is obtained from the nominal wake field inside the nozzle. On this wake field the induction of the nozzle is superimposed. Then the axial wake field is scaled such that the propeller absorbs 289 kW at 245RPM, which is the working point according to the trials. The result is shown on page F14.

Some inaccuracies exist in this method because the vortices stemming from the rudder do not enter the nozzle in the nominal case and are therefore not included in this wake field. This is one of the differences between the nominal and effective wake field.

Some vortices can be identified in the wake field however. The lower, larger vortex is due to the strut. This strut could benefit from a smaller thickness over chord ratio, creating less drag and disturbances.

The green area near the top is due to the boundary layer of the ship.

4.2 Pressure and cavitation

The pressure over the original blade is shown on page F15 in the upper figure. The red line is the cavitation limit. It is seen that the original propeller has a strong suction peak starting cavitation near the leading edge. This peak is seen during the full rotation of the propeller and is caused by the circle like leading edge.

Furthermore it is noted that there is a large margin against further cavitation. Thus when the suction peak is ignored, a much higher blade loading is needed to start cavitation. Therefore the blade area ratio could be minimized. Noted is that the condition used in this report is not at maximum blade loading.

An indicative redesign is made to show what could be achieved. The blade sections are changed by a NACA66 modified thickness distribution and an a=0.8 camber line which creates flat pressure distributions. The result is seen on page F16. The original design has significant cavitation during the full blade rotation. The adapted design has a significantly lower blade area ratio (from 0.85 to 0.62) and less cavitation. The flatter pressure distribution is shown on page F15 in the lower figure. In this way less vibrations can be expected and some efficiency is gained (about 1%).

5 CONCLUSIONS

The following conclusions summarize the findings of the analysis performed on the CFD computations written in this report:

On the viscous flow computations:

- The flanking rudders cause a decrease of forward thrust of 3%. Since these rudders are well aligned with the flow in this case, this should be seen as a minimum.

- The end plates of the flanking rudders are not aligned with the flow and therefore generate vortices that are ingested by the thrusters. These probably cause extra cavitation and vibrations of the propeller.

- The pressure resistance on the hull increases with a factor of four when the propeller action is taken into account. This is due to the concave shape of the aft part of the hull. The jet that comes out of the nozzles hit this part of the hull and increase its resistance, decreasing the effectiveness of the thrusters.

- There is some propeller induced flow separation in between the nozzles. Due to the high loading of the nozzles streamlines in between the nozzles close to the hull deflect to be ingested by the nozzle due to the high loading.

- The shallow water causes more water to be drawn to the thrusters from the side which means it flows around the relatively sharp edge of the aft part of the hull. This causes 3D flow separation and therefore strong vortices that are generated.

- The results of the resistance computations are sensitive to the size and shape of the separation regions. This is probably due to the combination of the instable nature of these regions and the steady state computations. This has an effect on the accuracy of the calculated resistance.

On the propeller computations:

- The propeller has a blunt leading edge causing sharp low pressure peak near the leading edge during the full rotation of the blade. This causes cavitation during the full rotation of the blade. Reshaping this leading edge reduces cavitation significantly. Blade area ratio can therefore be reduced and around 1% efficiency can be gained.

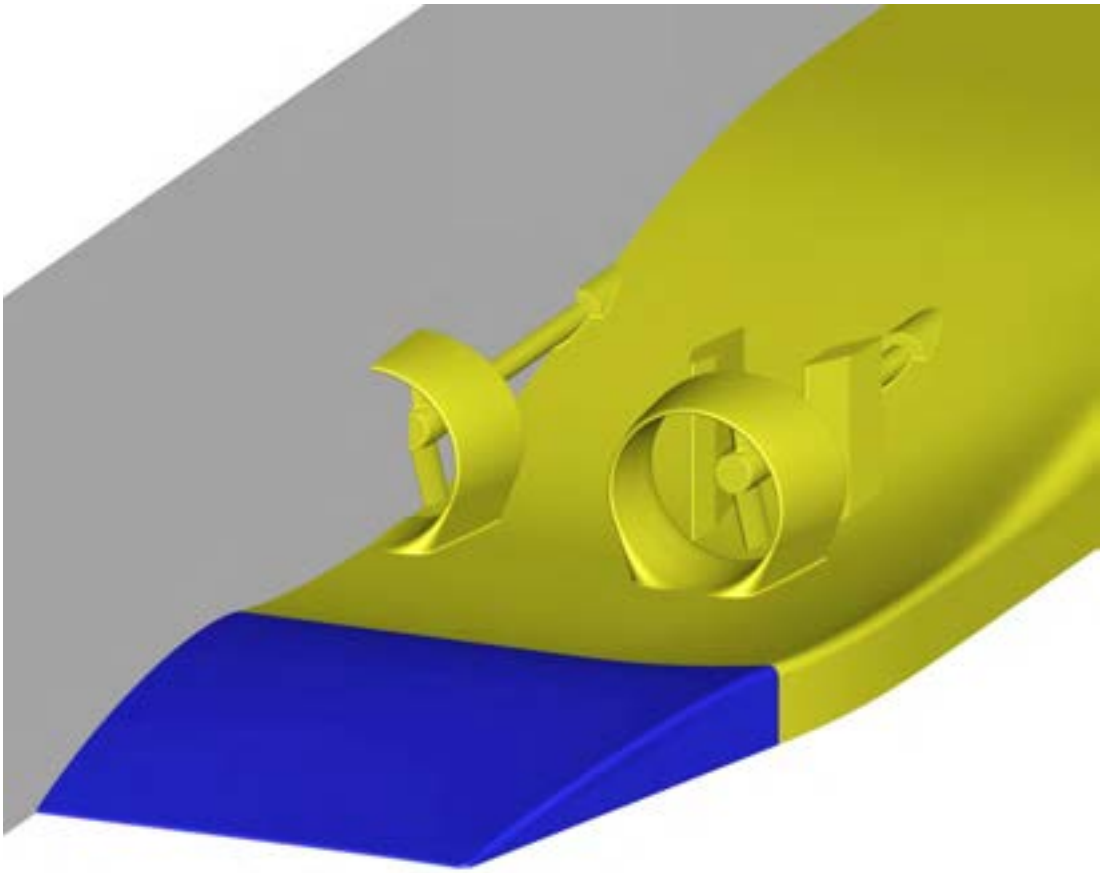

Figure 1: Geometry including stream cap in blue. In grey is the symmetry plane.

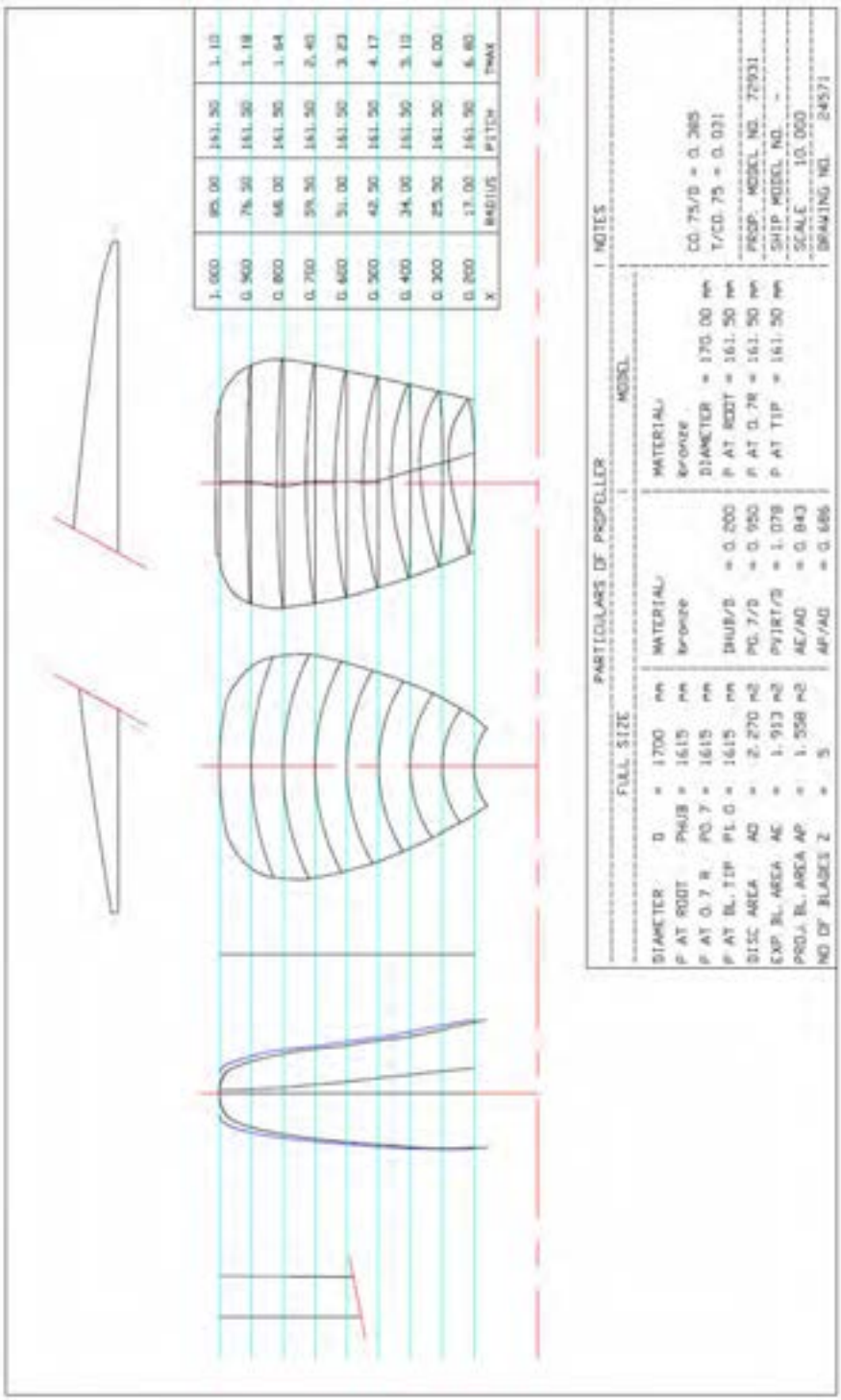

Figure 2: Form plan of the propeller as fitted on the Dunaføldvar

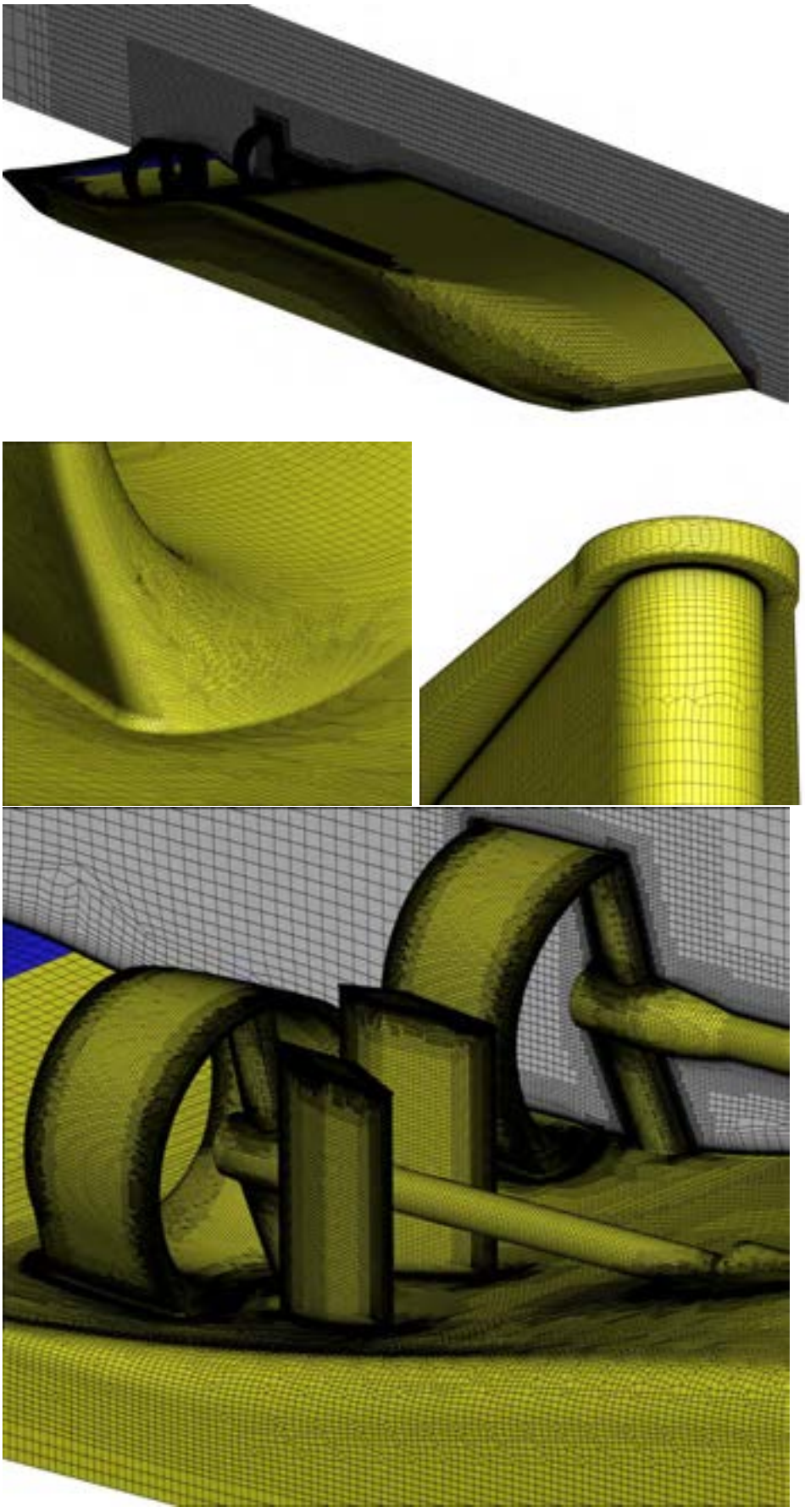

Figure 3: Impression of the computational grid

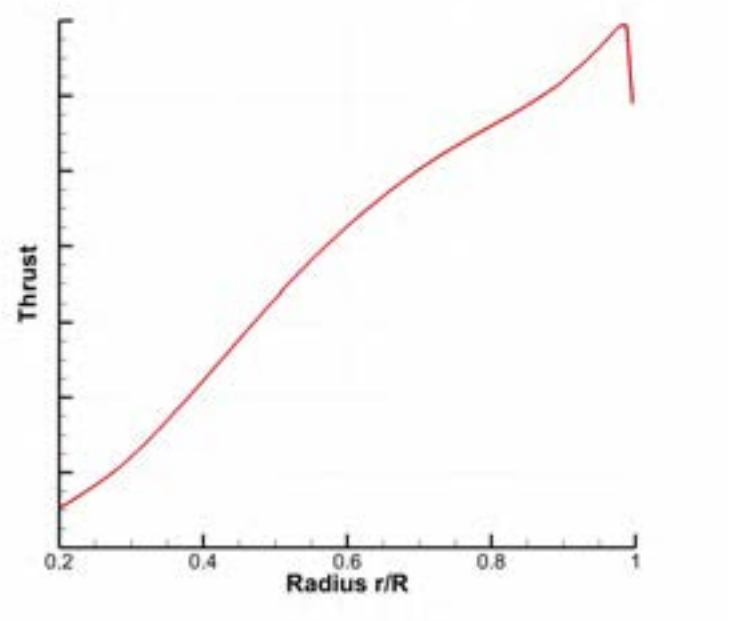

Figure 4: Radial loading of the actuator disk

Normal resolution grid

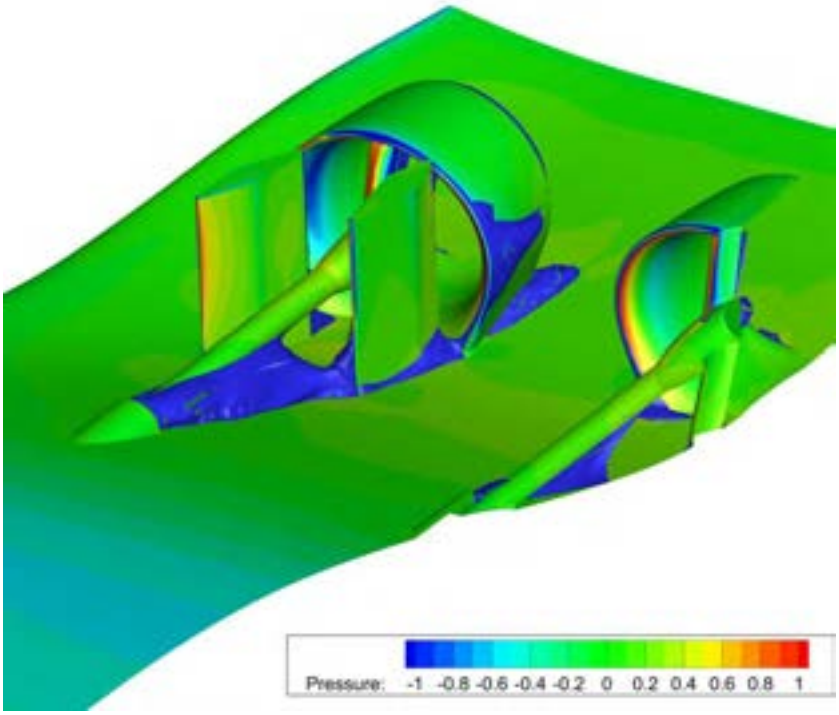

High resolution grid

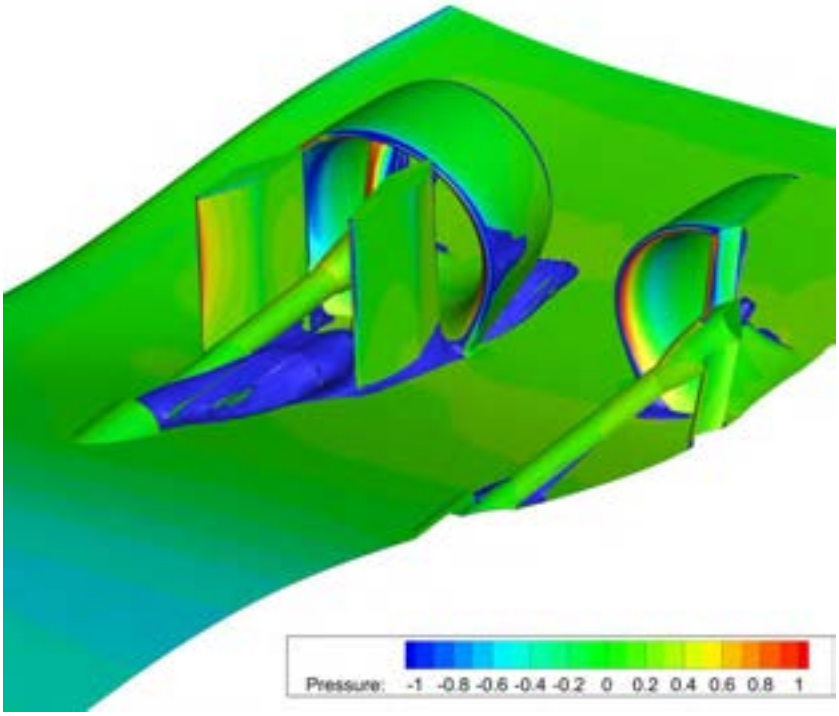

Figure 5: Resistance computations; Pressure scaled with incoming dynamic pressure; In blue are areas with flow in forward direction which is indicative for flow separation.

Normal resolution grid

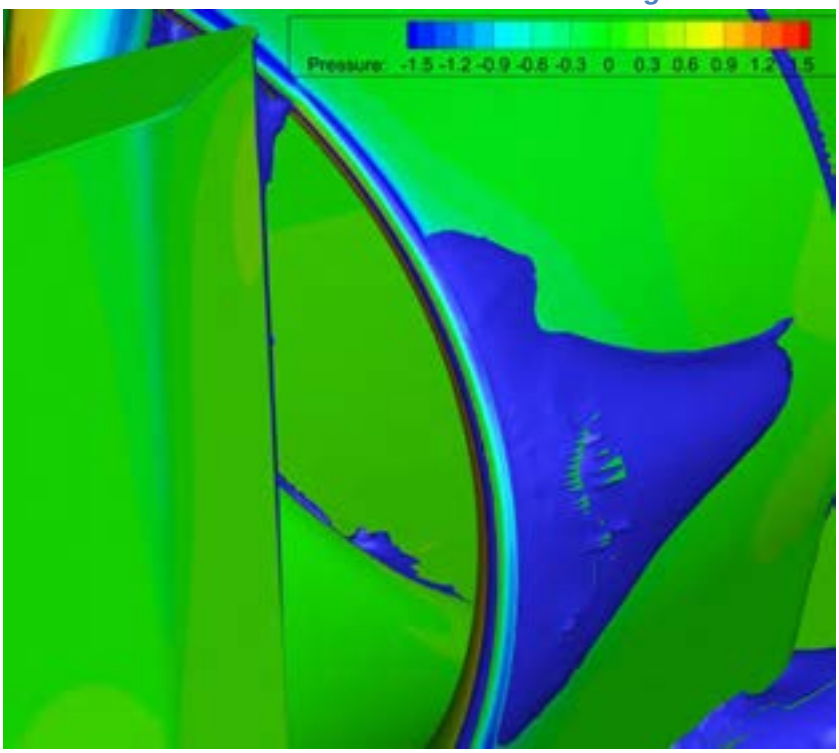

High resolution grid

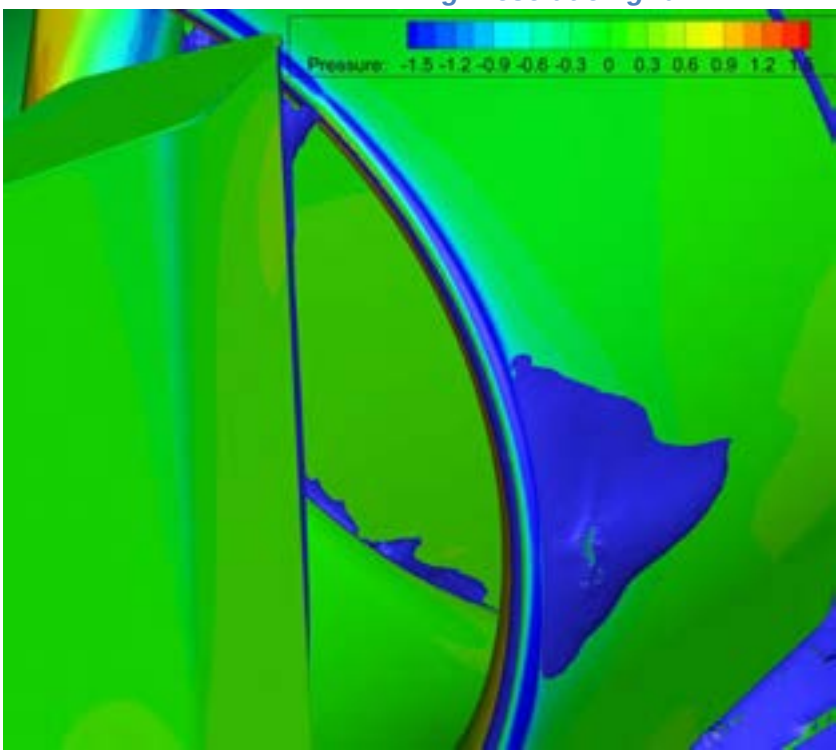

Figure 6: Resistance computations; Pressure scaled with dynamic pressure at inlet; In blue are areas with flow in forward direction which is indicative for flow separation.

Resistance computation

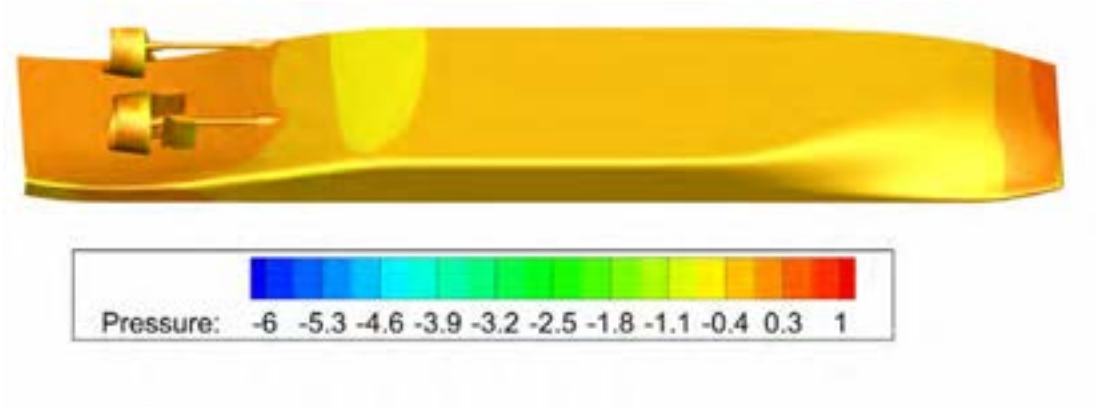

High resolution grid

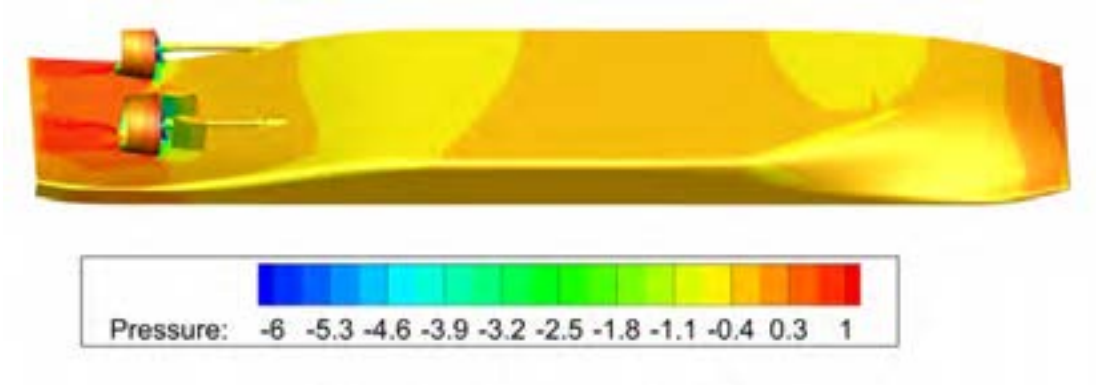

Figure 7: Comparison of pressure between resistance and propulsion computation; Pressure scaled with dynamic pressure at inlet.

Including flanking rudders

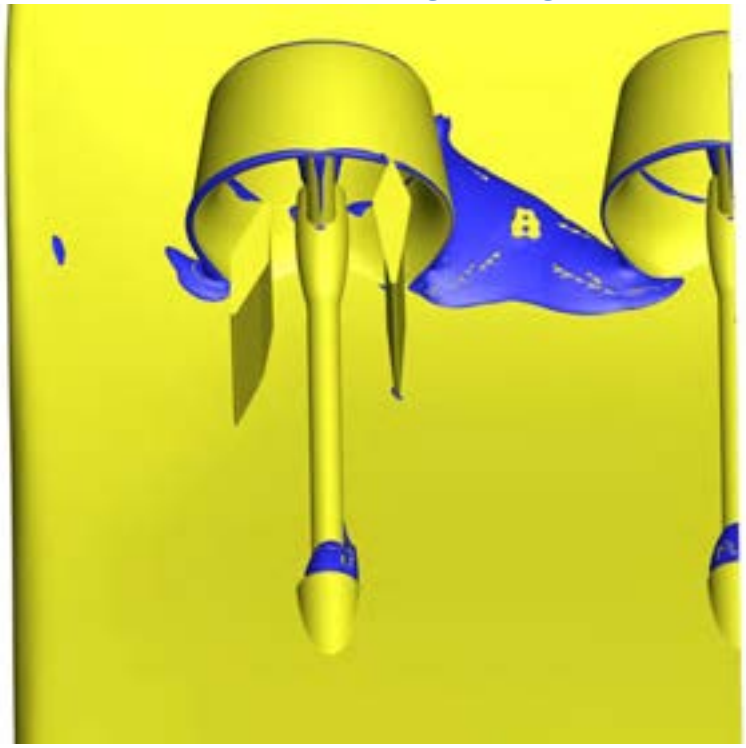

No flanking rudders

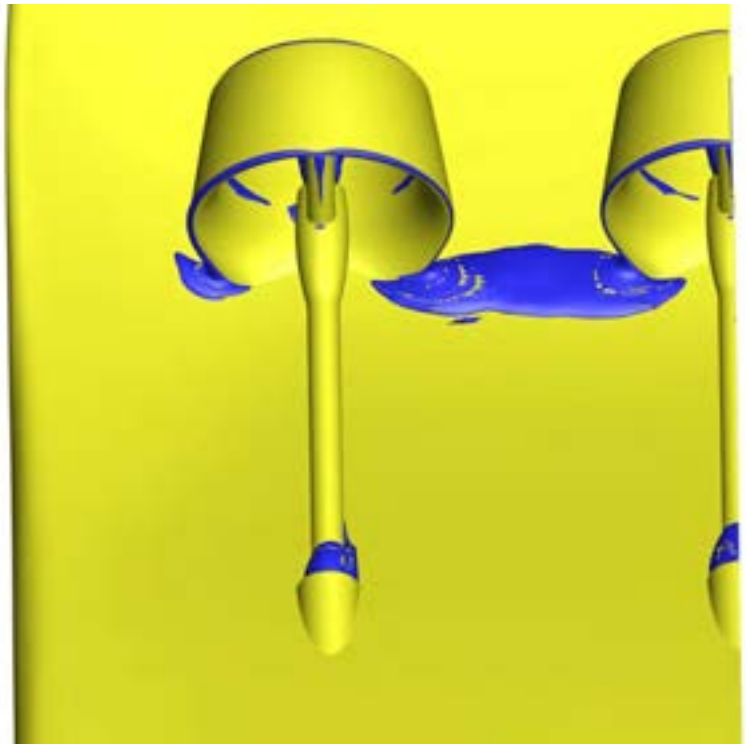

Figure 8: Propulsion computations; In blue are areas with flow in forward direction which is indicative for flow separation.

Including flanking rudders

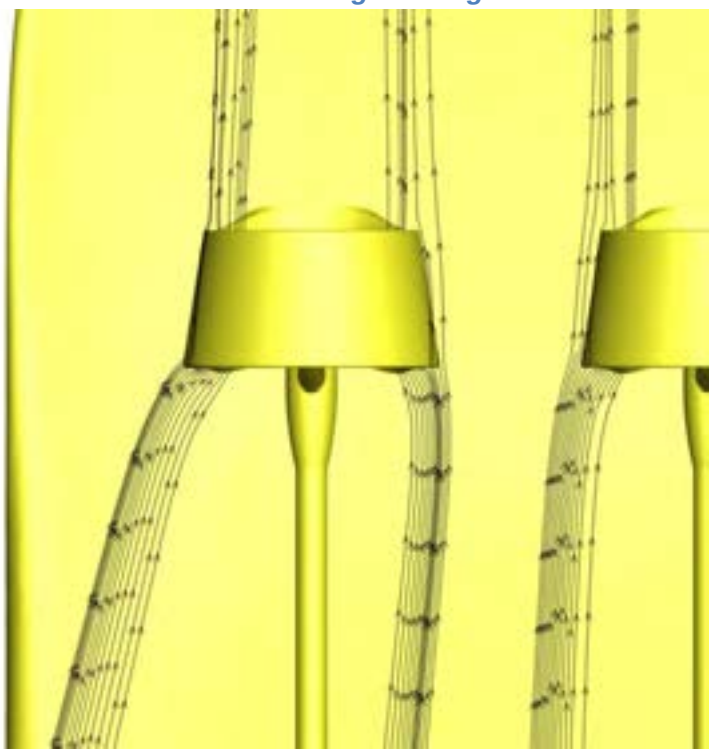

No flanking rudders

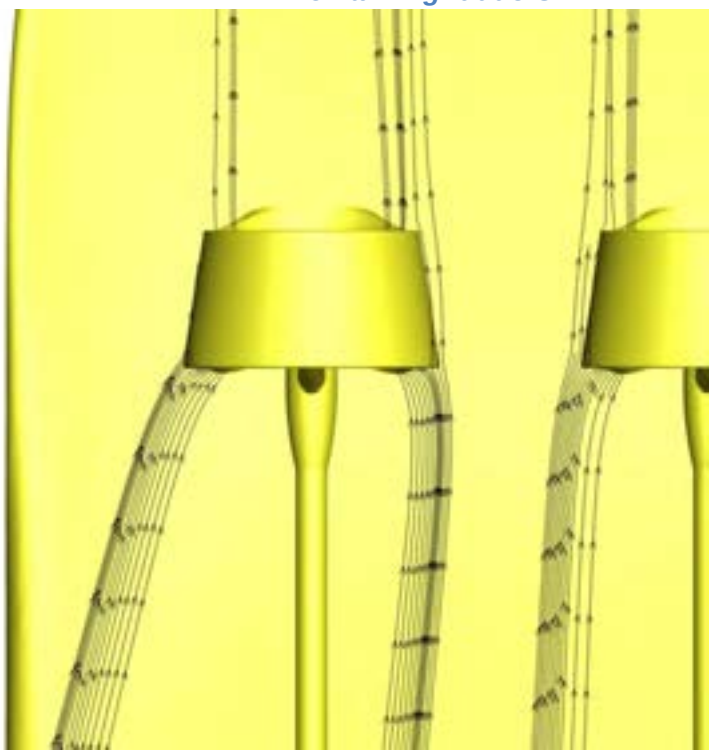

Figure 9: Propulsion computations; streamlines along the edge of the nozzle, note the high contraction of the flow at the inlet of the nozzle.

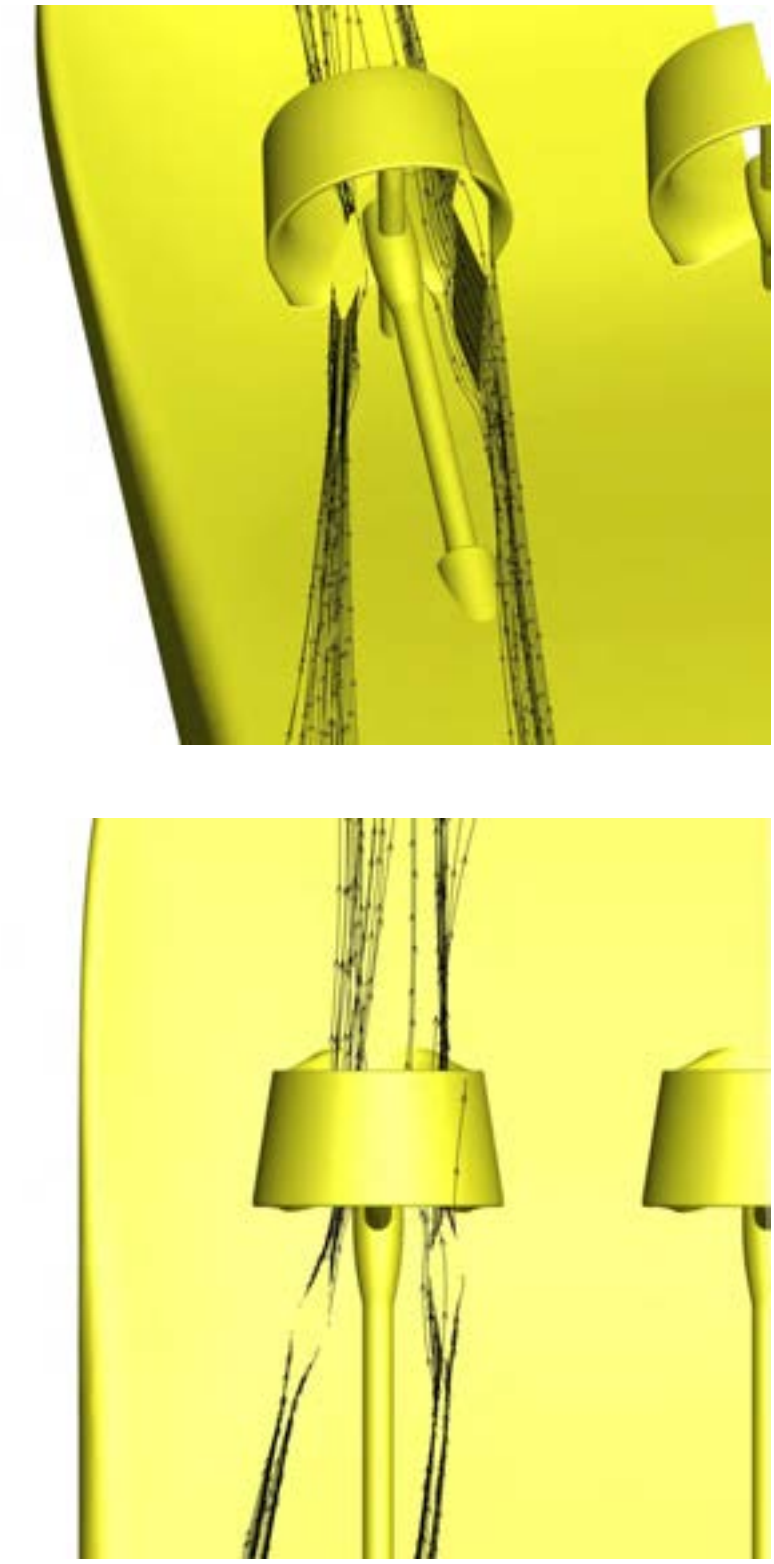

Figure 10: Propulsion computations; streamlines along the rudder.

Including flanking rudders

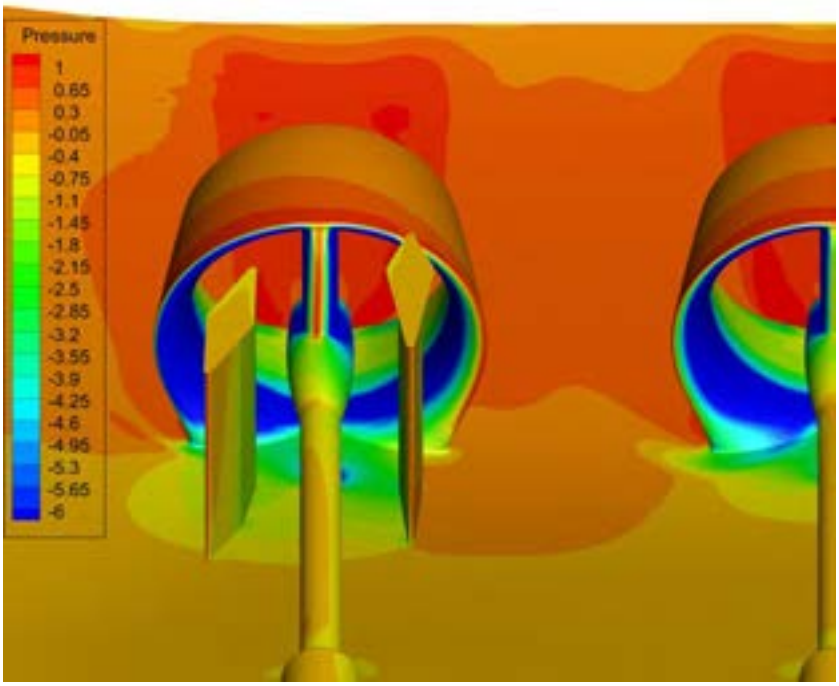

No flanking rudders

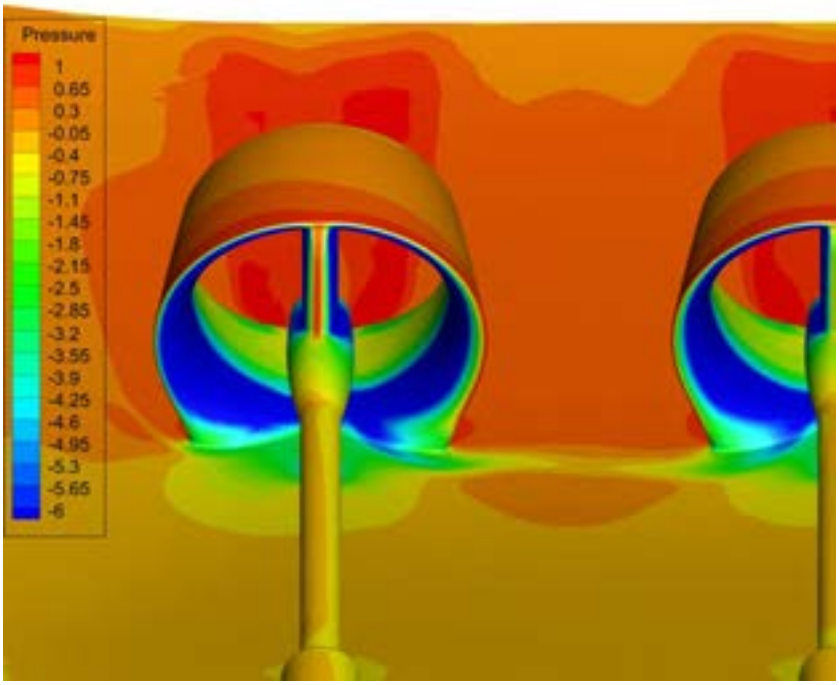

Figure 11: Propulsion computations; Pressure scaled with dynamic pressure at inlet.

Including flanking rudders

No flanking rudders

Figure 12: Propulsion computations; Streamlines

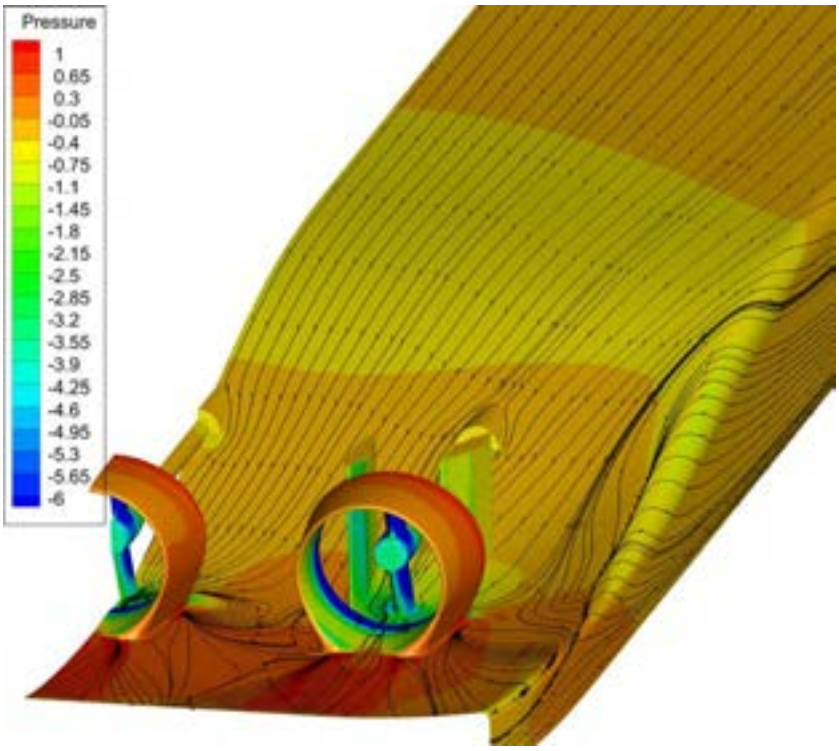

Propulsion computations; Limiting streamlines (direction of shear stress on the surface) and pressure; Pressure is scaled with dynamic pressure at the inlet.

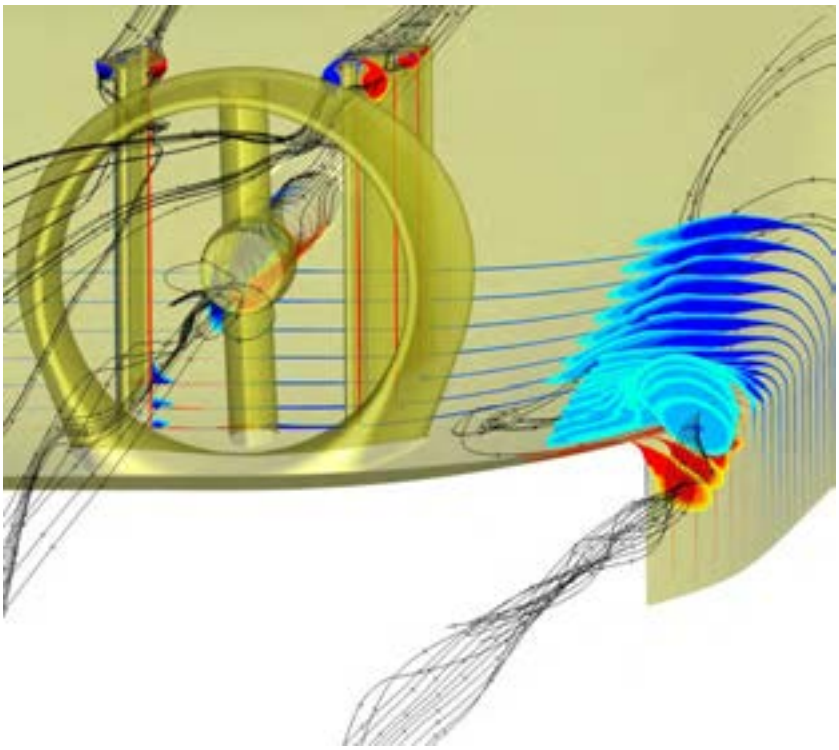

Figure 13: Propulsion computations; Streamlines and vorticity. This gives an impression of the vortices that are generated.

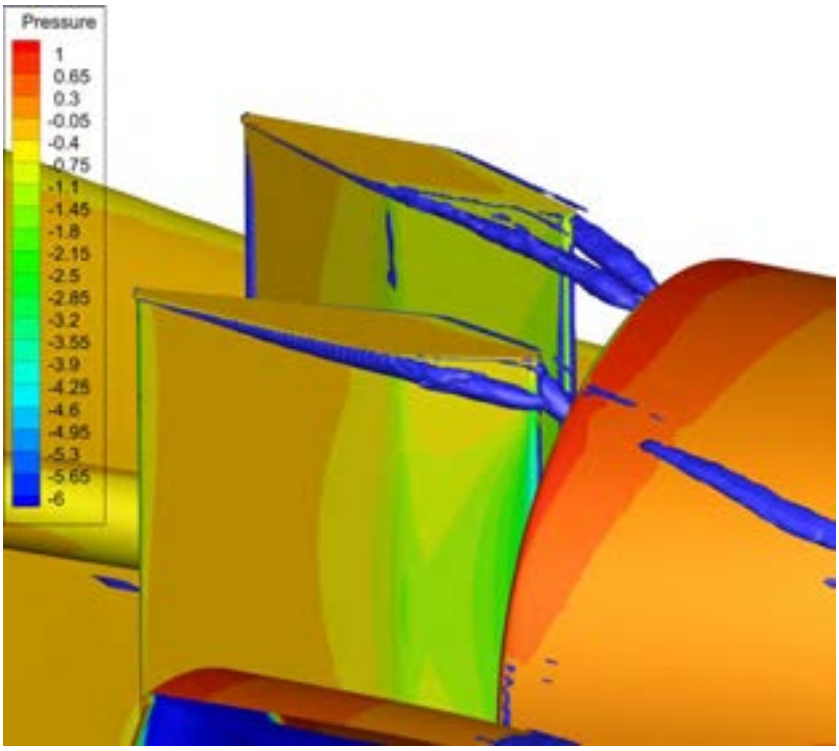

Figure 14: Propulsion computations; The blue regions are vortices; The vortices stemming from the rudder are diverted into the nozzle.

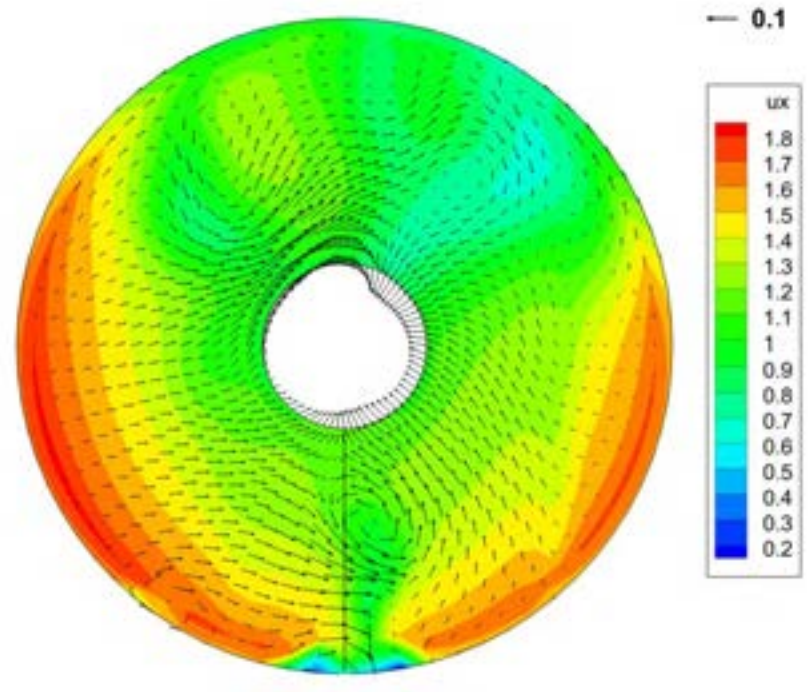

Figure 15: Wake field used in the PROCAL computations.

Original propeller

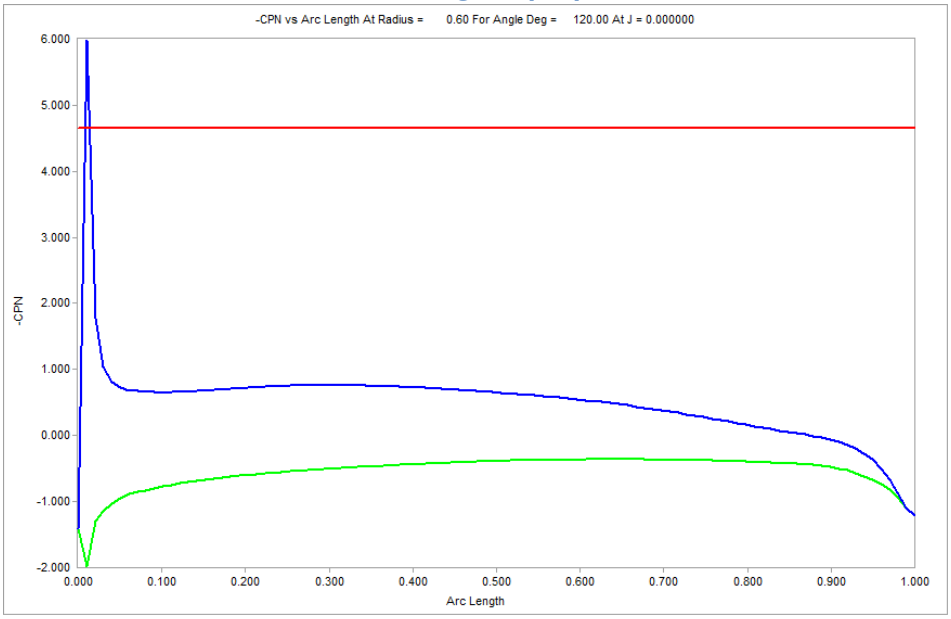

Adapted propeller

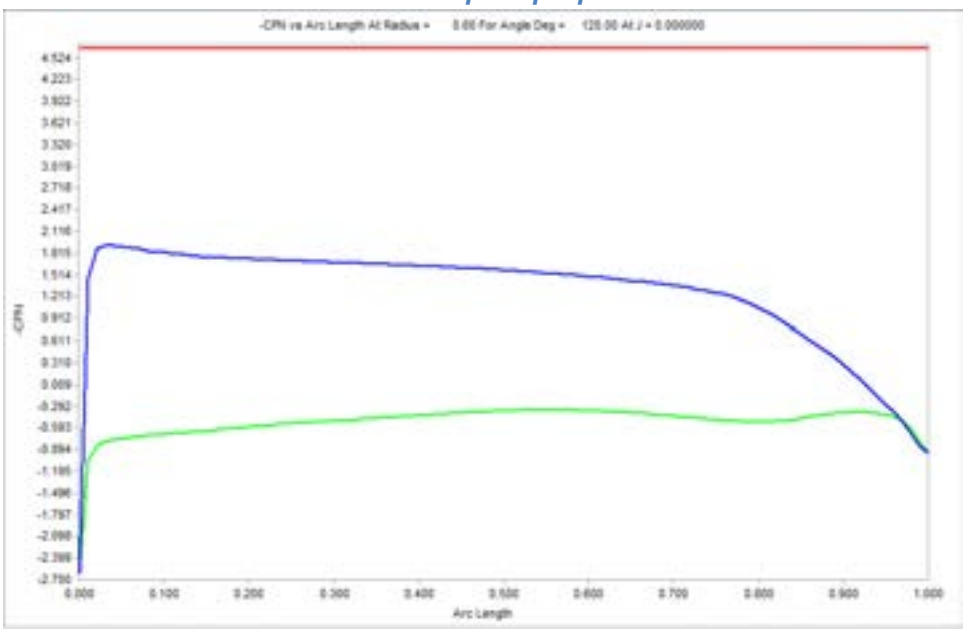

Figure 16: PROCAL; Pressure distribution from leading to trailing edge at blade position 120° (Starboard, Down) for the adapted propeller; The red line indicates the cavitation limit.

Original propeller

Adapted propeller

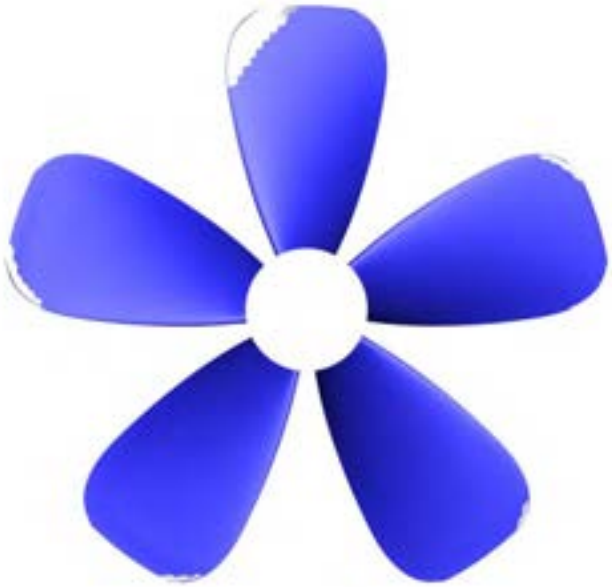

Figure 17: PROCAL; Cavitation areas on the blade shown in white;

CONCLUSIONS

Written by : MARIN – Ir. K.H. van der Meij

TABLE OF CONTENTS

1 CARPE DIEM

For the self propelled barge Carpe Diem two retrofit measures were investigated. First there was investigated with potential flow calculation if the wave making resistance could be reduced by modifying the bow. Based on these calculations the following could be concluded:

- The wave generated by the ship is good compared to that of similar vessels, therefore no significant gain is expected after modifying the bow.

Secondly the viscous flow around the gondolas was investigated. Based on this investigation the following recommendations were done:

- The gondolas should be oriented slightly inward in order to be aligned with the fluid and avoid the flow separation.
- The size of the gondolas are considered big. A reduction of it length is recommended.
- An increase of the distance from the end of the gondola to the propeller plane is recommended in order to improve the wake field.
- Smooth the end of gondola.

Based on this study, MARIN has proposed a hull modification of the ship Carpe Diem. For these new hull form only the aftbody of the gondolas was modified. A CFD calculation for the new ship hasn't been performed at the moment of writing this report, therefore no reduction in fuel consumption could be determined.

2 HERSO-I

The Herso-I is alsway sailing with the same barge in front, the Leonie SL. Between the barge and the vessel a large gap is present. In this study the effect of a trapeze was investigated. Therefore calculations with and without gap have been performed. Based on these calculation the following conclusions could be drawn:

- The flow around the bow of the Leonie SL shows a smooth transition from bow to bottom. The transition from the bow to the side is rather sharp due to the pram shape, which causes a large vortex.

- When not applying a smoothened transition the boundary layer along the pusher is rather thick due to the flow reversal behind the barge. When applying a smoothened transition the boundary layer becomes thinner. The thinner boundary layer is beneficial from resistance point of view; an indication for the resistance with and without smooth transition shows a resistance decrease of 20%.

- The transition as calculated might be impractical to build. A less drastic approach could be followed leading to less resistance decrease than indicated before. However, most of the resistance decrease is related to the removal of the flow reversal area.

- The axial velocity distribution just before the transom of the pusher shows two longitudinal vortices originating from the bilge area and the knuckle at the top of tunnel. These vortices increase the resistance of the vessel.

3 INLFEXIBLE

For the pushboat Inflexible there was investigated if the aftbody could be improved by retrofitting. Viscous flow calculation has been performed for the original hull lines, based on this calculation the following conclusions were drawn:

- Vortex sheet separation due to streamline convergence is seen on sharp edges at bow thrusters housing, bilges and bossing.
- Flow separation occurs at the bottom of the bow due to the strong curvature of the hull and the further deceleration on the flow caused by the downstream bow thrusters housing. When sailing with barges in front of the pusher, the local flow will be different.
- The shaft bossing is poorly aligned with the flow. This leads to the formation of a strong vortex, which crosses the propeller plane and causes vibrations
- Some flow separation is seen at the inner side of the bossing.
- The nominal wake field is characterised by various wake peaks stemming from different sources.
- The upper two struts are misaligned, locally at an angle up to 17° with the flow direction. The outer strut experiences just flow towards the centreline. However, the inner strut has incoming flow at both positive and negative angles. Please note that the calculation is performed for only one condition, variations in draught, trim and water depth can change the neutral angle.
- Rounding of knuckle lines substantially reduces the generation of strong vortices.

Based on these recommendations the bow thrusters gondola was smoothened as well as the shaft bossing. This resulted into an improved hull shape. For this new shape viscous flow calculations have been performed to determine the gain:

- The improved hull shape has an estimated 8 % reduction in resistance compare to the original shape. For the whole convoy this corresponds with a resistance reduction of 1 to 1.5 %

The following recommendations were done based on experience and the calculation results:

- **Nozzle**: The duct of the nozzle seems quite thick. Perhaps improvements can be made by using a more slender nozzle.
- **Knuckle lines**: Sharp edges in the hull can be made more rounded. Perhaps the depth of the bossing can be increased to accommodate this geometry change. Note that currently the duct is lower than the base.
- **Propeller**: Improvements can be made by using an optimized propeller. This is in the order of magnitude of 2 % power reduction
- **Rudder**: The rudders seem quite large and bulky. The more efficient design may increase manoeuvrability and decrease resistance.

- **Transom:** The transom immersion is relatively deep, creating a rather large recirculation zone behind the ship. A lower immersion reduces drag, but will necessitate geometry changes

4 DUNAFØLDVAR

The pushboat Dunaføldvar was equipped with flanking rudders. The retrofit measurement investigated for the Dunaføldvar was the effect of removal of the flanking rudders. Based on the calculations the following conclusions were drawn:

- The flanking rudders cause a decrease of forward thrust of 3%. Since these rudders are well aligned with the flow in this case, this should be seen as a minimum.

- The end plates of the flanking rudders are not aligned with the flow and therefore generate vortices that are ingested by the thrusters. These probably cause extra cavitation and vibrations of the propeller.

- The pressure resistance on the hull increases with a factor of four when the propeller action is taken into account. This is due to the concave shape of the aft part of the hull. The jet that comes out of the nozzles hit this part of the hull and increase its resistance, decreasing the effectiveness of the thrusters.

- There is some propeller induced flow separation in between the nozzles. Due to the high loading of the nozzles streamlines in between the nozzles close to the hull deflect to be ingested by the nozzle due to the high loading.

- The shallow water causes more water to be drawn to the thrusters from the side which means it flows around the relatively sharp edge of the aft part of the hull. This causes 3D flow separation and therefore strong vortices that are generated.

- The results of the resistance computations are sensitive to the size and shape of the separation regions. This is probably due to the combination of the instable nature of these regions and the steady state computations. This has an effect on the accuracy of the calculated resistance.

In addition some propeller calculations have been performed to investigate if an optimized propeller could increase the propulsive efficiency. Based on these calculations the following conclusion was drawn:

- The propeller has a blunt leading edge causing sharp low pressure peak near the leading edge during the full rotation of the blade. This causes cavitation during the full rotation of the blade. Reshaping this leading edge reduces cavitation significantly. Blade area ratio can therefore be reduced and around 1% efficiency can be gained.